THE DEVELOPMENT OF BIFACIAL DYE SENSITIZED SOLAR CELLS BASED ON BINARY IONIC LIQUID ELECTROLYTE

A THESIS SUBMITTED TO
THE GRADUATE SCHOOL OF NATURAL AND APPLIED SCIENCES
OF
MIDDLE EAST TECHNICAL UNIVERSITY

BY

MUSTAFA BURAK COŞAR

IN PARTIAL FULFILLMENT OF THE REQUIREMENTS
FOR
THE DEGREE OF MASTER OF SCIENCE
IN
METALLURGICAL AND MATERIALS ENGINEERING

JANUARY 2013

Approval of the thesis:

THE DEVELOPMENT OF BIFACIAL DYE SENSITIZED SOLAR CELLS BASED ON BINARY IONIC LIQUID ELECTROLYTE

submitted by **MUSTAFA BURAK COŞAR** in partial fulfillment of the requirements for the degree of **Master of Science in Metallurgical and Materials Engineering Department**, **Middle East Technical University** by,

Prof. Dr. Canan Özgen _____
Dean, Graduate School of **Natural and Applied Sciences**

Prof. Dr. Cemil Hakan Gür _____
Head of Department, **Metallurgical and Materials Engineering**

Prof. Dr. Ahmet Macit Özenbaş _____
Supervisor, **Metallurgical and Materials Eng. Dept., METU**

Examining Committee Members:

Prof. Dr. Ayşe Çiğdem Erçelebi _____
Physics Dept., METU

Prof. Dr. Ahmet Macit Özenbaş _____
Metallurgical and Materials Eng. Dept., METU

Assoc. Prof. Dr. Caner Durucan _____
Metallurgical and Materials Eng. Dept., METU

Assist. Prof. Dr. Yunus Eren Kalay _____
Metallurgical and Materials Eng. Dept., METU

Dr. Gülgün Hamide Aydoğdu Kuru _____
Senior Expert Engineer, ASELSAN

Date: _____

I hereby declare that all information in this document has been obtained and presented in accordance with academic rules and ethical conduct. I also declare that, as required by these rules and conduct, I have fully cited and referenced all material and results that are not original to this work.

Name, Last name : Mustafa Burak Coşar

Signature :

ABSTRACT

THE DEVELOPMENT OF BIFACIAL DYE SENSITIZED SOLAR CELLS BASED ON BINARY IONIC LIQUID ELECTROLYTE

Coşar, Mustafa Burak
M. Sc., Metallurgical and Materials Engineering
Supervisor: Prof. Dr. A. Macit Özenbaş

January 2013, 72 pages

In this study, we investigated the effect of electrolyte composition, photoanode thickness, and the additions of GuSCN (guanidinium thiocyanate), NMB (N-methylbenimidazole), and SiO_2 on the photovoltaic performance of DSSCs (dye sensitized solar cells). A bifacial DSSC is realized and irradiated from front and rear sides. The devices give maximum photovoltaic efficiencies for 70% PMII (1-propyl-3-methylimidazoliumiodide)/30%($EMIB(CN)_4$)(1-ethyl-3-methyl-imidazolium tetracyano borate) electrolyte composition and 10 μm thick photoanode coating which is considered to be the ideal coating thickness for the diffusion length of electrolyte and dye absorption. A significant increase in the photocurrent for DSSCs with optimum molarity of 0.1 M GuSCN was observed due to decreased recombination which is believed to be surface passivation effect at photoanode electrolyte interface suppressing recombination rate. Moreover, optimum NMB molarity was found to be 0.4 for maximum efficiency. Addition of SiO_2 to the electrolyte both as an overlayer and dispersed particles enhanced rear side illuminated cells where dispersed particles are found to be more efficient for the front side illuminated cells due to additional electron transport properties. Best rear side illuminated cell efficiency was 3.2% compared to front side illuminated cell efficiency of 4.2% which is a promising result for future rear side dye sensitized solar cell applications where front side illumination is not possible like tandem structures and for cells working from both front and rear side illuminations.

Keywords: Dye sensitized solar cell, ionic liquids, SiO_2 nanoparticles, bifacial sides illumination

ÖZ

İKİ BİLEŞENLİ İYONİK SIVI ELEKTROLİT BAZLI ÇİFT YÖNLÜ ÇALIŞABİLEN BOYA UYARIMLI GÜNEŞ GÖZELERİNİN GELİŞTİRİLMESİ

Coşar, Mustafa Burak
Y. Lisans, Metalurji ve Malzeme Mühendisliği
Tez Yöneticisi: Prof. Dr. A. Macit Özenbaş

Ocak 2013, 72 sayfa

Bu çalışmada elektrolit kompozisyonunun, fotoanot kalınlığının, GuSCN (guanidinium thiocyanate), NMB (N-methylbenimidazole) ve SiO_2 katkılarının boya uyarımlı güneş gözelerinin (BUGG) fotovoltaik performansı üzerindeki etkileri incelenmiştir. Boya uyarımlı güneş gözeleri hem ön hem de arka yüzden aydınlatılarak ikiyüzlü göze ölçümleri gerçekleştirilmiştir. Maksimum fotovoltaik verimlilik %70 PMII (1-propyl-3-methylimidazoliumiodide)/ %30 ($EMIB(CN)_4$)(1-ethyl-3-methyl-imidazolium tetracyano borate) elektrolit kompozisyonunda ve 10 µm fotoanot katman kalınlığında elde edilmiştir. Elektrolitin difüzyon mesafesi ve boyanın soğurma miktarları göz önünde tutulduğunda 10 µm fotoanot kalınlığı ideal kalınlık olarak ortaya çıkmaktadır. Elektrolit içerisine 0,1 M GuSCN eklendiği zaman BUGG fotoakımında büyük ölçüde bir artış gözlenmiştir. Gözlenen artış fotoanot ve elektrolit arayüzeyinde oluşan pasivasyon etkisi nedeniyle göze içerisinde ayrılan elektronların tekrar birleşme miktarlarında yarattığı önemli ölçüdeki azalma ile açıklanmaktadır. İkinci eklenti olan NMB 0,4M optimum miktarda maksimum verime neden olmuştur. SiO_2 yapı içerisine ekstra bir katman olarak ve elektrolit içerisine dağıtılmak suretiyle iki şekilde entegre edilmiştir. Belirtilen modellerin her ikisi de arka yönden yapılan ölçümlerde verimde iyileşme göstermekle beraber, ön yüzden yapılan ölçümlerde elektrolit içerisinde dağıtma modeli elektron taşınma mekanizmasının daha düzenli yapıya geçmesi nedeniyle verim açısından daha iyi sonuçlar göstermiştir. Maksimum göze verimi arka yönden yapılan ölçümlerde % 3,2, ön yüzden yapılan ölçümlerde % 4,2 olarak elde edilmiştir. Bu sonuçlar arka yönden de elektrik dönüşümünün kullanılabileceği muhtemel çift yönlü uygulamalar ve tandem yapıları için ümit vaat etmektedir.

Anahtar Sözcükler: Boya uyarımlı güneş gözesi, iyonik sıvılar, SiO_2 nanoparçacıkları, ikiyüzlü aydınlatma

To My Family

ACKNOWLEDGMENTS

First of all, I am very grateful to my supervisor Prof. Dr. A. Macit Özenbaş for his guidance, support during this work, and his great attention and patience on me from beginning until the end of my graduation.

I am very grateful to my laboratory colleagues Barış Çeltikçi, Halil İbrahim Yavuz, Kerem Çağatay İçli, Murat Güneş, Berk Akbay and Bahadır Can Kocaoğlu for their support and friendship at every stage of this study and my graduation. I am also very grateful to all the staff of the Department of Metallurgical and Materials Engineering for all the measurements.

This work was supported by the GÜNAM (Center for Solar Energy Research and Applications) at METU. I would like to thank to all the staff of the GUNAM for photovoltaic measurements.

Finally, I would like to express my deepest gratitude to my family for sharing my hard times with me and their love, support and patience during my life.

TABLE OF CONTENTS

LIST OF TABLES

TABLES

LIST OF FIGURES

FIGURES

CHAPTER 1

INTRODUCTION

Energy crisis in worldwide has been expressed by many journals, books and authorities since the realization of the diminishing of fossil fuel sources. Limited existence of fossil fuels in earth results in the growth of market prices and use of energy in a whole year raises a lot compared to the previous one. Therefore, energy demand of the countries has been increasing year after year. Today, although fossil fuel is still mostly used energy resource in worldwide, different energy resources will take the place of fossil fuels in industrial and basic applications. This overdue alteration will also propose a solution to the health and environmental problems which source due to fossil fuels. Mostly known and consumed fossil fuels are oil, coal and natural gas which are used in many distinct areas regardless of the used place. Therefore, people and natural life definitely exposure the negative effects of the fossil fuels in daily life. Most of the developed countries make an investment to the alternative energy resources which are also called as “Renewable Energy”. Wind, geothermal, biomass and solar energies are mostly pronounced renewable energies and they are tested in the aspects of abundance, adaptedness to whole world and performance. Solar energy is the most attractive, studied and invested candidate because above criteria are encountered in a best way by the solar energy. Solar energy has been investigated at several branches with different viewpoints. However, all the branches of solar cells suffer from different problems: High cost, not applicable to daily life and low efficiency may be some of them. Therefore, up to now, there is not a negotiation about which type of solar cell will become the future energy [1-2].

Photovoltaic researches have been introduced with silicon based solar cells because these cells showed promising results in efficiency values in their early period of studies. On the other hand, these cells had very important handicap which is the high production cost. Therefore, silicon solar cells in product form get into market quite a long time after the start of researches. Other disadvantages on commercialization of silicon solar cells are the high amortization time and decrease in efficiency out of laboratory conditions. Despite of the negative points, Si solar cells have been dominating the market for several years. Also, for 20 years, development in silicon solar cell industry decreases the cost of energy per watt from 100 USD to 4 USD. Although this price is again more than the fossil fuels, silicon solar cells look ahead more confident to replace with fossil fuels. Although there are good efforts to decrease the prices to lower values, generally these prices originate from the production technique of silicon wafers [1–3].

Since their invention in 1991, dye sensitized solar cells (DSSCs) have been attractive photovoltaic devices compared to conventional silicon based solar cells from an economical point of view [4]. Unique properties like low cost with moderate efficiency, energy production at adverse weather conditions (cloudy or rainy days) and applicability to window glasses and flexible substrates are the main reasons why DSSCs are the most suitable alternative to Si-based solar cells. However, commercialization of these devices requires high stability giving a life time of over 20 years.

Bifacial cell designs are mostly preferred for the classical p-n junction solar cells as a research and product. However, application of this topic to the DSSCs is restricted with a few researches. It will gain importance when products of DSSCs come into market because it will

supply same energy production from the much smaller cells. Although standard DSSCs can be illuminated from both sides, the ratio of the respective efficiencies for front- and rear-side illuminations are usually low because of the screening effect of the electrolyte. DSSC structures named as bifacial cells use a transparent layer between the photoanode and counter electrode which is used to increase the performance of the cell in the case of rear-side illuminations and thus the respective efficiencies for the front- and rear-side illuminations are increased. Such cells can be used with static solar concentrators and for tandem device design in near future applications [1, 5].

Mostly used electrolyte in high efficiency DSSCs is solvent based volatile liquid electrolyte (I^-/I_3^-) which causes degradation of the cells at ambient conditions. Volatile nature and high vapour pressure of these electrolytes make them problematic at outdoor uses. Main strategy to improve the stability of DSSCs is to find non-volatile counterparts of conventional solvents such as acetonitrile, valeronitrile, methoxypropionitrile, etc. Several groups have investigated application of different hole conducting mediums like ionic liquids, polymer electrolytes [6], organic-hole transport materials [7], and inorganic semiconductors [8]. However, none of these materials achieved 10% efficiency of solvent based electrolytes because of low diffusion rate of redox species and wetting ability. Besides all ionic liquids are promising candidates as they have thermal and electrochemical stability and hydrophobicity which also have comparable efficiencies with solvent based electrolytes [9]. Most popular ionic liquid used in DSSC applications contains imidazolium cations which suffer from increased viscosities causing low ionic mass transport when used with iodide/triiodide redox couple resulting in poor efficiencies [10].

One approach to compensate the reduction in viscosity is to employ a secondary anion in cooperation with ionic liquid (binary system). Mostly used anions in literature are bis-(trifluoromethylsulfonyl) imide (Tf_2N^-), thiocyanate (NCS^-) and tetracyanoborate ($B(CN)_4^-$. $(B(CN)_4)^-$ is the most appropriate anion among the alternatives because of its superior stability and low viscosity (19.8 cP) [10–13].

Different efficiency values ranging from 2.1% to 8% were found using different ionic liquid electrolyte compositions and high-molar extinction-coefficient sensitizers [14–19]. In order to suppress optical absorption of electrolyte for bifacial DSSC applications employing an additional SiO_2 layer on top of TiO_2 layer was investigated in a study which makes it possible to collect electrons efficiently [1]. An increase in the diffusion rate of electrolyte was also observed with the direct addition of SiO_2 nanoparticles to the electrolyte [20]. Although ionic liquids have more stabile structure compared to the solvent based electrolytes, they are also in liquid form and the stability of the cells after 20 years is not known. Also additions of SiO_2 nanoparticles into ionic liquid form a much better structure known as a quasi-solid [20, 21].

However, a detailed analysis of parameters like composition of electrolyte species seems to be essential for a proper understanding. This work aims to investigate compositional dependency on the efficiency of different electrolyte components. 1-ethyl-3-methyl-imidazolium tetracyanoborate ($EMIB(CN)_4$), guanidinium thiocyanate (GuSCN) and N-methylbenimidazole (NMB) with different concentrations were prepared and combined effects of these chemicals were observed and used in DSSCs employing titanium dioxide based mesoporous anodes sensitized with standard N-719 ([cis-di(thiocyanato)-N-N′-bis(2,2′-bipyridyl-4-carboxylicacid-4′-tetrabutyl ammonium carboxylate) ruthenium (II)]) dye. Therefore, the work presented in this manuscript gives optimum conditions for the molarity of additions and photoanode thickness on the cell performance using a systematic study. Also, the electrolyte composition 70% PMII / 30% ($EMIB(CN)_4$) used for this systematic study with GuSCN and NMB additions was not given in literature before.

A bifacial DSSC has been constructed and current density-voltage (J-V) curves of illuminated cells from both sides were recorded. As diffusion coefficient of different electrolytes varies, electron life time in mesoporous matrix changes and determination of optimum thickness has been carried out. In addition to electrolyte composition optimization,

effect of addition of a SiO_2 layer on photoanode and direct addition of SiO_2 nanoparticles into the electrolyte on the optical properties of the cell have been investigated and characterized by transmission measurements.

CHAPTER 2

LITERATURE SURVEY

2.1. Basic Information about Photovoltaic Cells

Photovoltaic effect has been known since 19th century by Becquerel's works. His works, on the other hand, depend on wet- photoelectrochemical process and it is not actually creating any background for today's solar cells. Present technology for solar cells was reported firstly by Chapman and Fuller at 1954 using semiconductor junctions. Up to 1980s, photovoltaic cells have been used widely at space satellites; then, crisis in energy supply direct the world to use photovoltaic energy sources instead of fossil fuels for potential domestic applications [2].

Solar energy has several advantages over conventional energy systems. Firstly, solar energy is a renewable energy source. Solar cells do not create any pollutant and damage on environment; in addition to fact that there is not any bad effect on human health. Solar energy conversion systems can be operated long time with low maintenance costs. Solar photovoltaic systems can be arranged in roofs and walls of buildings and also their reliability and silence attract consumers to produce their own energies. Solar cells can be used in several different areas from basic applications to complex ones which show the flexibility of them. Photovoltaic materials and systems have been investigated seriously by many institutes and companies since Becquerel's experiments; therefore, there is an extensive knowledge realted to them [2, 22].

Although there is a sharp decrease in price per watt and increase in efficiency and life time in the last 20 years, countries already supply only very small amount of their energy from solar cells. Because, initial costs of solar cells are more expensive to compare traditional energy sources. Companies do not act courageously to invest on the solar cells, due to the fact that high initial costs create longer amortization periods. Secondly, despite the enhancement of efficiency value of the cells, these values are still not sufficient for some of the applications. Final handicap is life time of the cells. Many companies and researchers work on to increase the operation time of cells and therefore use of cells in daily life. Many parameters are effective on performance of solar cells; availability, intensity and spectral composition of sunlight should be considered primarily [2].

2.1.1. Characteristics of Sunlight

Sun emits electromagnetic radiation, which is derived from nuclear fusion reactions, with a spectral distribution depend on its body temperature. Surface temperature of sun is nearly 6000 K and at this temperature sun behaves like black-body emitting light in the visible region (300 nm to 700 nm) with strongest energy peak in all temperature values.

62 MWm^{-2} power density of solar flux at sun surface is reduced to 1353 Wm^{-2} when it reaches to the outside of the earth atmosphere and this value is called as solar constant. Sunlight loses some energy when passing from atmosphere due to absorption, scattering and reflection. Atmosphere factor is explained by air mass which is the normalization of path which sunlight travels to the shortest possible path length (Figure 2.1) and it is given by:

$$Air\ Mass = \frac{1}{\cos\theta}$$

Eq. [2.1]

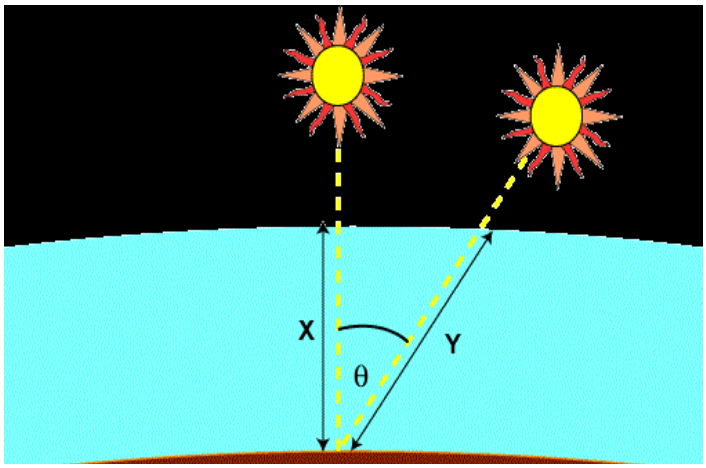

Figure 2.1 Shortest possible sun path length [23].

After the sunlight passes through Sun's atmosphere, it is referred as AM 0. Energy distribution spectrum of AM 0 is different from black body (6000 K) due to different transmissivity of Sun's atmosphere for each wavelength. For AM 1 condition, sun is directly overhead. AM 1.5 (when the sun is 48^0 to overhead) is accepted as standard for photovoltaic works with 1000 Wm^{-2} total power density. Figure 2.2 shows the energy distribution vs. wavelength diagram for the cases of AM 0, AM 1.5 and 6000 K Black body [23–25].

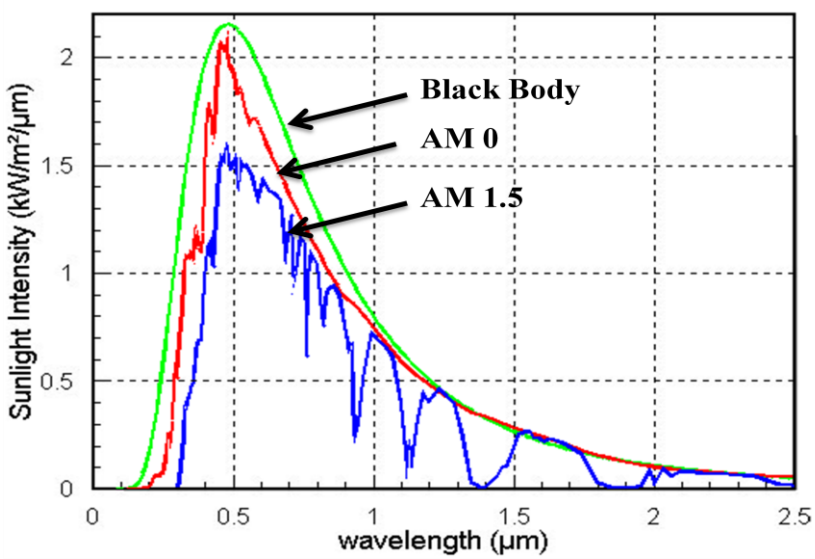

Figure 2.2 Spectral solar energy distributions of Black Body, AM 0 and AM 1.5 [23]**.**

2.1.2. Properties of Semiconductors

Materials can be grouped in three classes according to band structures as conductors, insulators and semiconductors. In the electronic configuration of materials, there is a forbidden energy band gap, which separates the valence and conduction band. Figure 2.3 reveals the band positions of 3 material groups.

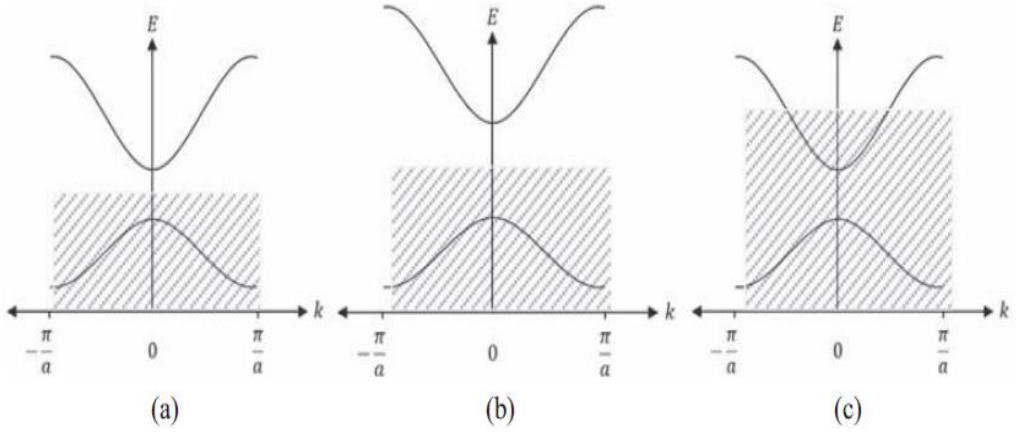

Figure 2.3 Energy levels of the different band structures (a) Semiconductor, b) Insulator, c) Metal) [26].

Semiconductors are preferred instead of metals and insulators for many electronic applications. In addition, they are mostly used in photovoltaic applications because; bands structure and band gap allow them to absorb visible light. They have fully occupied valence and non-occupied conduction band, which are involved in photon absorption and charge transportation. Also they possess optimum band gap which is so crucial for photovoltaics, because; electrons come back to valence state easily for small band gaps and visible light cannot be absorbed by large band gaps.

Group IV materials and compounds of group III-V and group II-VI of the periodic table constitute of the big majority of the semiconductors (Figure 2.4). Si, GaAs, CdTe and InP are the most important and favorite solar cell materials. In their ground state, valence band is full with electrons and conduction band is empty and therefore there is not any current flow. However, illumination or absorption of light broke the bonds in crystal structure which free electrons move to conduction band and holes occurs at valence band. This event creates current flow and these types of solar cell materials are called as intrinsic semiconductors [22 , 24].

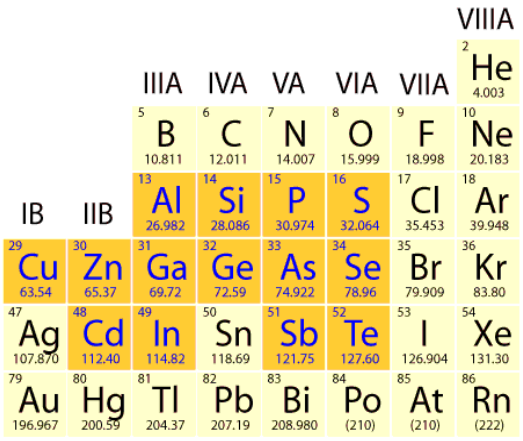

Figure 2.4 Potential semiconducting materials [23].

Furthermore, free carriers can be created with addition of impurity materials into the group IV materials and these are named as extrinsic semiconductors. Doping of materials into semiconductors create extra energy levels and alter the band gap of them. Additional level is formed as donor or acceptor according to types of impurity (Figure 2.5). Group V materials take the place of Si in crystal structure and supply additional electrons to system. Donor state is created by the supplied electrons and is called n-type doping. Group III impurity atoms substitute with Si atoms, therefore, amount of holes become more than electrons. Acceptor state is observed at band structure due to additional holes and is called p-type doping [22, 24].

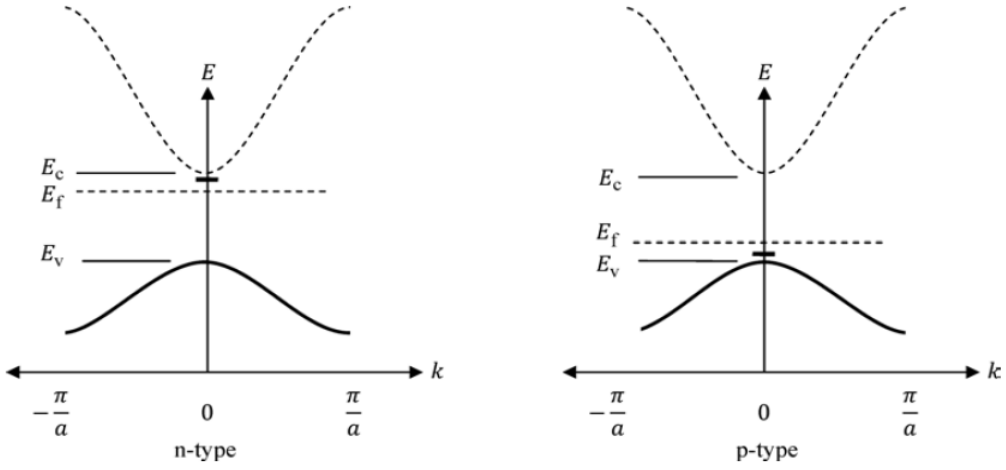

Figure 2.5 Donor (n-type) and acceptor (p-type) states in semiconductors [26].

2.1.3. The p-n Junction

While n-type semiconductors have abundance of electrons, p-type semiconductors are rich in terms of holes. When p-type and n-type semiconductors make contact with each other, p

-n junction, which is the fundamental of solar cell, is created. The p-n junction supply electronic asymmetry in semiconductors to separate charges for energy conversion. This asymmetric structure causes the flow of electrons from p-type to n-type semiconductor and diffusion of holes from n-type to p-type. In general sense, electrons and holes flow from higher amount region to lower amount region, however, leaving electrons from n type side and leaving holes from p type side create charge imbalance and form exposed positive charges at n side and negative charges at p side. An electric field is presented between p and n sides due to the exposed charges which tend to behave oppositely to natural diffusion event. The region of forming electric field is called as depletion region which tries to keep holes in p-type region and electrons in n-type region. These solar systems can reach equilibrium condition when it has only one Fermi level. Rearrangement of the conduction bands and valence bands makes the energy of Fermi level same for p and n side and this phenomenon is known as band bending. Figure 2.6 illustrates the p-n junction, depletion (or transition) region and band bending. When the bias is applied on junction, current flows from p side to n side [27-28].

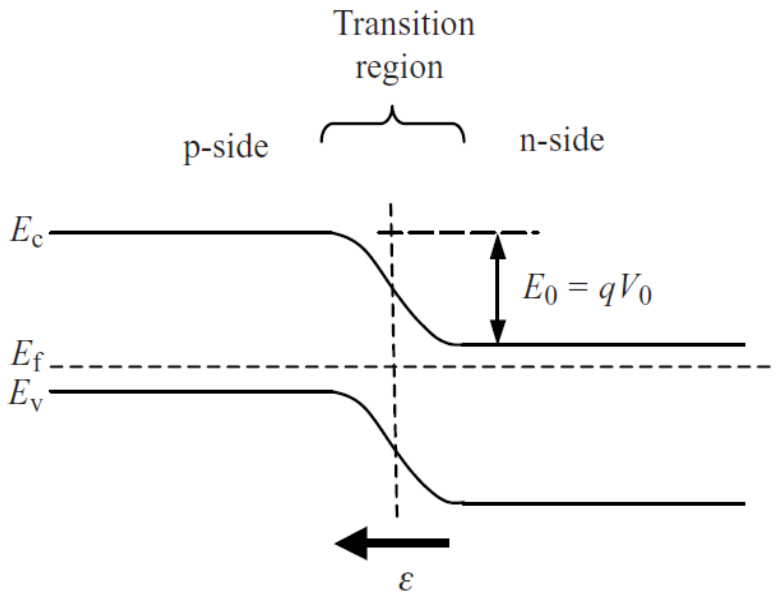

Figure 2.6 Band configurations after p-n junction [26].

2.1.4. Absorption of Light and Recombination Losses

Generation is a process of creation of free carriers with energy of light. When incident light hits the semiconductor, it can be reflected or transmitted through the semiconductor as lost mechanisms. Photons are transmitted or reflected, if they have lower energy than band gap energy. On the other hand, third process, absorption of incident light generates separated electron-hole pairs in semiconductor which is the principle of working mechanism of solar cells. Photons having larger energy than band gap energy are captured by the electrons at valence band of semiconductor. These electrons excited to unoccupied higher energy level (conduction band) and leave holes in the valence band.

Carrier generation is created by band to band transitions generally by optical absorption. Band to band transition can be observed in two ways according to band locations in crystal momentum. In direct band gap semiconductors, valence band and conduction band are

located at the same wave vector. On the other hand, minimum energy of conduction band and maximum energy of valence band are at different values of crystal momentum in indirect band gap semiconductors (Figure 2.7). Although only photon energy is enough to excite electrons to higher energy levels for direct band gaps, due to low momentum of it, photons cannot be sufficient to electron excitation in indirect band gap semiconductors. For indirect band gaps, a second particle which is referred as phonon involve in two step processes required for electrons to reach conduction band. Phonons have small energy and large momentum which is contrary to the properties of photons. Electrons primarily reach to minimum energy level of conduction band with photon absorption, then, change the wave vector with phonon emission and absorption. For indirect band gap semiconductors, large thickness should be provided to increase the absorption amount of light (due to the low value absorption constant), while there is no thickness requirement for the indirect band gap semiconductors, such as GaAs.

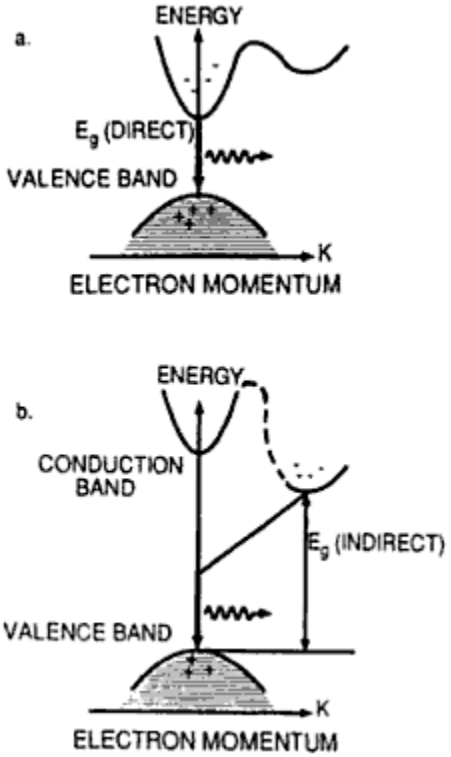

Figure 2.7 Direct (a) and indirect (b) band gap structures [29].

Also, different absorption processes can be observed in semiconductors. Occurrence of two step process in direct band gap semiconductors can be one of them when the condition of high photon energy. Second one is the excitation of the electrons at conduction band which is performed simultaneously with band to band transition due to the excess amount of carrier concentration which is called free carrier absorption. These processes do not create electron-hole pairs, on the other hand; they can be important for the cases of high-dopant impurity and strong illumination [24, 25, 28].

Electrons which exist in conduction band are at meta-stable state after separation of electrons from holes. These electrons are in tendency to go to lower energy levels to decrease their energies. They generally stabilize themselves recombining with holes at valence band which is called recombination process. Recombination processes can be

observed at bulk or surface state and it generally occurs due to charge energy inbalances. Processes can be generally classified as band to band transition loss, Auger recombination, recombination through defect levels and recombination from surface states (Figure 2.8).

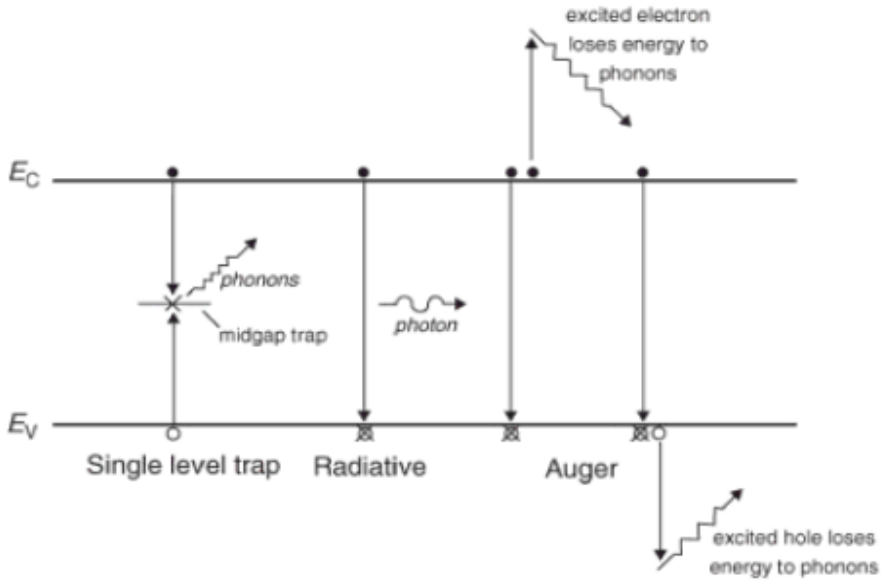

Figure 2.8 Potential recombination losses in semiconductors [30].

Band to band transition is commonly referred as radiative recombination and occurred unavoidably. Radiative recombination is just the opposite of the absorption of light which is returning of the excited electrons to their original states in valence band. Radiative recombination is observed mostly in direct band gap semiconductors due to only one step process. For indirect semiconductors, radiative recombination is very low, therefore it can be neglected. Auger effect which is another unavoidable recombination process is the interaction of holes with holes or electrons with electrons. Interaction between the same carriers causes a decrease in the energy of one carrier and an increase in the energy of other carrier with an amount of band gap of semiconductor. Then, excess energy is emitted by phonons. Auger recombination is faced for the systems which have low band gap and/or heavy doping.

Recombination via defect levels is mostly encountered at typical solar cells which directly depend on semiconducting material production and it can be minimized with changing some process parameters. Impurities in crystal or defects in crystal structure are the reasons of this recombination and create additional energy level in energy band gap. These levels enable the electrons to come back to valence state in two step process which is the relaxation of electron in conduction band to defect level and then from defect level to valence band. This recombination strongly depends on the purity of the materials and position of defect level in the band gap.

Surfaces present different behavior from the bulk structure as these regions include more defects and unbounded atoms than bulk regions. These disorders create several trap states in energy band gap which decrease electron-hole reaching time and cause high recombination with defect level mechanism. Surface passivation is a way to decrease surface recombination by growing additional layer, which fasten the unbroken bonds, on top of semiconductor surface [24, 28, 30].

2.1.5. Carrier Transport

There is no current flow at equilibrium condition of typical p-n junction. Electrons and holes separate from each other with an extra energy which is supplied by incident sunlight. Movement of these free carriers occurs with the help of two contributions: electric field moves the carriers to minimize the electrostatic potential energy which is called drift current and the second one, concentration gradient moves the carriers to minimize the statistical potential energy which is known as diffusion currents. These current terms form the transport equations which govern the electron (J_n) and hole (J_p) current density. Equations are given by:

$$J_n = q\mu_n n\varepsilon + qD_n\nabla_n \qquad \text{Eq. [2.2]}$$

$$J_p = q\mu_p p\varepsilon - qD_p\nabla_p \qquad \text{Eq. [2.3]}$$

μ_n and μ_p express electron and hole mobilities, D_n and D_p define electron and hole diffusion coefficients, ε is electric field and q is the elementary charge in these equations. First term of the equation refers to drift current and second one expresses the diffusion current. Drift current is directly affected by mobility term which changes with the density, temperature and electric field strength of the dopants. When dopant and impurity amounts increase, mobility of electrons and holes decreases due to enhancing of scattering events. Also high temperature and electric field decrease the time for the collision, hence the mobility decreases [24].

2.1.6. Solar Cell Output Parameters

Basically, solar cells convert the sunlight directly to the electricity with diode mechanism. When the light shines on the cell, cell tends to produce power. Current (I) - voltage (V) curve which represents the electrical output characteristic is the fundamental measurement for solar cell characterization. I-V measurements include many important parameters of solar cells such as short circuit current, open circuit voltage, fill factor and especially efficiency (Figure 2.9). Maximum power is calculated by the multiplication of all current values with corresponding voltage values. Obtained maximum value is maximum power and the data of current and voltage at maximum power is shown with I_{mp} and V_{mp}.

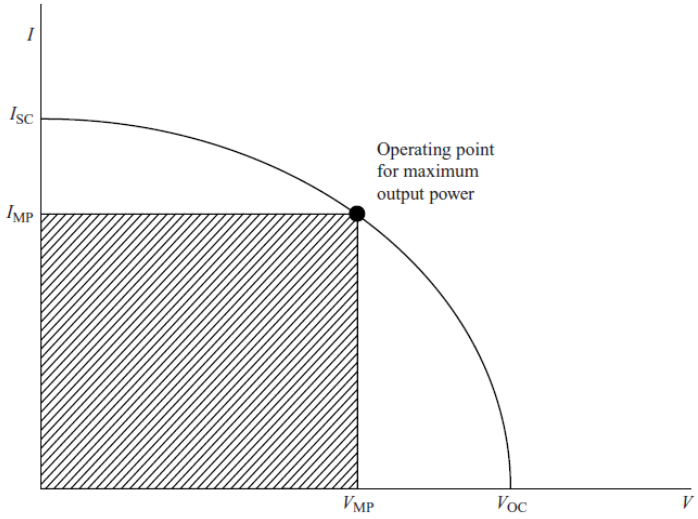

Figure 2.9 Outputs of solar cell characterizations [26].

Short circuit current (I_{sc}) is the current when the zero voltage passes through the cell at short circuit condition. Short circuit current is equal to the light generated current which is the largest current drawn from the cell. I_{sc} totally depends on the photon collection probability of cells, optical properties, spectrum of incident light and number of photons which are trapped by the cell. It is also directly related to the cell area, therefore; generally current density (J_{sc}), which is the current per area, is referred instead of current. Open circuit voltage (V_{oc}) is another important term. V_{oc}, which is the maximum voltage, occurs when the net current is zero. Open circuit voltage value is affected by recombination processes. Third parameter is the fill factor (FF) which defines the measure of squareness of the I-V curve. It also expresses the ratio of obtained maximum power to maximum obtainable power from cell.

$$FF = \frac{V_{mp} I_{mp}}{V_{oc} I_{sc}}$$

Eq. [2.4]

Shape of the I-V curves deviate from square shape due to the effect of parasitic resistances. Shunt (R_{sh}) and series (R_s) resistances are effective in solar cells and they reduce the fill factor and cell efficiency. Bulk and contact resistances are the reason of high series resistance. In addition, manufacturing defects are the reason of shunt resistances. These defects create alternative ways to flow of current and this decreases the shunt resistance of the cell. They are shown in Figure 2.10. To reach the square shape, R_s slope should go to zero and R_{sh} slope should go to infinity.

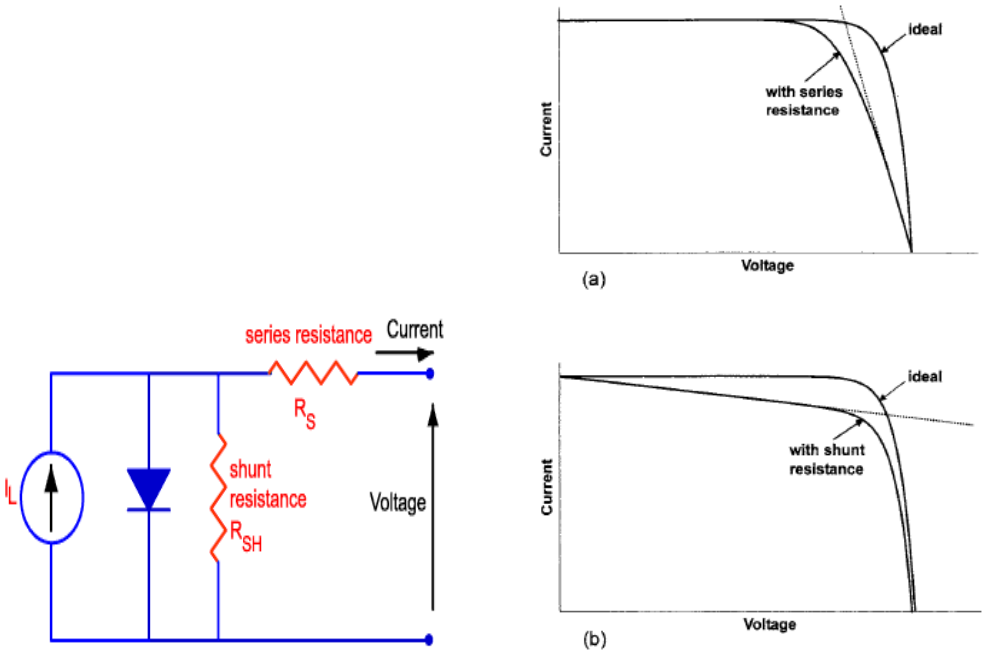

Figure 2.10 Shunt and series resistance [23, 31].

Final parameter which is obtained from I-V curve is efficiency (η). It is mostly used term to compare the photovoltaic performances of cells. It is the ratio of the output energy to the input energy (Eq. 2.5). Efficiency measurements are performed at standard AM 1.5 sunlight condition in order to compare devices with each other.

$$\eta = \frac{P_{max}}{P_{in}} = \frac{V_{mp} I_{mp}}{P_{in}} \qquad \text{Eq. [2.5]}$$

Quantum efficiency (QE) is another term for cell characterization. It is the ratio of the number of collected photons to the incident energy on the cell and it is given as a function of wavelength. Quantum efficiency measurement is performed using a xenon lamp coupled to a monochromator. This measurement technique gives some results about maximum absorbing point of dye molecules, light harvesting efficiency, electron injection efficiency and electron collection efficiency. Quantum efficiency (QE) curve is tending to square shape for the condition of minimum recombination processes Incident photon to current efficiency (IPCE) is another term which neglects the losses in transmitted and reflected photons. Therefore, to understand the cell performance, IPCE measurements give more sensible and reliable data when compared to quantum efficiency (Figure 2.11). Because, QE considers transmitted, reflected and absorbing photons; however, transmitted and reflected photons can be thought as direct loss for the solar cells [2, 22, 23, 31].

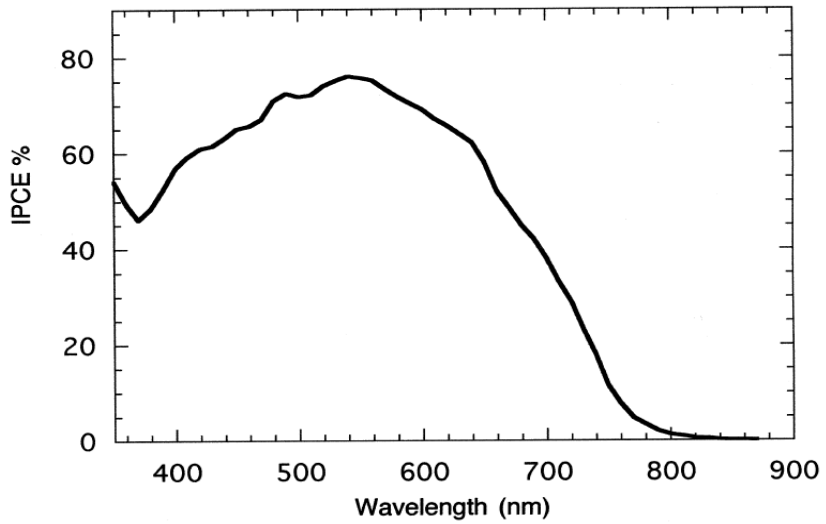

Figure 2.11 Schematic incident to photon conversion efficiency graph [2].

2.2. Types of Solar Cells

Solar cells are classified into four generations. Generations can be differentiated by the mechanisms of conversion. In the following parts, types of solar cells are explained in a detail manner.

2.2.1. Crystalline Silicon Solar Cells

Silicon possesses many interesting properties among the alternatives as an elemental semiconductor. High stability, advance chemical, optical and electronic properties make silicon the first choice for microelectronic industry. Also, success in applications directs the investments to crystalline silicon solar cell technology. These conditions present the 80% of the photovoltaic industry market occupied by crystalline silicon. Crystalline silicon solar cells can be divided as poly and single crystalline silicon.

Silicon solar cell is prepared from slicing of the large Si ingots. While poly-crystalline Si is produced direct casting of molten silicon, single crystalline Si ingots, which are obtained using a much complicated process, are fabricated by Czochralski crystal growth. Si ingots are generated by the pulling of a seed crystal on molten silicon at well optimized speed and temperature conditions. Crystal size and amount of impurity are the main factors affecting the cell performance, since defect recombinations are related to the impurity amount and current transport is related to crystal size. Thus, these terms are very crucial in cell performance and cost.

Silicon has also 1.1 eV band gap and this value is so close to the theoretical limiting efficiency in AM1.5 condition (1.5 eV). However, silicon is a weakly absorbing material and absorption should be increased by the thicker wafers with considering electron transport. To create the p-n junction, boron is added to molten silicon at impurity level; therefore starting material is p-type 300-500 μm thick wafers. Dopant amount of boron is determined by considering optimum diffusion length. Then these wafers are etched from smooth surface to rough surface. Phosphorus, as n-type emitter, is diffused on p-type silicon wafer as a very thin layer (0.5 μm) for high light passing. Also, series sheet resistance decreases with increase in dopant amount of phosphorus. After that, back and rear sides of the wafer are

cleaned from phosphorus by etching. Front surface is coated by the anti-reflecting coatings at 80-100 nm which can be tantalum oxide, titanium oxide and silicon nitride. By following, metal contacts (silver) are screen printed on front and rear side. Finally, cell is fired for good adhesion of anti-reflecting coating and metal contacts. Figure 2.12 represents the final architecture of the Si solar cell [24, 25, 27, 28].

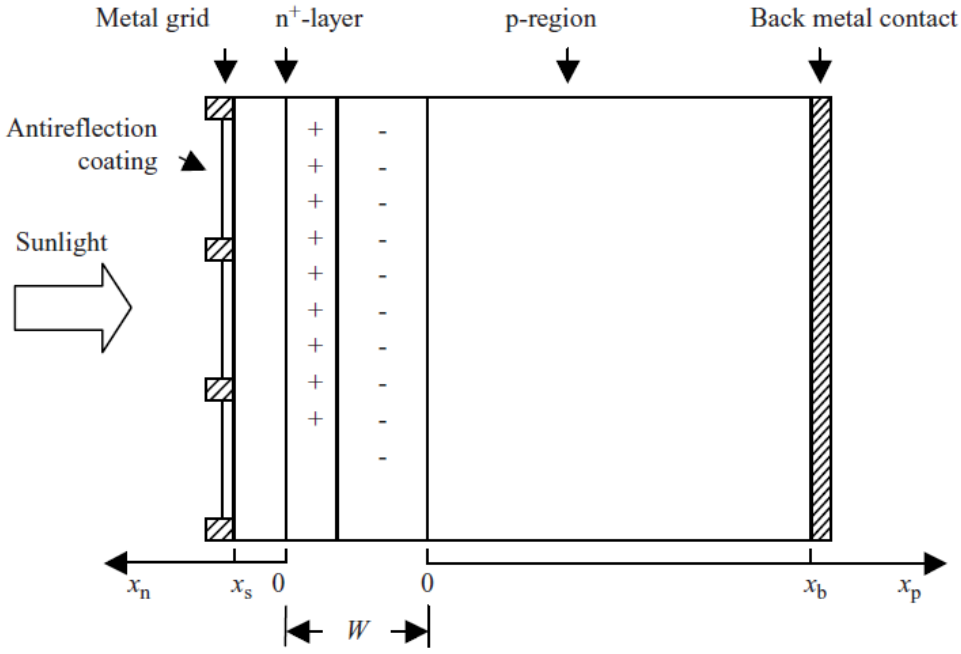

Figure 2.12 Cross-section image of typical silicon solar cell [26].

Silicon solar cells have been shown a marked improvement in efficiency and cost per watt values since the first use in market. Today, laboratory efficiencies are so close to the theoretical limitations as 27%. And the cost/watt of the silicon panels has been dropped to 1.2 USD from very high prices. Also, companies give 20 years warranties for service time for their products. Despite these impressive factors, panel prices are still very high compared to other solar cell technologies and companies have not reached to laboratory efficiencies in outdoor usage conditions, because of the fact that silicon solar cells should take sunlight at high light intensities and specific angle depending on the place.

2.2.2. Gallium Arsenide Solar Cells

Group III-V semiconductors have large potential in optoelectronic applications. Gallium arsenide (GaAs) is the most suitable semiconductor in III-V group for solar cell energy conversion with 26% efficiency. Energy band gap of GaAs is too near to optimum solar spectrum as 1.42 eV and it has also direct band gap structure. Therefore, GaAs solar cells strongly absorb the above wavelength of its band gap and there is not any thickness restriction due to high absorption. This nature makes GaAs popular for such complicated applications like space and electronic. Temperature and radiation, which both affect the cell performance adversely, resistances of GaAs solar cells are better than silicon solar cells.

Although GaAs has superior properties, their production costs are too much and it has already a maturing topic that Ga and As are both toxic materials. These factors limit the usage of GaAs in only space applications. Manufacturing of GaAs cells are performed by n and p type dopants. Silicon replacement with gallium atoms for n type and carbon substitution with Arsenic for p-type doping are preferred. Liquid phase epitaxy (LPE), molecular beam epitaxy (MPE) and metal-organic chemical vapour deposition (MOCVD) are mostly used in GaAs growth due to accurate composition and thickness control [28].

2.2.3. Thin Film Solar Cells

Thin film solar cells have many superior properties when compared to crystalline silicon solar cells such as low cost, robust and stability. Also, sunlight absorption of thin films is higher than crystalline silicon, therefore, there is no restriction in thickness and charge transportation. Non-crystalline silicon, II-VI binary compounds and I-III-VI ternary compounds can be used in thin film solar cell applications.

2.2.3.1. Amorphous Silicon Solar Cells

Amorphous Si (α-Si) solar cell has been used in daily life for 30 years as calculators. Advantages in production, price, performance and flexibility of α-Si make it popular in thin film solar cells. However, amorphous silicon suffers from the arrangement of atoms. In amorphous structure, long range order of atoms is not observed thus, distance between the atoms changes according to atom positions. Differences in distances create many dangling bonds as positively or negatively charged or neutral. Charged bonds directly affect the band energy diagram creating different energy level (recombination centers). Due to the high defect amount, p-n junction is not performed with dopants. Therefore, hydrogen passivation is performed to unbounded atoms to decrease the defect concentration of amorphous Si. Hydrogen atoms make bond with free neutral electrons in passivation. Although, passivation allows to doping of α-Si, defect states already remain in band gap and directly affect the charge transport. Moreover, defect density increases again with dopants. Therefore, p-i-n structure is used for amorphous silicon instead of p-n junction. An undoped α-Si intrinsic layer is coated between p and n doped α-Si in p-i-n junction.

Undoped silicon layer increases the thickness of cell, therefore it supplies an increase in photon absorption, also it helps the charge separation with drift mechanism creating an electric field. Sequentially, p doped, undoped and n doped amorphous silicons are deposited with variety of techniques, such as; plasma deposition of silane (SiH_4), sputtering and 'hot wire'. Despite the observed 13% efficiency, these cells suffer from Staebler-Wronski Effect which is about the destruction of α-Si:H with induced light [24, 26, 28].

2.2.3.2. Copper Indium Diselenide Solar Cells and Copper Indium Gallium Diselenide Solar Cells

$CuInSe_2$ (CIS) has a direct band gap nature which is nearly 1.0 eV. CIS solar cells took attention at 70's due to the fact that it has highest optical absorption in alternative semiconductors and it can be used at p and n type semiconductors. p-n homojunction type of these solar cells suffer from low efficiencies due to very high surface recombination and series resistances. Therefore, researchers directed two ways to increase efficiency: making heterojunction cells with CdS and adding Ga to CIS (CIGS).

Copper indium gallium diselenide solar cells are composed of solid solution of copper indium diselenide and copper gallium diselenide which belong to I-III-V group of periodic table. CIGS solar cells have cholcopyrite structure with tetrahedrally bonded nature. Its band gap changes between 1-1.7 eV according to the ratio of In/Ga. Due to the direct band gap nature, small thickness (2.5 μm) is enough for good photovoltaic performance. Cells are constructed

using the following procedure. CIGS is deposited on Mo coated soda lime glass where Mo is used for back metal contact. CIGS deposition is performed by co-deposition of copper, indium, gallium and selenium. And then, the structure is annealed under selenium vapour to selenization. Sequentially, CdS (for heterojunction) and ZnO (to increase conductivity) are coated on CIGS layer. CIGS is doped with p type defects and CdS is n-type to create heterojunction. CIGS cells are reached to 20% efficiency in laboratory conditions and now many companies start to produce a solar module for daily usage [24, 26, 28].

2.2.3.3. Cadmium Telluride Solar Cells

Cd-Te is the semiconductor from the II-VI group of periodic table with 1.45 eV direct band gap. Band gap value is so close to the band energy of theoretical maximum photo conversion value and CdTe has very high optical absorption. It can also be doped by both p and n type materials. Configuration of the cell is formed by the junction of p-CdTe with n-CdS. Most suitable technique for the materials deposition is sputtering moreover; many deposition techniques can be applicable for the depositions such as spray pyrolysis and chemical vapour deposition. Researchers reached to 18.3%, which was very far from the theoretical limit (29%). Also, CdTe own superior stability and is robust to outdoor conditions. However, the problems about tellurium supply and health problems offered by cadmium blocked the research and investment to CdTe [28].

2.3. Dye Sensitized Solar Cells

Starting point of the research at topic of dye-sensitized solar cells (DSSC) stand the sensitization of wide band gap semiconductors using dye molecules which was firstly observed by Moser doing research in field of photography. When the erythrosine dye is present on silver plates, an increase at photoelectric effect was observed by Moser at 19th century. After that, Gerisher and Memming did some experiments to understand electron transfer process which was performed by immersing ZnO and SnO_2 into redox electrolyte. Although DSSC has a long history, its conversion efficiency was limited to 1% up to 1990s due to weak absorption of sunlight. Then, Gratzel was conducted a milestone research and the efficiency hoped to 7% and then to 10%. Gratzel's research was about to increase the surface area of photoanode to enhance the amount of adsorbed dye molecules on photoanode. And then changing the chemical bonding behavior of the sensitizer, second hoping in efficiency value was realized. Architecture of conventional dye sensitized solar cells and components of the solar cell are shown in Figure 2.13.

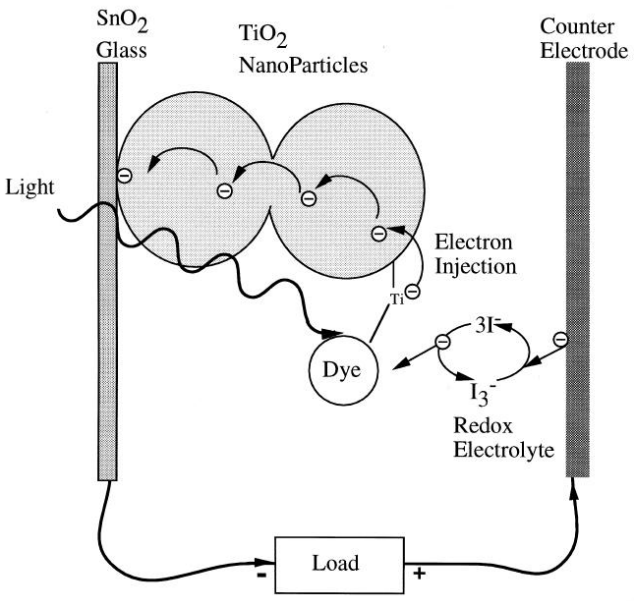

Figure 2.13 Structure and layers of conventional dye sensitized solar cell [2].

A structure is build between two transparent conductive oxide (TCO) glass substrates like a sandwich.TCO layers should not block the sunlight and should conduct the electricity. TCO layer is coated with a highly porous wide band gap semiconductor oxide and then, thick mesoporous photoanode layer is coated with photosensitizer. Photoanode surface area should be as high as possible to adsorb more sensitizer. Also, sensitizer should have HOMO and LUMO states for the excitation with photon absorption. Platinum or active carbon coating is made on counter electrode to catalyze the reactions. TCO glasses are sealed with the hot melt polymers or glass frits to prevent the leaking of liquid electrolyte outside the cell. Finally, the region between the sensitizer and Pt is filled with redox electrolyte couple for transferring carriers between the photoanode and counter electrode. Although various electrolyte species can be used in dye sensitized solar cells, solvent iodide/triiodide couple is the most preferred electrolyte for high efficiency [21, 32].

2.3.1. Main Components of Dye Sensitized Solar Cells

Main components of the dye sensitized solar cells are explained in the sequence of candidate materials, main requirements and performances in the following parts.

2.3.1.1. Transparent and Conducting Oxide (TCO) Substrates

TCO substrates have drawn attention to many opto-electronic applications due to their unique properties of low sheet resistance and high optical transparency at visible and near infrared region which makes also the most suitable substrate for DSSCs. Low resistance of TCO increases the number of excited electrons which can complete the circuit and high transparency provides that most of the photons reach the photoanode penetrating the substrate. In addition to the mentioned properties of TCO substrates, stability to the chemicals and durability to the high temperature sintering processes also supply advantages in using as a substrate of DSSC. Also glass substrates prevent the cell from the oxygen and water penetration in it. On the other hand, weight of glasses restricts the application areas of DSSC.

Impurity doped ZnO and the compounds between In_2O_3, ZnO, SnO_2, CdO are the main members of the TCO family. Table 2.1 shows different TCO materials and their electrical performances. Their optical performances change with electrical resistance, in other words, when sheet resistance value decreases, transparency of the glasses decreases. 80% in transparency is accepted in most of the DSSC applications. In this family, ITO (10% SnO_2 and 90% In_2O_3) stands out amongst the others with highly low resistance and high transparency. However, ITO is not the best candidate for DSSC applications. Because, photoanode sintering is performed at nearly 450-500^0 C in open atmosphere and conductivity of ITO films drops dramatically over the temperature of 300^0 C due to the filling the vacancies of ITO with oxygen. And also ITO does not make good contact with photoanode which is generally peeled off on ITO surface. Currently, most of the DSSCs are constructed using FTO (F: SnO_2) glass substrates with 8-15 Ω/square resistance and 80% transmittance at 550 nm. Fluorine doping to SnO_2, which is occurred by the changing of oxygen with fluorine, heals the performance of both conductivity and transparency. FTO coating on glass substrates is performed generally by physical vapour deposition systems and sometimes some other deposition systems can also be used for FTO coating like spray pyrolysis. Nearly half of the total prices of solar cells come from FTO glass layers.

Table 2.1 Electrical performances of different TCO glasses [33].

TCO Materials	Sheet Resistance (ohm/sq)
SnO_2:F	8
SnO_2:Sb	20
In_2O_3:Sn	6
ZnO:F	5
ZnO:Al	3.8
Cd_2SnO_4	7.2
ZnO:Ga	3

Researchers have focused on to use different substrates due to high weight and fragility of glass in recent years. Conductive oxide deposited polymer substrates are the most attractive topic for many electronic applications as well as DSSC due to the low weight and flexibility of these polymeric substrates. ITO-coated polyethyleneterephalate (PET) and ITO-coated polyethyleneaphthalate(PEN) are the well known examples of polymer substrates. However, polymeric substrates suffer from low temperature resistance, low electrical conductivity, and they are permeable to humidity. Second performance about substrates is that changing glass with thin metallic substrates like stainless steel and titanium. Metallic substrates supply good corrosion resistance against electrolyte while light transmittance is serious drawback [21, 32].

2.3.1.2. Mesoporous Photoanode

Wide band gap metal oxide semiconductors are generally preferred for the photoelectrode layer in DSSCs. Band gap of semiconductors should be larger than 3 eV for the transparency of mesoporous anode which, therefore, covers almost whole solar spectrum. Metal oxide should be produced at the structure of well interconnected colloidal nanoparticles which supply high porosity and large surface area. Large surface area is the main dilemma for high efficiency DSSCs because; the amount of absorbed dye molecules directly depends on the surface area of photoanode. Porous structure of mesoporous anode provides capillary action to electrolyte between the nanoparticles which regulate the total

current flow inside the cell. The elevation of DSSC at 90's stems from using large surface area structure and highly porous titania molecules in cells. Chemical stability, high electron mobility and high adhesion to TCO can be other requests from this layer. SnO_2, ZnO, Nb_2O_5, ZrO_2 and TiO_2 are the potential metal oxides which are examined in DSSC structures.

In candidates, highest efficiency is obtained by TiO_2 and thus, many researches in topic of DSSC realized the production using TiO_2. Porous structure and network between the titania particles is presented in Figure 2.14. Conduction band level of TiO_2 is slightly lower from the excited energy level of the dye molecules which supplies the efficient electron injection. And also, dielectric structure prevents the recombination of excited dye molecules which are attached on the surface of TiO_2 before reacting with redox electrolyte. It is also known that titanium dioxide nanoparticles are used mainly in paint industry and therefore, it can be obtainable at vast amounts.

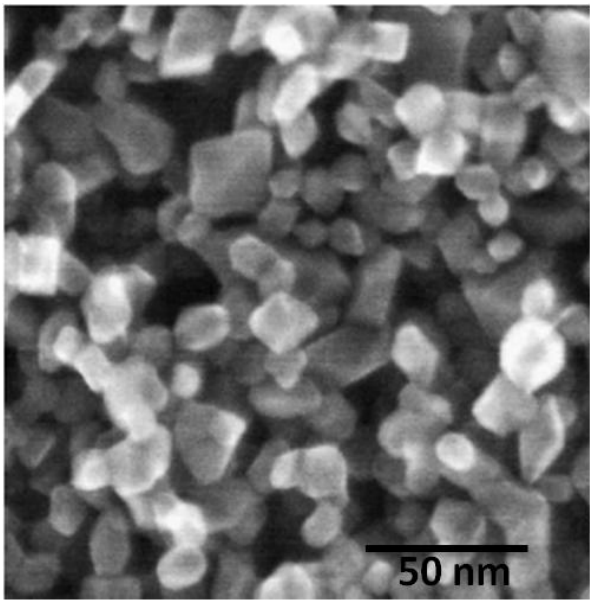

Figure 2.14 Mesoporous photoanode [34].

TiO_2 nanoparticles can be obtainable at three different crystal structures, brookite, rutile and anatase. In these forms, brookite phase has no interest in DSSC applications due to the difficulties in its production. Rutile and anatase are the common phases with 3 eV and 3.2 eV energy band gaps, respectively.

Rutile is the stable phase of titania, and possibility of rutile formation is increased at high temperatures (above 550°C) therefore the sintering temperature of titania is kept around 450-500°C to ensure anatase phase in the material. Prevailing properties of anatase is larger open circuit voltage due to 0.2 eV differences, more dye loading capacity and higher electron diffusion coefficient.

The performance of titanium dioxide photoanode layer can be improved using some modifications as stated below:

- $TiCl_4$ treatment is applied to TiO_2 surfaces to increase the density of specific binding sites (for more dye absorption),

- The use of TiO_2 nanotubes and nanowires instead of nanoparticles due to faster electron percolation nature,

- To add large TiO_2 nanoparticles (200-400 nm) on traditional layer to increase the amount of light absorbed in the cell,

- Covering the titania nanoparticles with different oxides (core-shell structure) to increase the electron path length.

While rutile is the thermodynamically stable state at macroscopic state, stability returns to anatase at microscopic state. Anatase phase is more preferable when the particle size is between 10-20 nm [35]. Also low particle size satisfies the large surface area dilemma. Therefore, to reach the required sizes, synthesis and coating methods of titania nanoparticles is significant. Sol-gel techniques are the common routes for the synthesis of anatase titania nanoparticles. An example is as follows;

- Synthesis starts up with hydrolysis of titanium (IV) alkoxides. R is an alkyl; commonly an ethyl, butyl or isopropyl group. Amorphous precipitates are formed with reaction.

$$Ti(OR)_4 + 2H_2O \rightarrow TiO_2 + 4ROH$$

Eq. [2.6]

- To produce sol, amorphous precipitates are peptisized in acid or alkaline water,

- Hydrothermal growth of the sol is performed in autoclave,

- Titania nanoparticles are dispersed by sonication,

- Concentration of these nanoparticles is done using evaporator (45^0 C, 30 mbar).

Titania paste production is performed by dispersing of nanoparticles into viscous fluids like polyethylene glycol or terpineol and adding stabilizers into this dispersion to prevent agglomeration. Triton-X 100, tetramethylammonium hydroxide and ethyl cellulose are the common surfactants. Viscosity of paste plays an important role to produce crack free titanium dioxide coatings, because coatings produced using nonhomogenous and low or high viscosity pastes are more probable to peel off the substrate. Therefore, the amounts of the additives are crucial from the point of coating quality. Then these pastes are coated on the glass surfaces by doctor blading, tape casting or screen printing. All of these techniques are cheap and not require any complex machine systems and conditions. Photoanode side is completed with a sintering procedure.

Many performances have been realized on photoanode to enhance the quality of dye sensitized solar cells. Different structures of titania, different types of photoanodes and some treatments have been tried and efficiency of the cells increases year by year by the help of them. Record efficiency is 11.4% where nanoparticles of anatase phase of titania were used in the production of this cell [21, 32, 36, 37].

2.3.1.3. Sensitizer

Sensitizer is the main component of dye sensitized solar cells. Primarily, it should absorb all solar spectrum from UV to near IR region and create electron-hole pairs by electron excitation. Then, it also should carry these excited electrons to conduction band of the photoanode with high quantum yield. Another important point is that sensitizer should be well connected with semiconductor for high electron injection. Positions of the HOMO (highest occupied molecular orbital) and LUMO (lowest unoccupied molecular orbital) level should match well with semiconductor and electrolyte to increase the number of excited electrons. To reach the high efficiency, LUMO level of the sensitizer should be higher than the conduction band of semiconductor to inject electrons easily and HOMO level of the sensitizer should be aligned with redox potential of the electrolyte to regenerate the oxidized dye molecules more effectively. Good thermal stability, good chemical stability and long life time (10^8 cycles, nearly 20 years) are the other common desires from the sensitizers. Table 2.2 shows the photovoltaic performances of devices which are produced using different dye absorbing materials.

Table 2.2 Efficiency values of cells produced using different dye molecules [32].

Dye Type	Efficiency (%)
N3	11.03
N719	11.18
Black Dye	11.10
Z910	10.20
K77	9.0 (IL elec.)
C106	11.4
D205	7.2 (IL elec.)

Due to the fact that, metal-organic dyes encounter the above conditions at maximum level, these dyes are the most preferred ones. Especially, Polypyridyl complex of ruthenium with one or more carboxylic acid groups becomes the main product and they are used to develop other dyes. Generally, carboxyl group is used to provide effective interaction of dye molecules with mesoporous photoanode. Furthermore, dramatic increase in efficiency is obtained with metal to ligand charge transfer (MLCT) in the case of N3 dye. MLCT changes the position of electron from Ru to the p* orbital which increases the electron injection rate to the conduction band of titania. After that, N-719 dye is obtained by changing the N3 bond structure. N719 shifts the conduction band of titania positively and increase the open circuit voltage of the cell. Although an increase in efficiency was observed with N719 dye, both of N3 and N719 cannot absorb the wavelengths above 600 nm of solar spectrum. Therefore, another dye was produced, N749 or black dye which provides the absorption at longer wavelengths and this means more current density. Z907 is another dye studied to solve the stability problem of the above dyes at temperature of nearly 80 ^{0}C. Z907 dye does not show any degradation for 1000 hours at 80 ^{0}C. K and C types of dyes are the commonly used other sensitizers. Their focus point is to increase the number of dye molecules sticking on the photoanode (high molar extinction coefficient) per unit length. These dyes are produced to face the problems encountered with ionic liquids. Because, photoanode thickness in the case of ionic liquids should be lower from the photoanode thicknesses when other electrolytes are used, due to the electron transfer rate deficiency of the ionic liquids. Also, many researchers studied the use of metal free organic dyes and quantum dots as sensitizers for the solar cells to decrease the dependence to rear earth metal ruthenium [12, 21, 32, 34]. Bond structure of different dye molecules are presented in Figure 2.15.

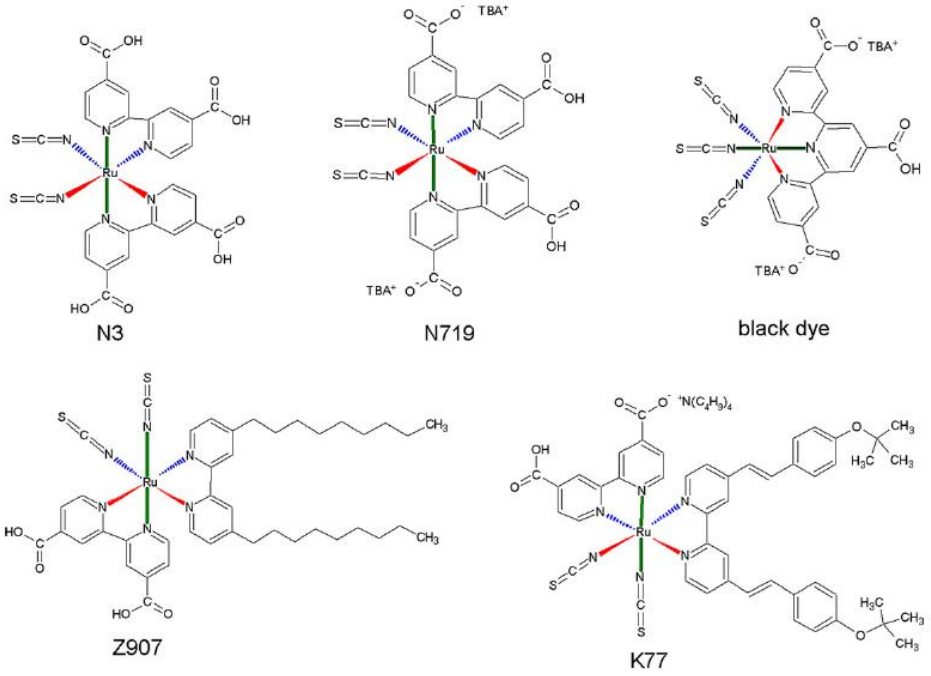

Figure 2.15 Structure of dye molecules [32].

2.3.1.4. Electrolyte

Electrolyte which is the next layer to the dye molecules provides the electron transportation between working and counter electrodes. The oxidized dye molecules should return to their original states using electrons from the electrolyte. Therefore, electrolyte should have some criteria to obtain better performance from the cell. Primarily, electrolyte does not react with excited dye molecules before they are injected into semiconductor. Then, electrolyte should react with oxidized dye molecules before they are reduced from the other dye molecules. To supply the above conditions, redox potential of electrolyte should be higher than the HOMO level of dye molecules and should be lower than the LUMO state of the semiconductor. Also, it should have low viscosity and high dielectric properties for high efficiency and low vapour pressure, high boiling point for the robustness of the cell.

Although many mediators have been studied for the electrolyte layer, solvent base iodide-triiodide electrolyte is the widely used and highest efficiency one. Iodide-triiodide is the redox couple of the electrolyte and acetonitrile, valeronitrile, proponitrile and 3-methoxypropionitrile are used as an organic solvent. Organic solvents are sometimes supported by the ester compounds like propylene carbonate and ethylene carbonate. Li cations are mainly added to electrolyte to decrease the screening effect of the electrolyte due to its dark inherent. Therefore, it supplies an increase in short circuit current density. The fame of the solvent based iodide-triidoide electrolyte originates from the low viscosity nature. Low viscosity of electrolyte causes fast electron injection to dye molecules and high efficiency. Although solvent based electrolytes have some superior properties, corrosive, low boiling point and high vapour pressure characteristics make them unreliable for the outside applications and sometimes closed environmental operations. When the temperature reaches to boiling point of the electrolyte, electrolyte degrades the sealing material and finally it terminates the working of cell.

Many alternative systems have been tried to obtain better stabilities. Cobalt, bromine and copper redox couples were tried as electrolytes however, their efficiencies stayed too low compared to solvent ones. Solid electrolytes, quasi solid electrolytes and ionic liquids are the other electrolyte species which are used in solvent free cells. Therefore, they do not suffer from volatility problems. Since they are not viscous, they suffer from low electron transport and low efficiency. Inside the alternatives, ionic liquids are the most common challenge for the solvent based electrolytes with improved stability and close cell performance [9, 21, 32, 38–40].

2.3.1.5. Counter Electrode

Iodide ions oxidized to triiodide by reducing the dye cation are regenerated at the counter electrode by recombining with photoelectrons coming over the external load. Rate of this chemical reaction has to be very high and overpotentials which in turn lower the maximum photovoltage have to be prevented. For this purpose a catalyst is applied to counter electrode surface which is the interface between electrolyte and conducting oxide glass. Most common catalyst is platinium where gold and carbon also can be applied. Coating can be deposited by sputtering or evaporation resulting films of up to 100 nm. Pt coating can also be performed by thermal decomposition of H_2PtCl_6 or screen printing of the Pt paste. Alternatively carbon base products and conductive polymers are tested instead of Pt for the catalyst layer due to economical reasons and high photovoltaic performance expectations. Also some other designs are performed without using counter electrode layer which is called monolithic design [21, 37, 41, 42].

2.3.2. Working Mechanism of DSSC

Solar light and cell interactions create a sequence of reactions. These reactions start with absorption of the solar light by the dye molecules. The electrons are excited from HOMO level to LUMO level of dye molecules by the help of solar energy absorption. Excited electrons in dye molecules are injected to the conduction band of the photoanode. Injected electrons move from the mesoporous network to transparent conductive oxide and then they travel from the external circuit to counter electrode. Oxidized dye molecules come back to original state by the electron donation from electrolyte species. I^- anions are oxidized and converted to I_3^- anions to perform the electron donation. Finally, electrons which reach to counter electrode, realize the reduction reaction of electrolyte which is the back reaction from I_3^- to I^-. In the presence of catalyze species; this reaction occurs with high rate and high efficiency. Electrolyte mediator provides this cycle by giving and receiving electrons while the process lasted. All reactions are completed in nanosecond time ranges thus; low time does not permit any other reactions different than the ones mentioned. This event supplies to prevent any decrease in cell performance. S, S*, S^+ are the dye molecule, excited state of dye and dye cation and also I^- and I_3^- are the redox species [21, 32]. Figure 2.16 shows the layers, energy bands and sequential reactions and these reactions are following the sequence given below.

$$S + h\nu \rightarrow S^*$$

Eq. [2.7]

$$S^* \rightarrow S^+ + e^-$$

Eq. [2.8]

$$2S^+ + 3I^- \rightarrow 2S + I_3^-$$

Eq. [2.9]

$$I_3^- + 2e^- \rightarrow 3I^-$$

Eq. [2.10]

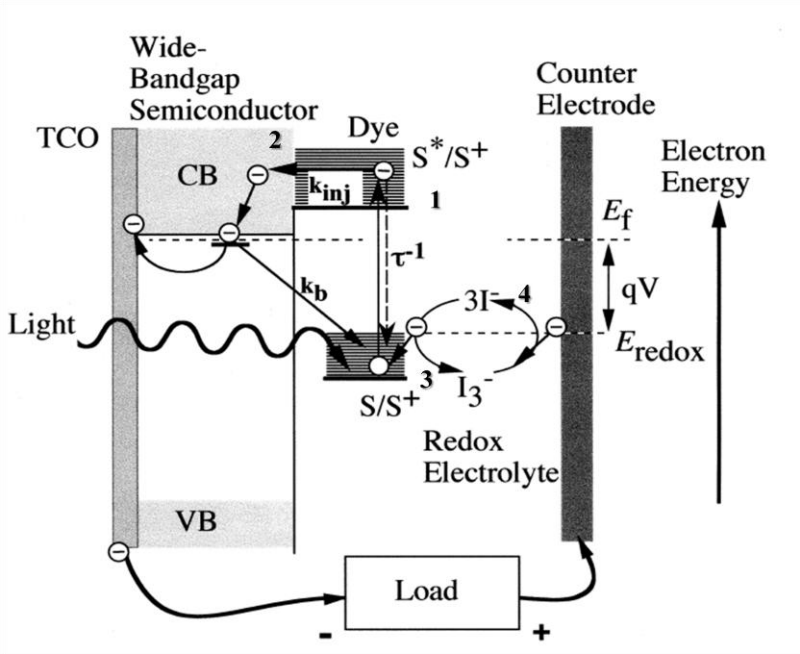

Figure 2.16 Working Mechanism of DSSC (Numbers 1 to 4 indicate the sequential reactions given in equations 2.7 to 2.10) [2].

2.3.3. Kinetic Processes in DSSCs

Since the increasing attention of dye sensitized solar cells with Gratzel idea, many performances have been carried out to understand the absorption, separation, transport and recombination processes in these cells. Because, DSSCs are differentiating from the classical solar cells at fundamental operations [43]. These differences are as follows:

- Light absorption and charge transport are occurred at the same material in classical solar cells, while these two operations are separated in different materials in DSSCs. Absorption process occurs at dye molecules and transport processes are realized in photoanode and electrolyte species.

- Second issue is the charge separation which is provided by the electric field in traditional solar cells. On the contrary, charges are separated in DSSCs due to kinetic events between the photoanode/dye/electrolyte interfaces.

- Electrons and holes are mobile in the same material for pn junction solar cells and this condition is dependent on the purity and defect free structures for good performance. On the other hand, electrons are mobile in photoanode and holes are mobile in electrolyte for the DSSCs. This mechanism restricts the recombination processes to only photoanode and electrolyte interfaces.

2.3.3.1. Light Absorption

Light absorption is provided by the dye molecules which are well-tuned with photoanode layer. Well-tuned structure is formed by the adsorption of dye molecules to TiO_2 surfaces. Carboxyl groups (COOH) of dye molecules are responsible for this adsorption with proton donation to photoanode. It is mentioned that light absorption occurs by excitation processes

in dye molecules. The excitation of Ru metal complexes is explained using metal to ligand charge transfer (MLCT). In MLCT, HOMO level of dye molecules are positioned near to metal particles and oppositely LUMO level of the dye molecules are positioned near ligands. In the excitation process, electrons are raised from HOMO to LUMO level. LUMO level is directly in contact with anchor carboxyl group and therefore very close to photoanode surface. This structure creates an overlap in electron wave function of LUMO level and conduction band of photoanode which is the primary reason of the fast electron transfer at the dye-photoanode interface [2, 27, 32, 36, 43].

2.3.3.2. Charge Separation

Charge separation is related to the processes of electron transfer from dye to photoanode and hole transfer from oxidized dye to electrolyte. This issue which determines the electron transfer quality depends on the energy level matching of the LUMO level of dye and conduction band level of TiO_2 photoanode. Electric field basically separates the charges in classical solar cells which is invalid for the nanoparticle electrode and electrolyte interaction. Small particle sizes do not allow creation of space charge layers inside the particles. Furthermore, there is no electric field present between the nanoparticles when investigated at macroscopic scale. In addition to above ones, electrolyte covers all nanoparticles and screens the existing electric fields (for the thick films) by decoupling the particles. Because of these reasons, band bending is not observed in DSSCs.

The major mechanism of charge separation is based on the energy level positions of LUMO level of dye and conduction band level of TiO_2 photoanode. LUMO level of dye molecules is above the conduction band level of TiO_2 and HOMO level of dye is below the chemical potential of the redox electrolyte and these settlings create driving force to separate charges. Another driving force comes from the entropy differences between the dye and photoanode. Electrons are tending to move in the direction of photoanode due to large number of delocalized states compared to dye molecules. Final mechanism is created by the anchor carboxyl group of dye molecules. To supply the adsorption of dye to photoanode, a photon is donated from anchor group to photoanode. Therefore, the photoanode surface is more positive and dye surface more negative which help to separate charges and reduce recombination [2, 27, 32, 36, 43].

2.3.3.3. Charge Transport

In DSSCs, electron movement in the photoanode and hole movement in the electrolyte constitute the charge transport. Both charge transport mechanisms play an important role for the solar cell operation and many points already wait explanation about fundamental questions.

2.3.3.3.1. Electron Transport in Mesoporous Photoanode

Mesoporous structure of photoanode which is also called network structure is mainly used as a large surface area substrate for dye molecules. Also, this structure supplies a real advantage for electron transport process which creates a path for the electrons to reach to the electrode. There is an unclear situation about the nature of the electron transfer whether the electrons are transported by the electric field or diffusion. As mentioned above, there is no electric field to drift the electrons in DSSC due to nano sized structure. When the excited electrons move from LUMO level of dye to conduction band of TiO_2, high electron concentration is created at positions near the dye molecules compared to photoanode - TCO interface. Due to the electron concentration gradient between the layers, electrons move with hopping actions one from the other interconnected nanoparticles by the diffusion mechanism to reach the TCO layer.

Diffusion coefficient distribution directly affects the electron diffusion performance. Furthermore, surface traps at different depths in photoanode are responsible for the electron hoping which is a related issue with distribution of diffusion coefficient. These trap regions are localized energy states and they are very important for transport mechanisms. They do not create any recombination in the bulk state, however, they create low photocurrent and photovoltage at surface transport processes. Diffusion coefficient is also affected from the quasi Fermi energy level under illumination. Illumination level is important in diffusion coefficient value which is very low for the low light condition due to only deep traps participate in transfer while for the high light intensity, transport occurs by the help of not only deep traps but also shallow traps. Therefore, conductivity of the photoanode increases with light level intensity due to the filling of trap states [2, 27, 32, 36, 43].

2.3.3.3.2. Ion Transport in Electrolyte

Redox electrolyte which is the main part of the cell has the property of hole conduction. Its mission starts with the regeneration of the oxidized dye molecules which remain after electron separation from the excited dye molecules [44]. The reactions are given below:

$$2S^{+} + 3I^{-} \rightarrow 2S + I_3^{-}$$

Eq. [2.11]

$$I_3^{-} + 2e^{-}(Pt) \rightarrow 3I^{-}$$

Eq. [2.12]

I_3^{-} is produced at the electrolyte and semiconductor interface and it moves from here to the counter electrode by diffusion mechanism. Furthermore, I^{-} is directed in opposite way from counter electrode to photoanode after it is produced. Therefore, redox electrolyte is similar to hole carriers in p-n junction solar cells. Electrolyte feeds the electrodes and maintains the redox potential with fast redox reactions. Even if it seems that only one reaction is happened in electrolyte, occurred reactions in electrolyte compose from successive charge transport and fast chemical reactions which are given below:

$$(I^{-} \rightarrow I + e^{-})\ x\ 2$$

Eq. [2.13]

$$2I \rightarrow I_2$$

Eq. [2.14]

$$I_2 + I^{-} \rightarrow I_3^{-}$$

Eq. [2.15]

2.3.3.4. Recombination

Generated electrons in photoanodes have the tendency to recombine with holes in a similar manner with classical solar cells but using different mechanisms. Mainly recombination is realized at defect sites of Si solar cells thus, high purity is extremely important. Due to different charge separation mechanisms of p-n junction solar cells and dye sensitized solar cells, DSSCs do not suffer from recombination which originates from large particle numbers and surface areas (grain boundaries). Also, DSSCs do not have any hole at photoanode.

Therefore, recombinations are totally different from silicon solar cells. Most important advantage of the DSSC is that both dye/TiO_2 and dye/electrolyte reactions are very fast.

Possible recombinations in DSSCs are given in Figure 2.17. Possible recombinations: excited electrons can recombine with Homo level dye molecules, injected electrons may recombine with dye molecules at HOMO level or holes in the electrolyte. Electron movement from LUMO to HOMO level is not encountered so much due to the low reaction rate. Reactions between dye and titania are one of the fastest reactions known. Recombination of the injected electrons with HOMO level dye molecules seems negligible for the most electrical models except the condition for the electron accumulation at photoanode. Most effective mechanism is the recombination of the injected electrons with holes in electrolyte due to fast reaction rate. However, this recombination also does not tend to go forward due to the kinetic reasons. Although main reaction (Eq. 2.12) is fast, it constitutes from three different reactions as given in Equations 2.16 to 2.18. Since electrons should pass through two interfaces (dye/electrolyte and dye/TiO_2) to realize recombination, 3rd reaction is a slow reaction and determines the overall reaction rate. Therefore, the rate of recombination is low due to the low electron diffusion rate in the third reaction [2, 27, 32, 36, 43].

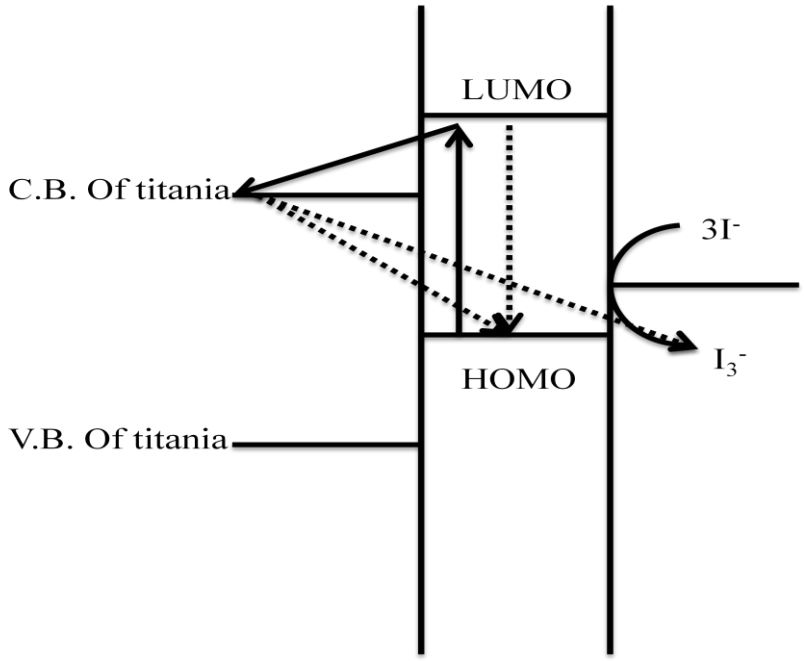

Figure 2.17 Possible recombination reactions in a DSSC.

$$I_3^- \rightarrow I_2 + I^- \text{ (1)}$$

Eq. [2.16]

$$I_2 + e^- \rightarrow I_2^- \text{ (2)}$$

Eq. [2.17]

$$2I_2^- \rightarrow I_3^- + I^- \text{ (3)}$$

Eq. [2.18]

2.3.4. Ionic Liquid Electrolytes for Dye Sensitized Solar Cells

It is known that all high performance DSSCs have been carried out using solvent based electrolytes which are prepared by mixing of iodine into a solvent (acetonitrile, valeronitrile, methoxypropionitrile etc.). On the contrary to high performance, solvent based electrolytes limit the usage of DSSCs in industrial applications. Problems in sealing of device and the volatility characteristics of solvent based electrolytes make them untrusting from the point of view of stability and life time. Many researchers work on some alternative electrolytes to compete with solvent-based ones in cell performance. Ionic liquids which are also known as molten salts are the most attractive alternatives to solvent-based electrolytes due to fairly good efficiency and high device stability. Although alkyl imidazolium salts, alkyl pyridinium salts and tri-alkyl methylsufonium salts are the well-known ionic liquids, especially, imidazolium based electrolytes have been widely used in dye sensitized solar cells [9, 40].

These solvent-free electrolytes contain ionic compounds which are formed from ions and ion pairs. They generally melt at room temperature and it means that their melting points are low. Other important advantages and properties of ionic liquids can be given as:

- High chemical stability
- High thermal stability
- Negligible vapour pressure
- Non-flammability
- Solubility with most organic and inorganic materials

The most important drawback of ionic liquids is the relatively high viscosity nature when compared to solvent-based ones. High viscosity nature of ionic liquids can be explained by high polarity and localized charge density on iodide. Also, viscosity of ionic liquids increases with the alkyl chain length of ionic liquid. Van der Waals interaction increases with chain length and therefore, viscosity of electrolyte increases. High viscosity nature causes low diffusion of redox ions. Although the minimum viscosity of ionic liquid is 10 times of the organic solvents and it is expected that diffusion rate becomes 10 times lower and their cell performances can compete with organic solvent ones. This situation is explained by another transport mechanism which is called as Grotthus type or non-diffusional hoping mechanism. In this mechanism, I_3^- ions move to the counter electrode with exchange reactions addition to the diffusion mechanism. Low diffusion rate occurred due to these electrolytes can be healed by increasing the amount of I_2 which in turn gives I_3^- ions. Decrease in viscosity and increase in conductivity are determined by the concentration I_3^- in the electrolyte. Several works in the literature show that short circuit current density increases up to saturation concentration of I_3^- and after that it decreases with increase in the concentration of I_3^-. Decrease in J_{sc} can be explained by the photon absorption of I_3^- and slow diffusion nature of it[21].

Second weak point of ionic liquids comes from the behavior of them against light intensity. While cell performance of solvent based electrolytes linearly enhances with increase in light intensity, ionic liquids shows restricted increase due to the low transport nature of I_3^- in ionic liquid. Another disadvantage of ionic liquids comes from the quantity of imidazolium iodide. If the concentration of imidazolium iodide is very high, this high amount of imidazolium ions reacts with excited dye molecules and causes quenching of dye molecules. 25% of dye molecules is exposed to quenching and this elicits a low cell performance. Below reaction shows the excited dye quenching:

$$D^*/TiO_2 + 2I^- \rightarrow D^-/TiO_2 + I_2^-$$

Eq. [2.19]

In the literature, many ionic liquids have been used to find alternative electrolytes to the solvent based electrolytes. Table 2.3 shows some studies about the ionic liquid electrolytes. 1-hexyl-3-methylimidazolium iodide (HMII), 1-ethyl-3-methylimidazolium iodide (EMII), 1,3-dimethylimidazolium iodide (DMII), 1-butyl-3-methylimidazolium iodide (BMII) and 1-propyl-3-methylimidazolium iodide (PMII) are the mostly used active ionic liquids. In the above active ionic liquids, PMII is one of the electrolytes commonly used due to its lowest viscosity and highest conductivity value at room temperature. The first approach is about to decrease viscosity by adding non-active ionic liquids. Non-active ionic liquids which mean electroinactive imidazoluim salts with various anions decrease the viscosity of pure PMII ionic liquid and increase the efficiency dramatically. For this issue, 1-ethyl-3-methylimidazolium triflate (EMITf), 1-ethyl-3-methylimidazolium thiocyanate (EMISCN), 1-ethyl-3-methylimidazolium dicyanamide (EMIDCN), 1-ethyl-3-methylimidazolium tricyanomethanide (EMITCM), 1-ethyl-3-methylimidazolium tetracyanoborate (EMIB$(CN)_4$) and 1-ethyl-3-methylimidazolium bis(trifluoromethanesulfonyl)imide (EMITFSI) are added into PMII to decrease viscosity and to increase the diffusion of ionic liquids. Second approach depends on the healing of PMII performance by adding some system regulator chemicals. These additives are 3-phenylpropionic acid, tert-butylpyridine, N-alkylbenzimidazoles, N-methylbenzimidazoles and guanidinium thiocyanate. Some of them show healing in open circuit voltage and some of them show healing in short circuit photocurrent [9, 21, 32].

Table 2.3 Photovoltaic performances of some different ionic liquids [9].

Ionic liquid	Efficiency (%)
DMHIII-EMIF2,3HF	2.1
PMII-EMISCN	7.0
PMII-EMIDCN	6.6
PMII-EMITCM	7.4
PMII-EMIBCN_4	7.0
PMII-EMITFSI-EMITf	6.7

2.3.5. Quasi-Solid Ionic Liquid Electrolytes

Using of ionic liquids can solve many problems about stability which are faced at using organic solvent electrolytes. On the other hand, they are already in liquid form and this issue also can create many problems in device sealing and long term usage. Therefore, solidification of the ionic liquids can be the final solution to stability problems. Solid and quasi-solid electrolytes are studied widely as hole mediators to remove the liquid part. Solid electrolytes suffer from low charge carrier mobility and their performances are far from the organic solvents. Nevertheless, quasi-solid electrolytes present promising results for the future studies. For the solid structures, full-filling of photoanode surface by the electrolyte is the most critical issue because, all the regions, which are not filled, become the source of electron-hole recombination. Quasi solid electrolytes are produced using three general approaches:

- The use of low molecular weight gelators,
- Polymerization of ionic liquid media,
- The use of inorganic materials for solidification of ionic liquids.

Physical thermoreversibility characteristic of low molecular weight gelators is the main reason of using them as an ionic liquid solidifier. They can easily fill the photoanode surface at higher temperatures for the sol-gel transition and after cooling they can produce mechanically stable electrolyte. This property originates from forming of intermolecular hydrogen bonds between the oxygen atom in the urethane group and the hydrogen atom in the amide group. The gelling agents are composed of poly(vinylpyridine) and ($HOOC(CH_2)_n$ COOH) and the gelation occurs with a reaction between these two groups. Cell performance decreases 10-20% with the gelling agent included corresponding to the non-gelled ionic liquid electrolyte. Decrease in cell efficiency comes from the decrease in diffusion rate. Second performance to obtain quasi-solid electrolyte is based on the polymerization of ionic liquids. Polymerization is initialized using two constituents: polypyridyl-pendant poly(amidoamine) dentric derivative (PPDD) and multifunctional halogen derivative (like 1,4-dibromobutane or polyethyleneoxide (PEO)). PPDD is responsible from the solidification of electrolyte by in-situ polymerization. Although, this kind of electrolyte observes 50% decrease in cell performance, they preserve the cell performance much longer compared to ionic liquids.

The last strategy to make quasi solid electrolyte is the production of composite electrolyte using ionic liquid electrolyte and inorganic nanoparticles. SiO_2, TiO_2 and Al_2O_3 nanoparticles are extensively used to synthesize quasi–solid electrolytes which form a network structure. Primarily, these kind of quasi solid electrolytes reveal increase in efficiency when the inorganic nanoparticles are added in small quantities, on the contrary to the other quasi-solid electrolytes where a decrease in efficiency is observed about 20 to 50%. Grotthus type transport mechanism is also observed in quasi-solid electrolytes with an enhancement (for the type of inorganic material addition), since the network structure in these types of electrolytes provides a more ordered path for I_3^- transport during exchange reactions. It can be seen that anions can move more easily in this composite structure (Figure 2.18). Therefore, overall diffusion rate increases which is contrary to the expectations [20, 21, 32].

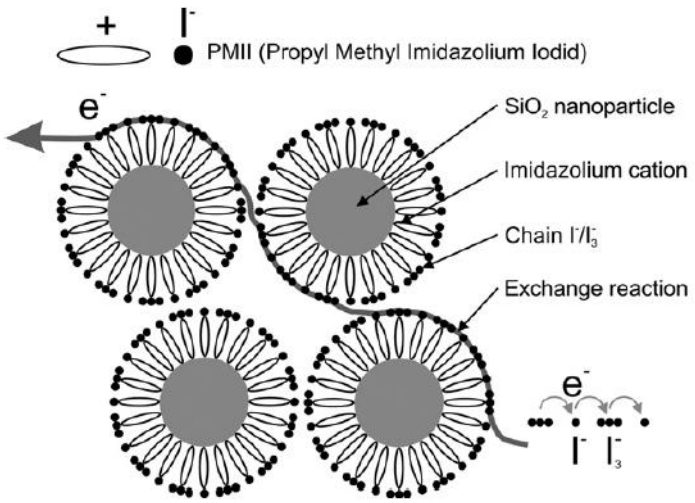

Figure 2.18 Quasi solid ionic liquid electrolyte [20].

2.3.6. Bifacial Electron Transfer

Producing electricity using both sides of the cells is a hot topic not only for the classical solar cells but also for the dye sensitized solar cells. Their importance comes from the increase in cell performance up to 50% when two sides of the cells work together. Back sides of the cells are responsible for the collection of the reflected photons from the surroundings, which is called as Albedo radiations. Albedo radiations can be maximized with integrating cells on the reflective surfaces with an optimum angle and a distance. This condition is absolutely not suitable for many applications such as roof applications. However, static solar concentrators should be most suitable and important way of providing advantages from the back side illuminations. They can also be used in alternating positions such that one side looks to the west and the other side looks to the east. With this position, solar cell can produce electricity both in the morning and in the evening.

When dye sensitized solar cells are irradiated from rear side, cells can produce electricity with 1/3 decrease in efficiency compared to front side irradiation. The loss of cell performance originates from the screening effect of electrolyte. Electrolytes have dark color and filter the most of the photons before they reach to dye molecules. Also, photons should overcome the Pt layer, because it also reflects the most of the incident photons. Therefore, photon numbers which reach the dye molecules, for the front illumination are nearly the twice of the rear side measurements. Although the decrease in photon number is nearly 50% and the decrease in efficiency is about 33% for the rear side measurements in DSSCs. Electron motions in both front and rear side illuminations are given in Figure 2.19. While the electrons spend most of their time in the electrolyte for front side irradiation, electrons follow a long path at photoanode for rear side illumination. As an advantage, long life time in photoanode directly enhances the open circuit voltage of the cell. Second advantage of the electron pathway is about the resistance in electrolyte structure and electrons move through the electrolyte as fast as possible for the rear side illuminations which causes minimum resistance [1, 5, 45].

In this thesis, bifacial DSSC has been constructed and current density-voltage (J-V) curves of illuminated cells from both sides were recorded. Although standard DSSCs can be illuminated from both sides, the ratio of the respective efficiencies for front- and rear-side illuminations are usually low because of the screening effect of the electrolyte. DSSC structures named as bifacial cells use a transparent layer between the photoanode and counter electrode which is used to increase the performance of the cell in the case of rear-side illuminations and thus the respective efficiencies for the front- and rear-side illuminations are increased. Such cells can be used with static solar concentrators and for tandem device design in near future applications [1, 5]

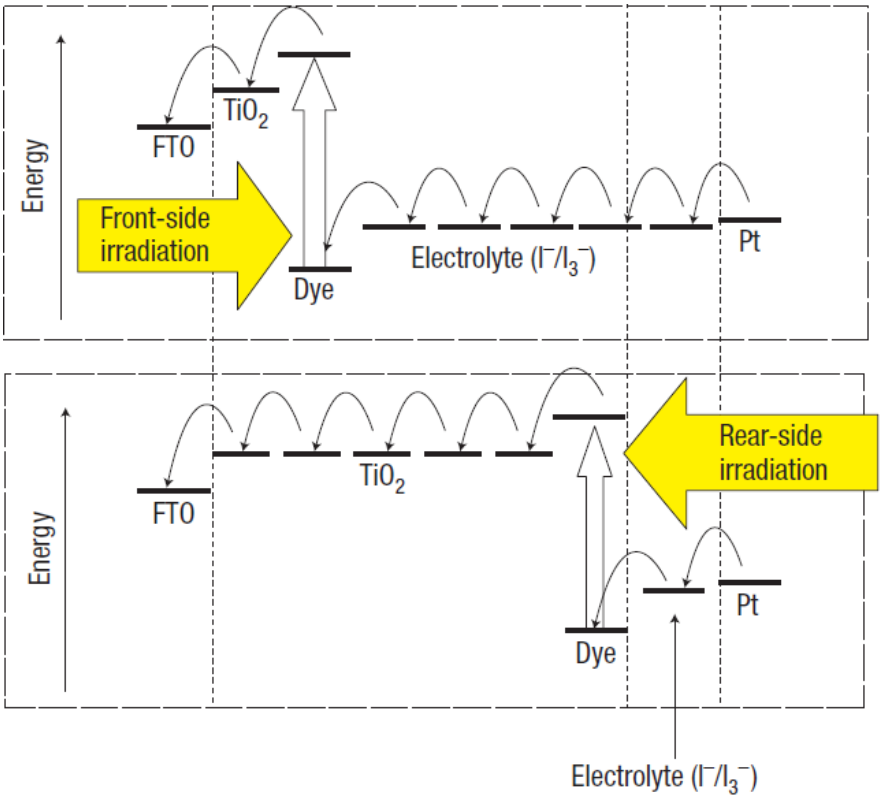

Figure 2.19 Electron transport for the front and rear side illuminations [1].

CHAPTER 3

EXPERIMENTAL

In this chapter, all fabrication steps of dye sensitized solar cells are analyzed in detail. Also, some key points and performance healing activities which are critical to obtain high performance cells are given in the following parts. Titanium dioxide nanoparticles which are purchased from Degussa were the starting point of this work. TiO_2 paste was prepared using these particles and the paste was coated on the pre-cleaned conductive glass substrates. Coating procedure determines the photoanode thickness and the effect of photoanode thickness on cell performance is evaluated in discussion section of the thesis. Surface of photoanode and conductive glass were treated using titanium tetrachloride. Enhancement of the cell performance using surface modification is known and generally the technique used in applications. Production of electrolyte with different additives and chemicals constitute the main goal of this work. Effect of using different composition of electrolytes and adding different molarities of chemicals are analyzed in the perspective of photovoltaic cell performance. Another parameter used in this thesis is the integration of silicon dioxide to the cell in a paste form. Therefore production and coating of SiO_2 is another important issue. Experimental studies conclude with production of complete cells and characterization of them. XRD and SEM characterizations were made after the production of thick films and solar cell parameters, transparency and quantum efficiency analysis were made after the production of complete cell. In the following part all experimental steps are given in the normal sequence of cell production.

3.1. Substrate Preparation and Cleaning

FTO (fluorine-doped SnO_2) conductive glass is most widely preferred substrate for DSSC applications due to its superior properties among alternatives. FTO shows an opposite behavior with respect to conductivity and transparency. For the high performance, FTO substrates should have as low resistivity and high transparency as possible. In this work, FTO glass substrates which have 15 ohms/sq electrical resistivity and 85% optical transparency (Tec 15-Pilkington) were purchased. All substrates had 4mm thicknesses. These substrates were cut into desired size depending on the active area of the photoanode to obtain best electrical contact for the measurements. Clean and dust free substrates are very essential for the good adhesion of films. Therefore, substrates should be cleaned in a way to prepare compatible surface for the coating materials. Conductive glasses are dipped into different chemicals in an ultrasonic bath at different time periods. Firstly, they are dipped into detergent solution to clean the organic chemicals on the surface for 20 minutes. These glasses are then treated in tap water, pure water and ethanol sequentially for 15 minutes in the ultrasonic bath. The cleaned FTO substrates were kept in ethanol till the deposition process [37, 41].

3.2. $TiCl_4$ Treatment

In the process scheme of DSSC production, titanium tetrachloride treatment is performed two times. First treatment is applied on pre-cleaned electrode before coating of photoanode to supply better mechanical contact between substrate and photoanode. Using this first $TiCl_4$ treatment, thick TiO_2 films stick more rigidly to FTO substrates. Other treatment is applied

after the thick film deposition. Surface roughness factor increases with treatment and it causes an increase in dye absorption amount of TiO_2 and photocurrent value of the cells.

Both of the treatments are realized using the same solution of $TiCl_4$. Firstly, an aqueous stock solution is prepared with addition of $TiCl_4$ (Merck) into pure water at 2M. This reaction is extremely exothermic and therefore water should be kept in ice bath to decrease the temperature of the water during the process. This aqueous stock solution is kept at constant temperature at 4°C and for all treatment processes. A final solution is prepared as 40 mmol $TiCl_4$ solution using the stock solution. Electrodes are soaked in vertical direction into the final solution using a fixture and they are heated to 70ºC and hold 30 minutes in drying oven. Reaction time should not exceed the determined time too much because, the thickness of the nanocrystalline TiO_2 produced on the substrate increases and it creates a blocking layer for the initial light photons. Finally, treated glasses are cleaned with pure water and ethanol [37, 41].

3.3. Production of TiO_2 Paste

For the photoanode layer, anatase phase titania is the most preferred material due to the advantages in performance since conduction band level of it is just below the LUMO level of the ruthenium dye complexes. Furthermore, it has several properties to increase the performance of DSSCs like large surface area and good interconnection of nanoparticles between each other. However, another critical point is the size and shape of the TiO_2 nanoparticles. To obtain more dye absorption, surface area of the photoanode should be as large as possible. Maximum surface area can be obtained using spherical nanoparticles due to its minimum energy. Size of the particles is also critical because when the particle size is between 10-20 nm, particles tend to become in the anatase phase.

It this work, 20 nm titania particles were purchased which have 80% anatase-20% rutile composition as Degussa-P25. The following production steps are used to prepare titania paste. Preparation is done in agate mortar and powder is crushed in the mortar to prevent the agglomeration. While crushing, acetic acid (Merck), water and ethanol (Merck) are added to the mortar drop by drop. When the mechanical crushing is finished, solution is taken from the mortar with excess amount of ethanol. Then solution is homogenized using stirrer and ultrasonic horn. Terpineol (Fluka) as a carrier and ethyl cellulose (Sigma-Aldrich) as a binder are added into sonicated solution and the whole solution is concentrated using evaporator at 35ºC at 10mbar. Evaporation should be finished before evaporating the terpineol because, the viscosity of paste is crucial to prepare a good coating and terpineol plays an important role in the viscosity [21, 37, 41]. Detailed titania paste production is given in Figure 3.1.

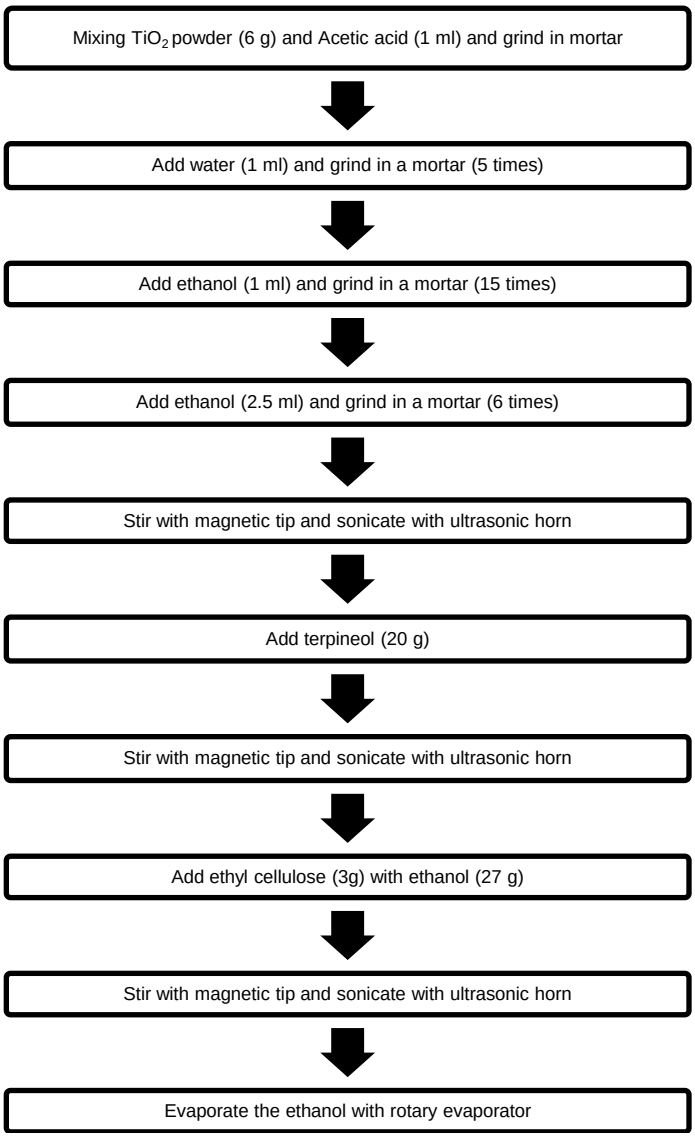

Figure 3.1 Scheme for titania paste production [37]

3.4. Screen Printing of Pastes

Screen printing is a cheap, easy and flexible thick film coating technique for the pastes and inks and it can be applied on any kind of substrates. It has been known and applied in many applications for several years and it is also known as silk screen, serigraphy and serigraph printing. The equipment of screen printing generally composes of a frame and a screen (Figure 3.2). Frame can be made from wood or aluminum and silk, polyester or metallic meshes can be used as a screen. Important point is the blocking of the unwanted areas on screen with stenciling technique. In this technique, desired open areas are printed on transparent paper with black color. Then, screen is coated with emulsion materials and the paper is placed on the screen. Screen is exposed to ultraviolet light to ensure for the sticking of the blocking layer on the unwanted regions. Finally screen is washed with water to clean the regions which are not exposed to the light and pattern is produced using photo emulsion method.

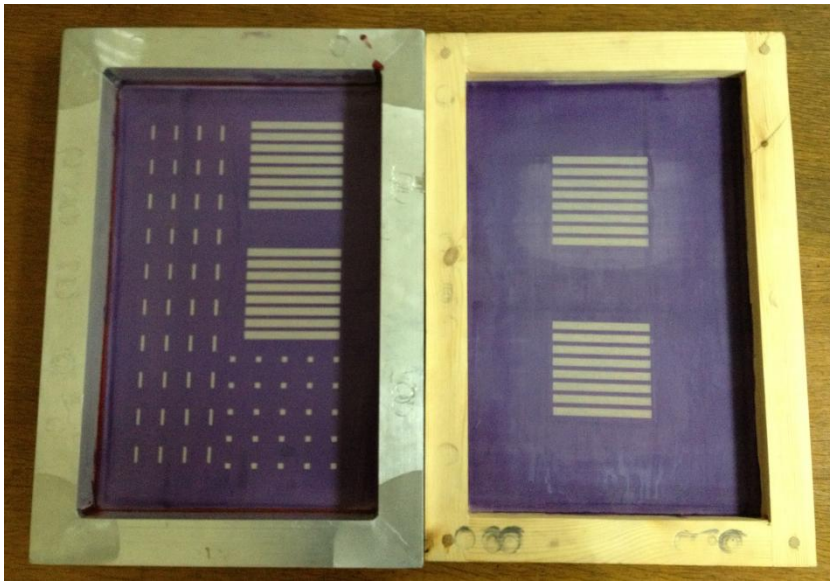

Figure 3.2 Aluminum and wood case screens.

To have a good screen printed coating, mesh size of the screen should be selected considering the particle size and paste fluidity. In this work, 90T mesh/cm screens were used with a pattern of 0.5 cm X 0.5 cm open area. It means that active area for the cells is 0.25 cm^2. In printing procedure, screen is placed on top of the substrate without contact and prepared pastes are put in front of the opened pattern region. Paste is moved on opened region using a rubber blade. Rubber blade should be pulled with 70-80° angle from the horizontal by applying power from the starting point to final point of pattern. Paste is pumped or squeezed in patterns with capillary actions. Deposition of paste can show differences according to the mesh thickness and pattern. When the rubber blade comes to the final point of pattern, screen and substrate separate (snap-off) from each other and desired pattern is coated on the substrate (Figure 3.3). TiO_2 and SiO_2 pastes were deposited using similar screens in a class 10000 clean room environment.

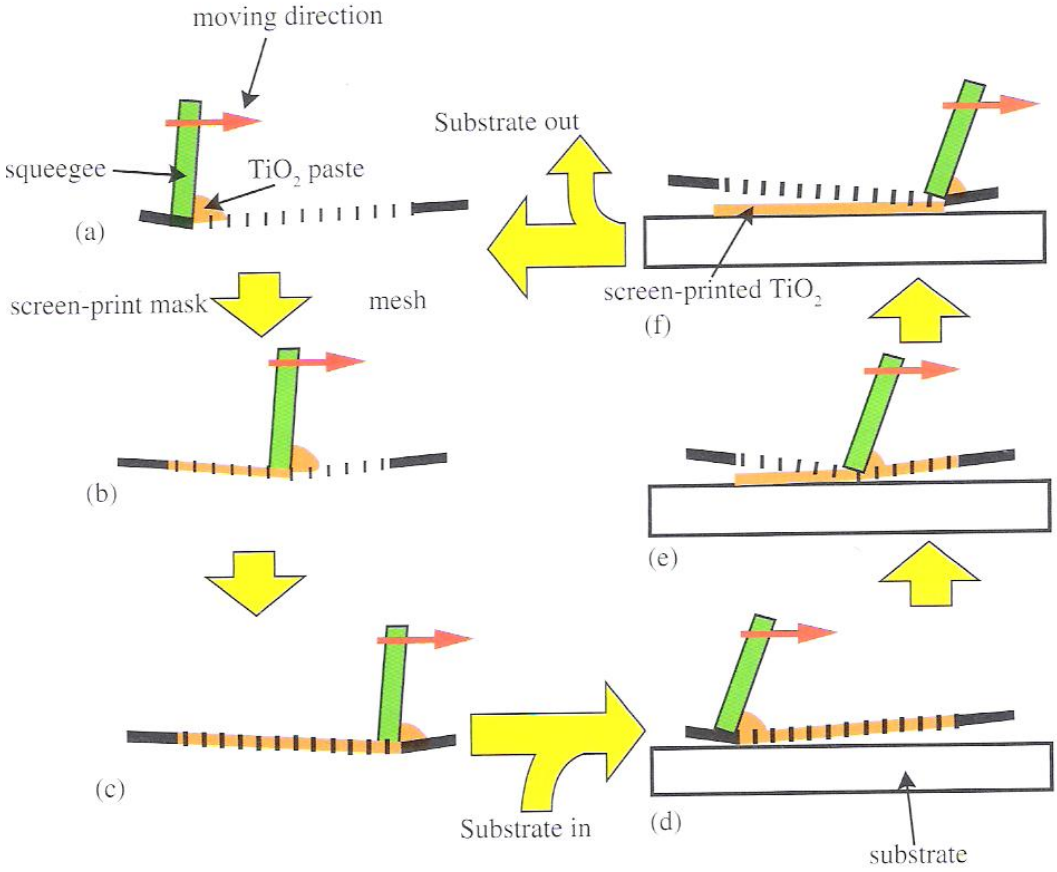

Figure 3.3 Actions in screen printing operation [21].

After coating titania paste, glass is placed on a paper wetted via ethanol in a clean box. Ethanol vapor supplies leveling of titania paste on the substrate, in other words, paste relaxes and surface irregularities are removed. Also, some fabrics which come from screen printing are removed with leveling. Although leveling time depends on the operator observation, it nearly takes three minutes. If waiting time exceeds three minutes, paste can separate or spread on the surface. After leveling step, glass with titania paste is placed into a drying furnace at 125°C for 5-10 min. 2 µm thick titania layer were deposited as a single layer and therefore, process steps which were coating-leveling-drying, were repeated until the desired thickness value was obtained. In this work, to investigate the relation between the photoanode thickness and cell performance, one to six screen printing operations were performed and six different coating thicknesses were obtained [21, 37, 41].

3.5. Heat Treatment

Heat treatment is a very critical process step in DSSC production. In this work, FTO coated soda lime glasses (Si(62.77%), Ca(16.71%), Na(13.96%), Mg(4.03%), Al(1.04%), K(0.99%), Fe(0.23%)) with low iron contents were used from Pilkington and their softening point is nearly 600ºC. Heat treatment should be applied at a temperature below this softening point not to damage the substrates. In addition, titania changes its phase from anatase to rutile over 550ºC. Most appropriate temperature for sintering is about 500°C for both titanium dioxide and tin dioxide. Another critical issue is the heating rate of the films where sudden

changes in temperature result in thermal stresses, which cause cracking of the film and peeling off from the substrate. As long as the films contain organic binders, these binders have to burn completely before the sintering of particles starts, otherwise organic residues are trapped between interconnected particles and causes failure during the operation of the cell. Therefore, sintering of titania layer should be performed using step wise temperature increases to prevent the thermal stress and to obtain desired surface roughness. In this work, the temperature in the furnace is increased 10ºC per minute and the following sequential temperature and time combinations are used: 325ºC for 5 min, 375ºC for 5 min, 450ºC for 15 min and 500ºC for 15 min. Additives are leave from the photoanode with partial by partial at above temperature steps. After sintering at 500ºC, cooling is performed in closed furnace ambient. Following to the cooling process, second $TiCl_4$ treatment is carried out on the photoanode. When the treatment is finished, photoanode is washed with absolute ethanol and another sintering process is applied at 500ºC for 30 min to sinter the particles on the photoanode surface due to this last $TiCl_4$ treatment and anode is cooled in the furnace again [21, 37, 41].

3.6. Dye Staining

When the furnace temperature is around 80ºC, photoanode is taken out from the furnace and directly immersed in dye solution. Photoanode was placed in solution horizontally and all the active areas of photoanode should be in contact with dye molecules. Dye solution was prepared adding 0.5 mmol N-719 ([cis-di(thiocyanato)-N-N′-bis(2,2′- bipyridyl- 4-carboxylic acid-4′-tetrabutylammonium carboxylate) ruthenium (II)]) (Solaronix) into the acetonitrile (Merck) and tert-butyl alcohol (Merck) (1:1 volume ratio) solution. Solution is mixed until the dye molecules are dissolved in the mixture completely. Prepared dye mixture should be kept in air-tight boxes to preserve the solution from the gaseous and liquid water molecules under storage conditions. Because, dye molecules easily attract water molecules and this condition is detrimental for the cell performance. Keeping the dye solution in a storage box is also essential to preserve the solution from evaporation, dye molarity of the solution increases with evaporation of acetonitrile. Although process time for complete dye staining is nearly 24 hours at room temperature, it can be decreased to lower values when the dye staining occurs at higher temperatures. Sensitized photoanode is removed from the solution and it is cleaned with plenty of acetonitrile to remove the unbounded dye molecules from the surface of photoanode. Finally, cleaned photoanodes should be immediately used in cell assembly to prevent the absorption of water molecules by dye [21, 37, 41].

3.7. Counter Electrode Preparation

Counter electrode is an electron donor for the electrolyte, while the process rate is very slow. Therefore, surface of the substrate used for the counter electrode is coated with reaction catalyst chemicals. FTO coated substrate has again 15 ohms/sq electrical resistivity and 85% optical transparency (Tec 15-Pilkington), however a 1 mm hole is drilled using water jet for electrolyte injection. Also they were cut to dimension of 1.5 X1.5 cm and same cleaning steps are followed for the counter electrodes as front electrodes. Cleaned substrates are heated to 400 ºC for 15 min to remove the organics and they are cooled in furnace to 200 ºC. Then, hexacloroplatinic acid solution in isoproponol (Solaronix) is dropped on the surface of counter electrode at 200 ºC. Solution is spread on the substrate and heated in thefurnace at 400 ºC for 15 min. After removal of counter electrode from the furnace, cell assembly should be performed as soon as possible to keep the catalytic surfaces clean [21, 37, 41].

3.8. Electrolyte Production

Electrolytes were produced using different compositions of PMII (1-propyl-3-methylimidazolium iodide) (Merck) and $EMIB(CN)_4$ (1-ethyl-3-methyl-imidazolium

tetracyanoborate) (Merck). To investigate the effect of $EMIB(CN)_4$ addition on PMII, electrolyte compositions of 25%, 50%, 70%, 85% and 100% (PMII amounts) were prepared using 0.2 M I_2.They were mixed and stirred in a beaker nearly one day to obtain homogenous electrolyte mixture. Then, cells were produced using these electrolytes and the highest cell efficiencies were recorded for the electrolyte composition containing 70% PMII and 30% EMIB(CN)4. Therefore, this composition was selected as the optimum composition for the further studies in this work.

Then, GuSCN (guanidinium thiocyanate) (Merck) and NMB (N-methylbenimidazole) (Merck) were added to the electrolyte at different molarities. 0, 0.05, 0.1, 0.2 M GuSCN and 0, 0.25, 0.4, 1 M NMB were added separately to the electrolyte of 70% PMII and 30% (EMIB(CN)4) composition to observe the GuSCN and NMB dependence of the electrolyte during the photovoltaic action. 0.1 M GuSCN and 0.4 M NMB were found to be the optimum concentrations of these materials which yielded maximum efficiencies in the DSSCs.

Using optimum electrolyte, NMB and GuSCN compositions, experiments were repeated. Firstly GuSCN and NMB amount were taken constant at 0.1 and 0.4 M and PMII and $EMIB(CN)_4$ were mixed in different molarities and cell performances were observed. Then, electrolyte composition and NMB were kept constant and GuSCN were added in different molarities. Finally, electrolyte composition and GuSCN were kept constant and NMB were added in different molarities. Thus, combined effect of electrolyte, GuSCN and NMB compositions were investigated.

3.9. Integration of SiO_2

In this work, additional silicon dioxide nanoparticles of 7 nm (Aldrich) in size were employed in the system in two different ways. The first one is the preparation of a SiO_2 paste and coating it on the TiO_2 layer and the second one is the dispersion of nanoparticles into the electrolyte directly. SiO_2 paste was formed by following the same procedure of TiO_2 paste. As a SiO_2 layer, a thickness of 3 μm was deposited on top of TiO_2 photoanode using same mesh size screens as titania after the heat treatment of TiO_2 paste. Then, it was dried and heated to 500 ºC for 30 min. After cooling to 80 ºC, it was immersed in dye solution for 24 h. Silica nanoparticles do not absorb the dye molecules and allow passing of them to reach the titania layer. Due to this property, silica can be used as an overlayer on TiO_2. Secondly, nanaoparticles were directly added into optimum electrolyte compositions at 0.1 M. Electrolyte should be stirred at 600 rpm and for 24 h to mix the nanoparticles with electrolyte fully and to obtain a homogenous solution at the end of the process [1, 20].

3.10. Assembly

Dye-covered photoanode and Pt coated counter electrode are assembled using a sandwich type structure. Coated sides of the electrodes are placed in a way looking one another and a hot melt polymer is placed between the electrodes to perform the sticking. In this work, photoanode active area is nearly (0.5X0.5 cm) 0.25 cm^2, therefore 25 μm thick Surlyn (Solaronix) is cut as a frame. Surlyn frames are shaped as a hollow square using scalpel at 0.5X0.5 cm sizes and 1 mm wall thickness. Surlyn frame is placed around the active area of photoanode and hole on the counter electrode. Hole on the counter electrode should be aligned to the edge of the active area of the photoanode, because hole on the counter electrode can easily scatter the incoming light for the back side measurements and it can cause a sharp decrease in cell performance. Then, this stack is placed on the hot plate and temperature is adjusted to 120 ºC. A slight press is applied on the stack to spread to Surlyn film between the electrodes homogeneously and the stack is cooled slowly to room temperature and it is inspected visually to observe any defects like surpassing of Surlyn film on photoanode or non-adherent Surlyn regions.

Most critical point in assembly is the filling of electrolytes between two glasses. Direct injection of electrolyte into the cell does not supply full wetting due to air in the cell. Therefore, another filling method is applied, which is vacuum back filling. In this method, cell is placed into a glass beaker and electrolyte is dropped on the hole of counter electrode. Then, air in the beaker is evacuated by a rotary pump. The air bubbles inside the cell are also evacuated during the process. When bubble exit is ceased, vacuum is broken and electrolyte moves into the cell from the hole using the pressure of the air. Finally, hole is sealed by UV curing glue and it is solidified by UV light. Thus, electrolyte is confined between two glass electrodes. The architecture of the dye sensitized solar cells used in this study is given in Figure 3.4, where the front and rear side illuminations are indicated. The positions of TiO_2 photoanode and SiO_2 nanoparticles are also shown in the same figure [21, 37, 41, 46].

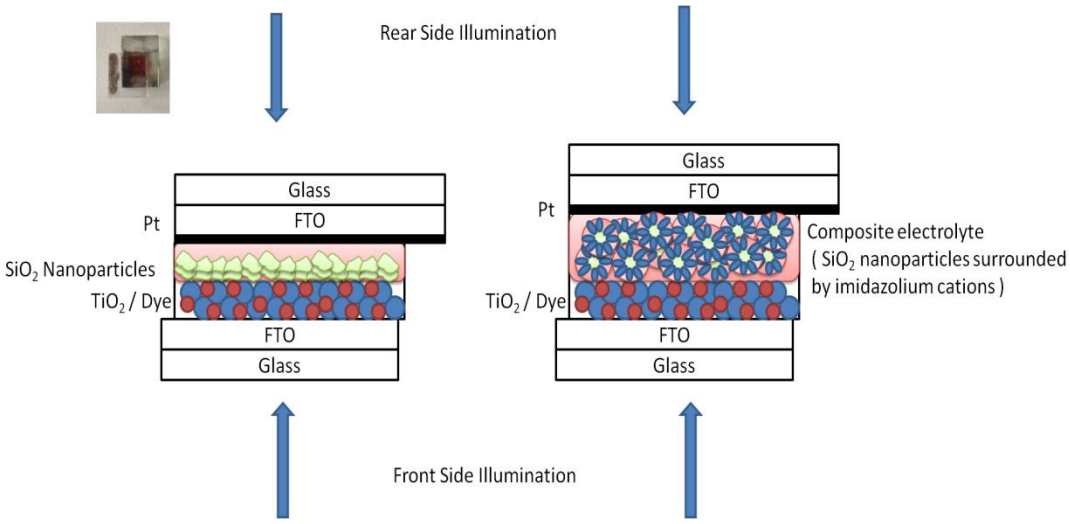

Figure 3.4 The schematic of the bifacial transparent DSSC with the photo of the device [46]

3.11. Characterization

Morphologies and shapes of TiO_2 and SiO_2 nanoparticles, microstructure and film qualities of thick TiO_2 and SiO_2 films, total thicknesses of photoanodes and chemical compositions of layers were analysed by field emission scanning electron microscope (FESEM, FEI–Nova NanoSEM 430) in Metallurgical and Materials Engineering Department of METU. Crystal structures of the phases were investigated by Rigaku D/MAX 2200/PC diffractometer, Metallurgical and Materials Engineering Department of METU.

The devices, which have 0.25 cm^2 active area, were characterized by a Keithley 2440 sourcemeter under standard AM 1.5G filtered irradiation (100 mW cm^{-2}) from a Newport 91192 model 300 W Solar Simulator in Physics Department of METU to observe the photovoltaic performance of devices. IPCE (incident photon-to-electron conversion efficiency) spectra for the DSSCs was measured by Oriel IPCE measurement kit which involves 300 watt xenon arc light source, CS260 Monochromator, Merlin lock-in amplifiers, optical chopper and Si detector in Chemistry Department of METU to investigate the spectral behavior of the devices. Transmittivity spectra for the DSSCs were taken by Cary Varian 100 Bio UV-visible spectrophotometer in Metallurgical and Materials Engineering Department of METU to understand the effect of silica nanoparticles on transparency.

CHAPTER 4

RESULTS AND DISCUSSION

All the experiments have been performed to create a promising solution to the problems in conventional redox electrolyte. For this purpose, many cells were produced using titania and silica nanoparticles and produced cells were filled with different electrolyte mixtures. Different characterizations were conducted to investigate and compare the performances of the cells. Measurements were applied in two stages: at sub-device form and device form. Sub-device form characterizations were applied to understand the photoanode morphologically and structurally, on the other hand, measurements in device form were performed to analyze the solar cell characteristics.

XRD, SEM and EDX characterizations were done in sub-device form. Titania screen printed glasses were characterized using XRD to analyze the crystal structure of titania powders. Then, SEM analysis were conducted on photoanode layers to observe the morphology and shape of the titania powders, adherence of thick layer on glass, surface irregularities and to measure the photoanode thicknesses. Possible impurities in photoanode layers were investigated by EDX analysis.

J-V curves, IPCE and transmittance measurements were performed for a complete device. Photovoltaic performances of the devices with different electrolyte compositions were characterized using Solar Simulator. By analyzing the output of the solar simulator (J-V curves), several photovoltaic properties can be obtained like open circuit voltage, short circuit current, fill factor and cell efficiency. Incident photon to electron conversion efficiency measurements were conducted on devices to obtain the spectral cell performance of the devices. Finally, transmission measurements were applied to examine the optical transparency of the cells and to reveal the relation between the cell performance and transparency.

4.1. X-ray Analysis of the Photoanode

XRD analysis was performed on titanium dioxide coated FTO glasses to determine the existing crystal structures, approximate size of particles and relative ratios of the phases. The measurement of diffraction analysis was performed between 10º and 80º. The XRD spectra of the titania are given in Figure 4.1. Results show that titania is composed from anatase phase with small fraction of rutile. Relative amounts of anatase and rutile phases were calculated using the software of Rigaku and their relative ratios are quite similar to data for the precursor of the titania paste production (P25- Degussa). Anatase to rutile ratio was approximately 80% to 20%. Characteristic peaks of SnO_2 also exist in the spectrum and SnO_2 peaks are located around 26º, 34º, 52º, 63º and 66º. The peaks of anatase phase were observed at 25º, 38º, 48º, 54º, 63º and 68º with a fairly good crystallization. These two theta values correspond to (101), (200), (105), (211) and (204) planes of anatase according to JCPDS 21-1272 card values. Also, tin oxide peaks match with JCPDS 46-1088 and peaks of the rutile phase of titanium match with JCPDS 21-1276 card values. Generally, sharp peaks have higher particle sizes than the broadened peaks. In this work, titania precursor was purchased containing approximately 20 nm particle size.

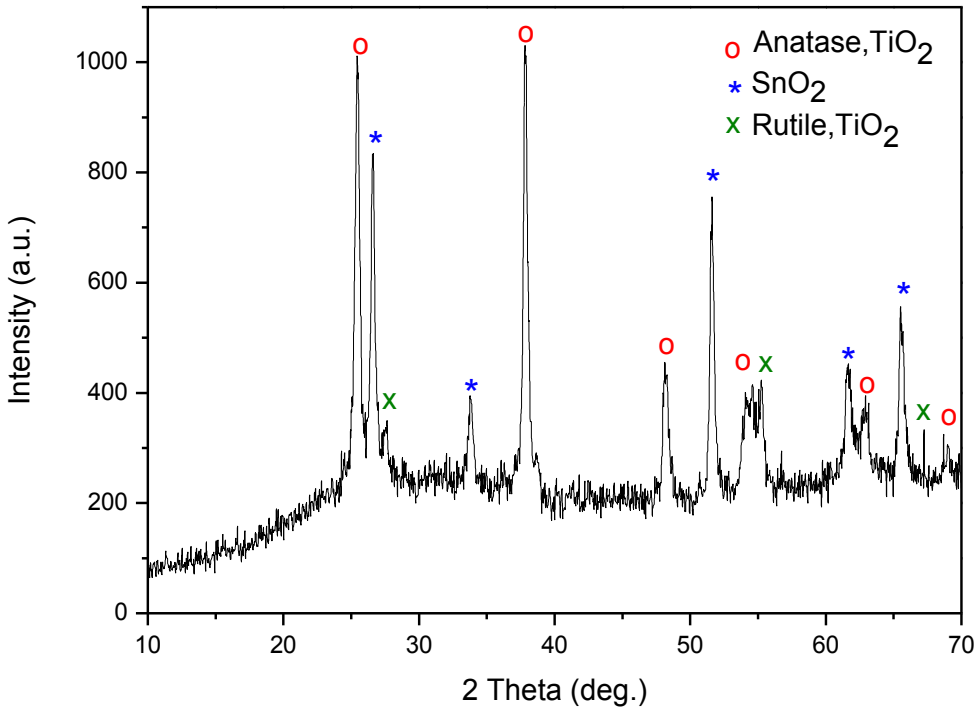

Figure 4.1 X-ray spectra of titania nanoparticles on FTO glass.

4.2. SEM Analysis of Photoanode Thick Films

The prepared titania pastes were coated on FTO glass by screen printing method and to characterize and observe the particle size, film quality, paste quality, porous structure, surface quality and thickness, SEM analysis were performed on titania coated FTO glasses. For thickness determination, glasses were cut and cross sections of the films were observed using SEM. Also, EDX analyses were carried out for compositional analysis for Ti and O and also it was used to determine the impurities due to production stages. Due to the low conductivity nature of the photoanode, few nanometers thick gold was coated on the photoanode.

SEM image of the nanocrystalline porous TiO_2 layer is presented in Figure 4.2. It shows that most of the spherical titania particles are distributed homogeneously. Also, titania particles are well organized and they make a good network. Whole structure is highly dense and it has well surface coverage. Another output is the highly porous structure of the layer which is

critical for the maximum dye absorption. Sizes of the particles are nearly 20 nm and this data is consistent with the supplier information and XRD results. However, some small and large agglomerations can be seen in the SEM images.

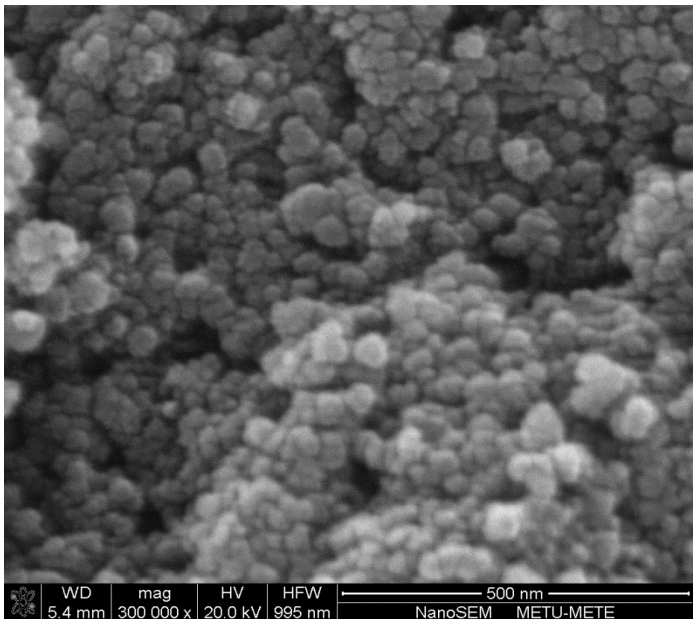

Figure 4.2 Magnified SEM image of the titania layer.

Figure 4.3 shows the surface of the photoanode layer. Although surface smoothness and uniformity were fairly good, some small and large aggregates can be seen on the surface, which create some roughness. It is an inevitable result of screen printing coating technique. However, when the size of agglomeration is about the micron levels, they are called as large aggregates which form the origins for small cracks in the porous titania layer. These cracks are due to the shrinkage occurring at large aggregates during the sintering process. To obtain a good electron transport, photoanode layer should be crack free. Therefore, these cracks may create some decrease in the photovoltaic performance.

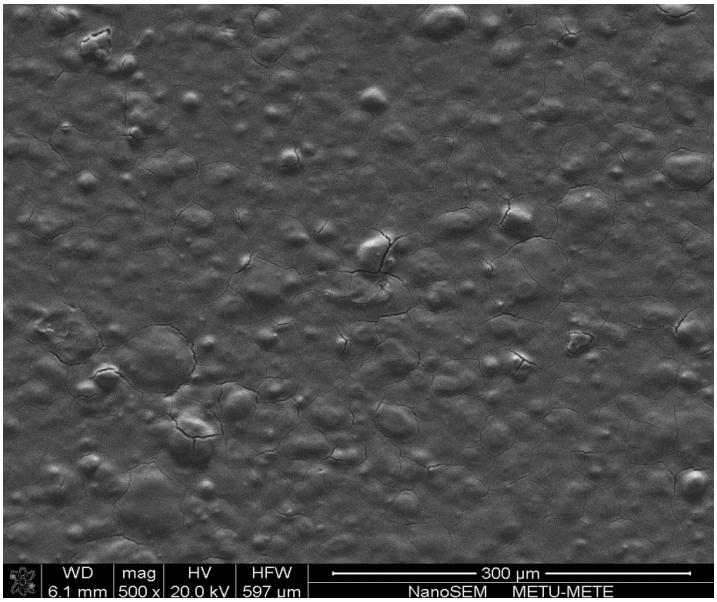

Figure 4.3 Top view of the thick titania layer.

Cross-sectional SEM image of the photoanode and conductive glass can be seen in Figure 4.4. To image the lateral surface, samples were cut into two pieces. Cutting procedure should be performed carefully not to damage the samples. Damage can occur with peeling off photoanode layer on the surface. The glass and photoanode interface can be seen in this figure where the photoanode TiO_2 layer adheres well on the surface of substrate and any peel off was not observed.$TiCl_4$ treatment is the main explanation of the high quality of adherence. In the same figure, dense and uniform structure of titania particles can also be observed. Investigation of the lateral surface gives values about the thickness of the photoanode layer as nearly 7 μm. This thickness layer can be obtained using 3 coating cycles by screen printing method. The thickness uniformity of the film is also homogeneous.

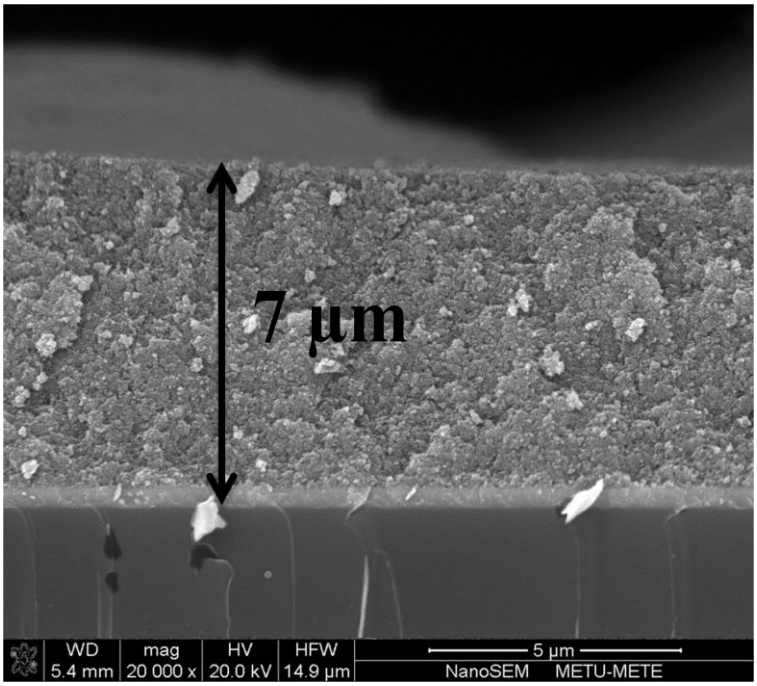

Figure 4.4 Cross-sectional image of the photoanode.

Cross sectional image of the SiO_2 layer on titania thick film is presented in Figure 4.5. Titania layer is obtained using two cycles of coating and it has nearly 5 μm thickness and silica is coated as a single layer and it is nearly 1.5 μm in thickness. Silica nanoparticles adhere well on titania particles. However, silica particles show some agglomeration due to the small particle size of the silica nanoparticles.

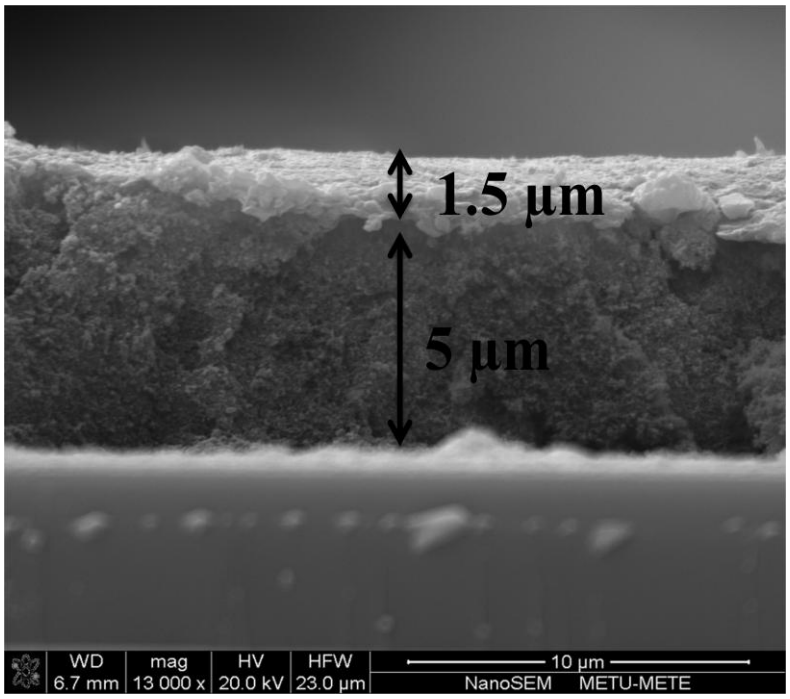

Figure 4.5 Cross-sectional image of the silica and titania layers.

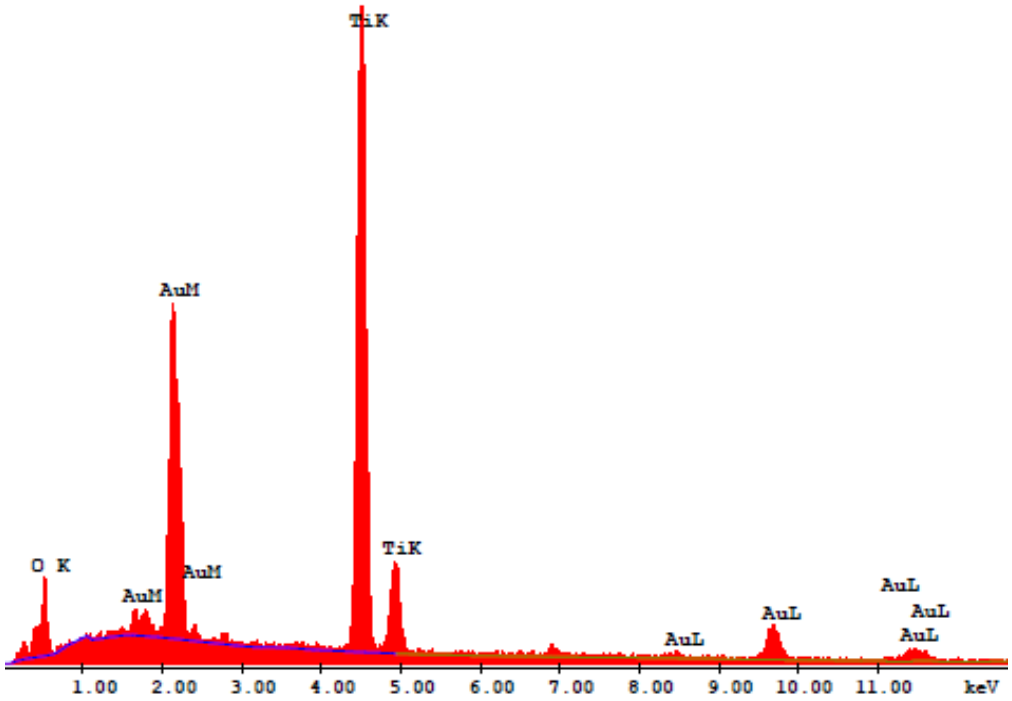

Figure 4.6 EDX spectra of titania nanoparticles.

Figure 4.6 shows the EDX spectra of the titania nanoparticles on FTO glass. Ti, O and Au elements are detected in this analysis. Gold comes into diagram due to coating layer for SEM observation. When the small gold peak (near to 2keV) is neglected in the calculation, atomic percentage of Ti is nearly 31% and O is nearly 69%. Layer does not include any contamination, it is important for the quality of the film. As a result, purchased precursor is clean and photoanode layer is not contaminated during the preparation of the film.

4.3. Photovoltaic Characterizations of the Cells

Amount of different additives are optimized using data which was obtained from the photovoltaic measurements. Therefore, the work presented in this thesis gives optimum conditions for the molarity of additions and photoanode thicknesses on the cell performance using a systematic study.

4.3.1. Effect of Binary Electrolyte Composition on Photovoltaic Performance

Figure 4.7 and Table 4.1 summarize the effect of ($EMIB(CN)_4$) added to PMII on photovoltaic properties of DSSCs which were prepared using 0.1 M GuSCN and 0.4 M NMB additions to the electrolyte composition. All devices were constructed using 10 µm TiO_2 photoanode thickness. It is observed that efficiency and photocurrent density increase until the optimum value of 70% PMII above which they start to decrease. Also open circuit voltage makes maximum at this composition. It is obvious that addition of low viscosity electrolyte increases the diffusion coefficient and electron lifetime, therefore the open circuit voltage increases causing an increase in the efficiency. However, when the composition of PMII changes below 70% open circuit voltage and efficiency start to decrease. A likely reason for this effect is the increase in the probability of capture of a conduction band electron resulting in increased recombination rate. In this work, it was seen that rear side illuminated cells show the same behavior as the front side illuminated ones (Figure 4.7). Rear side illuminated cells give a value of approximately 3/5 of photocurrent and efficiency values compared to the front side illuminated cells, where this reduction is expected since incoming photons are captured by electrolyte and Pt layer.

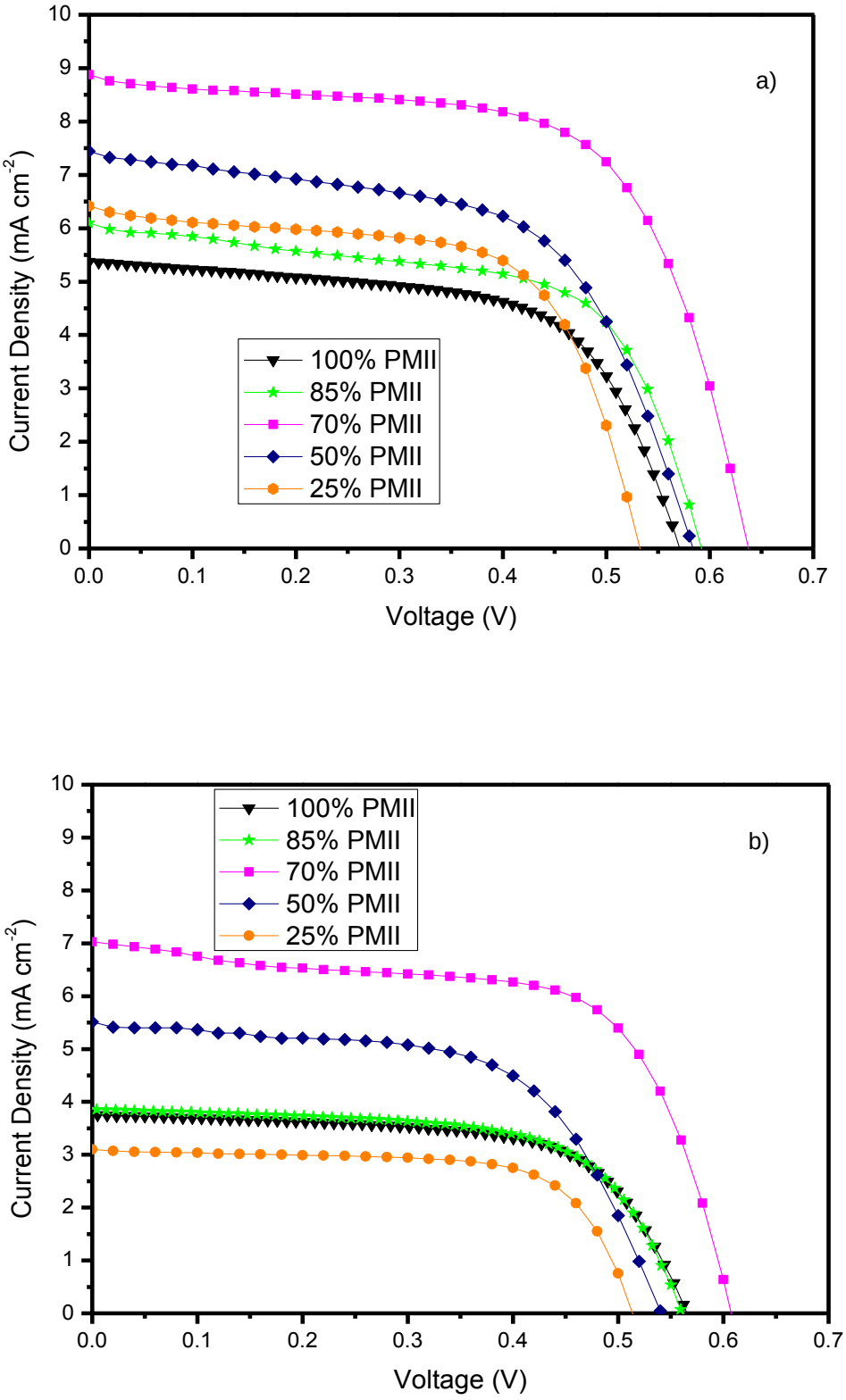

Figure 4.7 J-V characteristics curves for the DSSCs constructed using different compositions of (PMII- $EMIB(CN)_4$) irradiated from a) front and b) rear sides [46].

Table 4.1 The photovoltaic characteristics of DSSCs constructed using different compositions of (PMII - $EMIB(CN)_4$) [46].

	Composition of PMII (%)	V_{oc} (V)	J_{sc} ($mA.cm^{-2}$)	FF	η (%)
Front Side Illumination	100	0.57	5.38	0.62	1.91
	85	0.59	6.10	0.61	2.20
	70	0.64	8.88	0.61	3.63
	50	0.59	7.44	0.62	2.53
	25	0.53	6.42	0.63	2.16
Rear Side Illumination	100	0.56	3.76	0.64	1.37
	85	0.56	3.87	0.64	1.39
	70	0.61	7.03	0.63	2.76
	50	0.55	5.51	0.65	1.80
	25	0.51	3.10	0.69	1.10

4.3.2. Effect of Photoanode Thickness on Photovoltaic Performance

Cross-sectional scanning electron microscopy (SEM) images of screen printed films with different thicknesses are given in Figures 4.8-4.13. They were produced using different screen printing cycles. Screen printing was performed from 1 to 6 cycles and corresponding coating thicknesses are 2.4–4.6-8.1-10.5-12.4 and 15.4 μm. Optimization of TiO_2 thickness is another important factor to improve the photovoltaic performance of binary ionic liquid electrolyte. The use of non volatile electrolyte decreases the mass transport rate, in other words, diffusion length is shorter than solvent based electrolytes which means that diffusion limited current occurs at shorter distances. Therefore, photoanode thickness is expected to be shorter compared to solvent based electrolytes and it should be optimized for different electrolyte compositions. Generally, for solvent base electrolytes optimum photoanode thickness is nearly 14-19 μm [37]. Photon absorption by the photoanode increases with photoanode thickness, on the other hand, thickness should not be more than 19 μm due to diffusion limitations of redox couple [1]. In this work, nearly 10 μm TiO_2 thickness gives the highest efficiency for PMII/($EMIB(CN)_4$) electrolyte for both front and rear side illuminated cells as 3.63% and 2.75%, respectively. The photovoltaic characteristics of DSSCs constructed using 70% PMII and 30% ($EMIB(CN)_4$) electrolyte together with 0.1 M GuSCN and 0.4 M NMB additions are summarized in figure 4.14 and table 4.2. Dye is absorbed on the photoanode irrespective of the thickness of TiO_2 layer. However, the ratio of dye-excited area of the photoanode to non-excited area decreases with increase in the thickness. Although, current density increases with the increase in photoanode thickness, above condition causes a decrease in the open circuit voltage after averaging the electron density [1]. The reduction in fill factor with increasing photocurrent density is a result of high series resistance at high current densities.

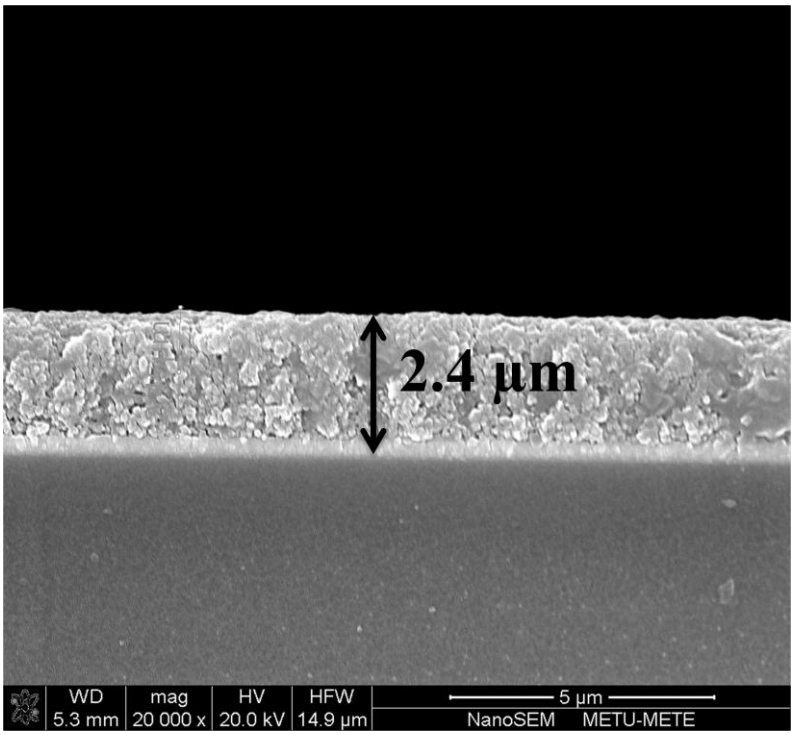

Figure 4.8 Cross-sectional image of the titania photoanode layer screen printed using one cycle.

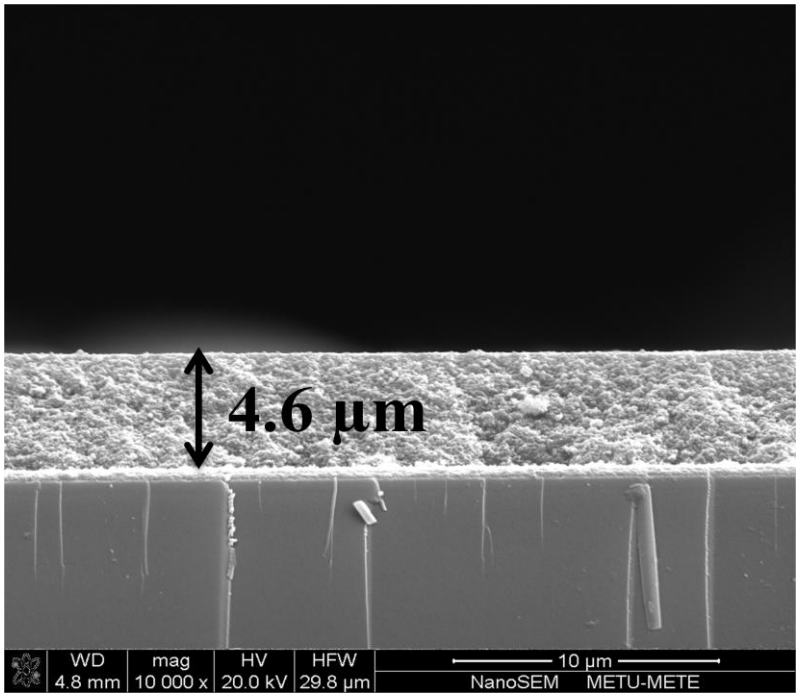

Figure 4.9 Cross-sectional image of the titania photoanode layer screen printed using two cycles.

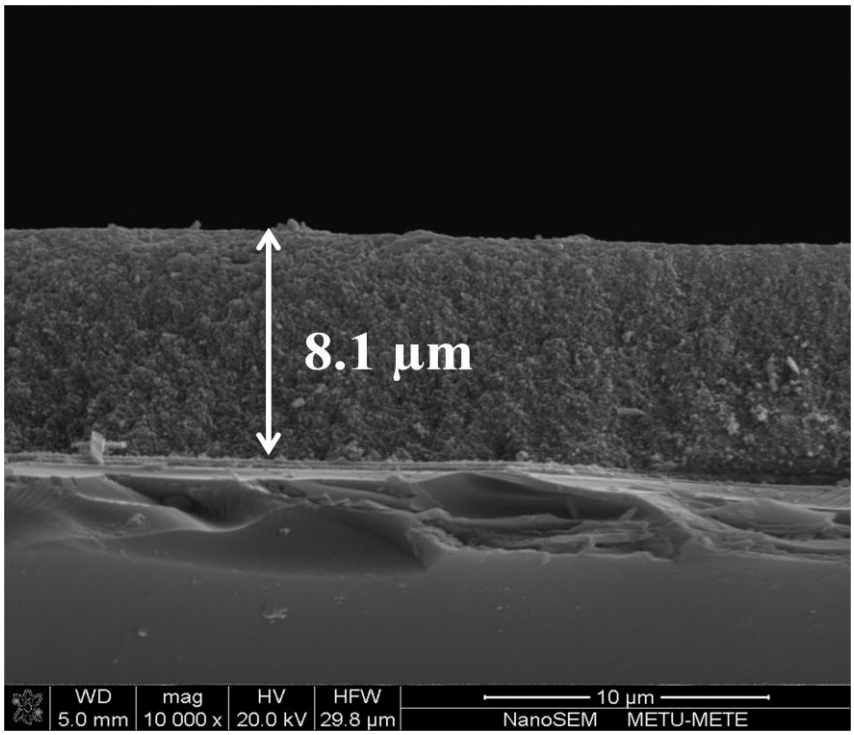

Figure 4.10 Cross-sectional image of the titania photoanode layer screen printed using three cycles.

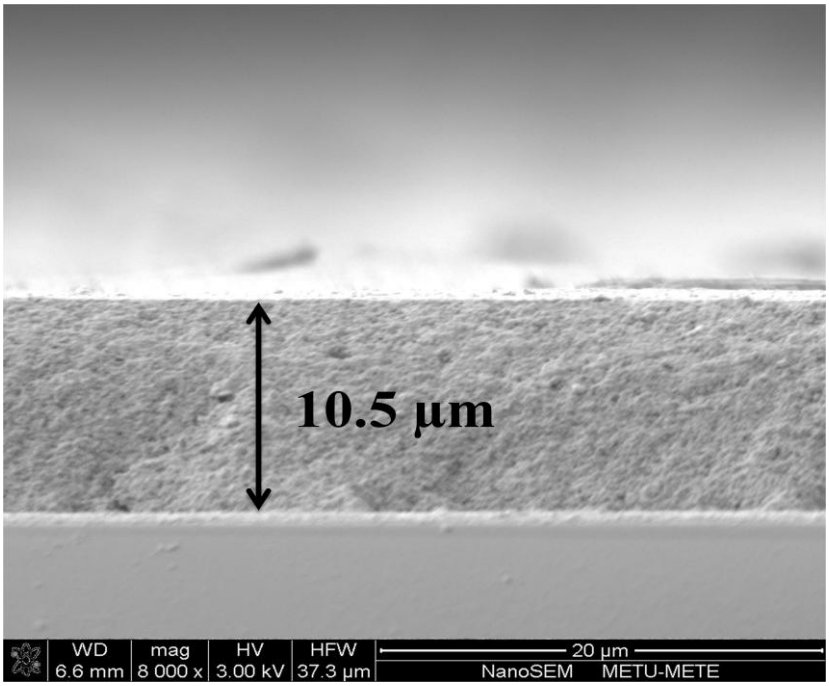

Figure 4.11 Cross-sectional image of the titania photoanode layer screen printed using four cycles.

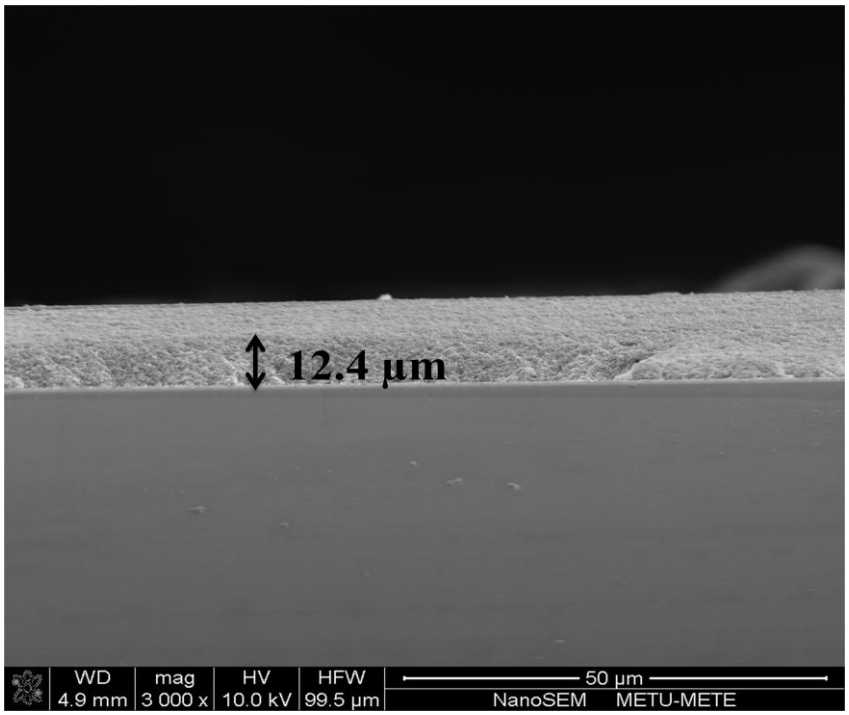

Figure 4.12 Cross-sectional image of the titania photoanode layer screen printed using five cycles.

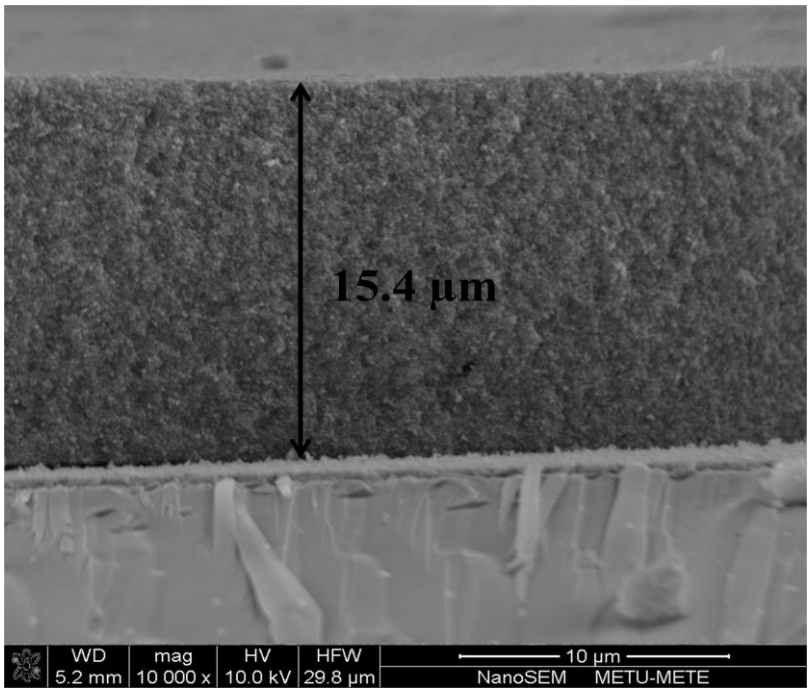

Figure 4.13 Cross-sectional image of the titania photoanode layer screen printed using six cycles.

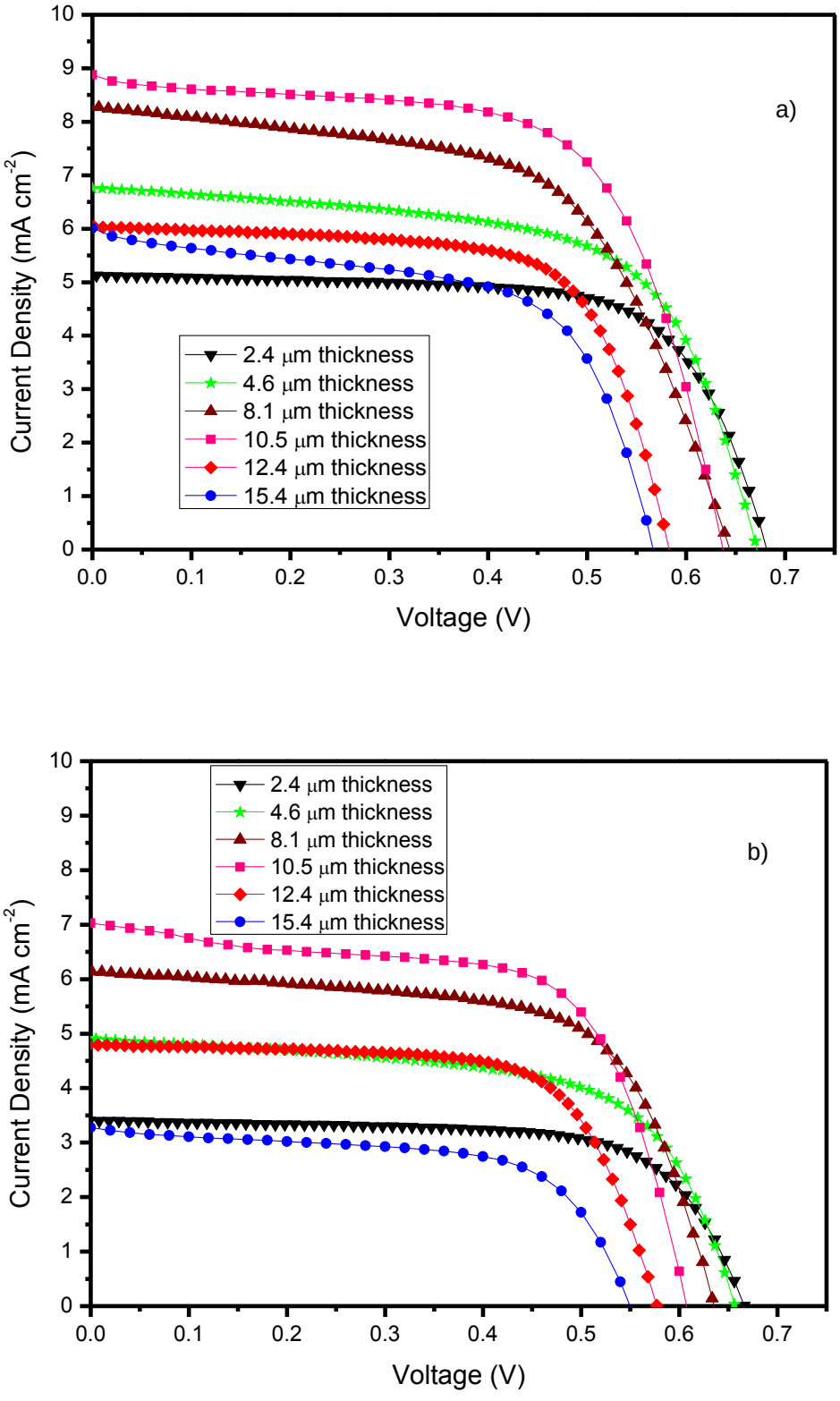

Figure 4.14 J-V characteristics curves for the DSSCs constructed using different coating thicknesses of TiO_2 films irradiated from a) front and b) rear sides [46].

Table 4.2 The photovoltaic characteristics of DSSCs constructed using different coating thicknesses of TiO_2 films [46].

	Thickness (μm)	V_{oc} (V)	J_{sc} (mA.cm^{-2})	FF	η (%)
Front Side Illumination	2.4	0.68	5.13	0.69	2.41
	4.6	0.67	6.76	0.64	2.87
	8.1	0.65	8.3	0.62	3.14
	10.5	0.64	8.88	0.61	3.63
	12.4	0.58	6.04	0.63	2.40
	15.4	0.57	6.00	0.66	2.04
Rear Side Illumination	2.4	0.66	3.4	0.69	1.56
	4.6	0.65	4.91	0.65	2.01
	8.1	0.63	6.14	0.64	2.54
	10.5	0.61	7.03	0.63	2.75
	12.4	0.57	4.80	0.66	1.90
	15.4	0.55	3.28	0.68	1.12

4.3.3. Effect of the Addition of Guanidinium Thiocyanate and N-methylbenimidazole on Photovoltaic Performance

Addition of guanidinium thiocyanate and N-methylbenimidazole into the electrolyte was shown to have a positive effect on photovoltaic efficiency [47]. As given in Figure 4.15 and Table 4.3, addition of GuSCN into 70% PMII and 30% ($EMIB(CN)_4$) electrolyte containing 0.4 M NMB addition results an enhancement in photocurrent density values almost a factor of 2 up to 0.1 M, while Voc increases slightly in this range. It was reported that GuSCN cations are absorbed together with the dye molecules thus facilitating the formation of a compact monolayer. This monolayer of GuSCN cations and dye molecules prevent the recombination causing a surface passivation effect and positive shift in TiO_2 conduction band probably increasing the injection efficiency of the excited dye molecules [47–49]. However, the photovoltaic performance parameters of the DSSCs showed a decrease when GuSCN concentration is above 0.1 M possibly. Since the transmittance values are increasing from 30.1 % to 32.4 % in the range of 350 nm-800 nm (on the average) when GuSCN molarity increases from 0.1 to 0.2 M, high quantities of GuSCN could lead to the decrease of DSSC performance because of the decrease of the photon absorption by dye molecules (Figure 4.16).

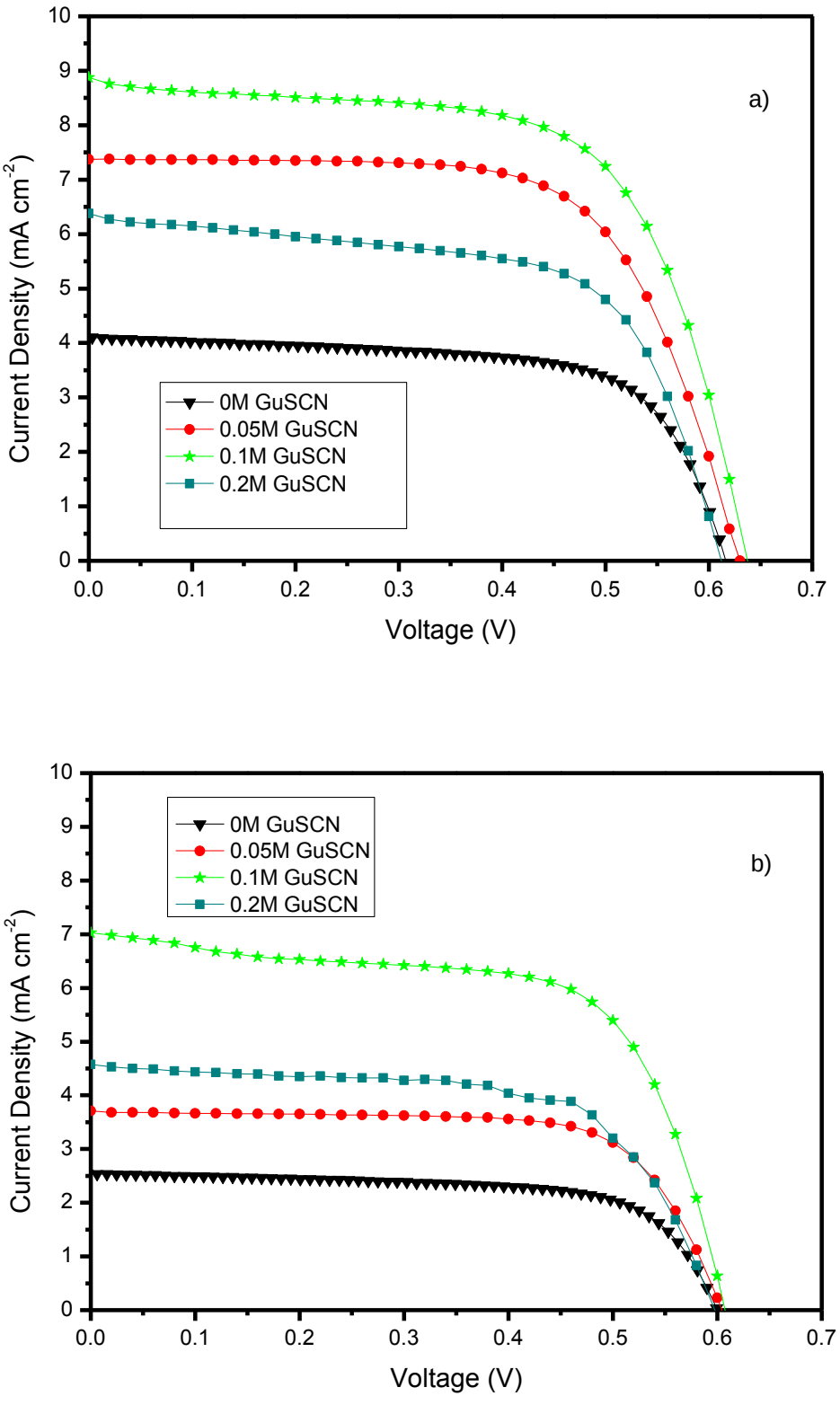

Figure 4.15 J-V characteristics curves for the DSSCs constructed using different compositions of GuSCN irradiated from a) front and b) rear sides [46].

Table 4.3 The photovoltaic characteristics of DSSCs constructed using different compositions of GuSCN [46].

	Molarity of GuSCN (M)	V_{oc} (V)	J_{sc} (mA cm^{-2})	FF	η (%)
Front Side Illumination	0	0.62	4.10	0.67	1.69
	0.05	0.63	7.37	0.66	3.08
	0.1	0.64	8.88	0.61	3.63
	0.2	0.61	6.38	0.63	2.44
Rear Side Illumination	0	0.60	2.54	0.67	1.03
	0.05	0.62	3.71	0.69	1.59
	0.1	0.61	7.03	0.63	2.76
	0.2	0.60	4.58	0.65	1.79

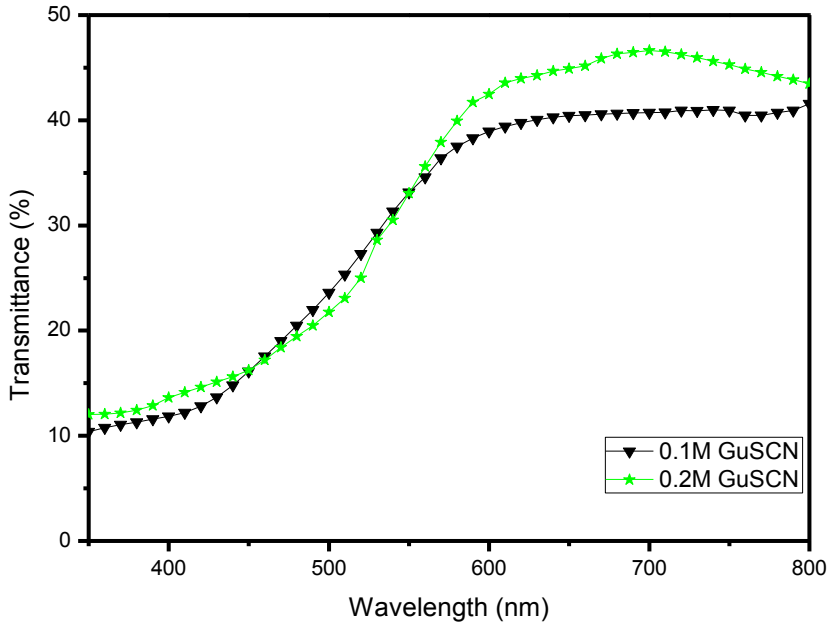

Figure 4.16 Transmittance spectra of the DSSCs constructed using 0.1 and 0.2 M of GuSCN molecules.

Another chemical agent used to improve electrolyte performance is N-methylbenimidazole. Photovoltaic characteristics of the DSSCs constructed using different compositions of NMB added into 70% PMII and 30% ($EMIB(CN)_4$) electrolyte containing 0.1 M GuSCN are summarized in Figure 4.17 and Table 4.4. Maximum efficiency was observed for the cells containing 0.4 M NMB composition as 3.63% for front side illuminated devices. On the contrary of GuSCN, NMB directly affects and heals the performance of open circuit voltage. Photocurrent density is improved with the addition of NMB only slightly compared to GuSCN. Moreover, addition of NMB more than 0.4M decreases Jsc considerably. NMB is another surface passivating agent suppressing recombination and dark current resulting in enhanced efficiency and open circuit voltage. NMB forms a crystalline product in ionic liquid electrolytes which causes a negative shift of the conduction band causing a longer electron lifetime in the TiO_2 film under open circuit conditions [9, 47]. Both GuSCN and NMB additions to the electrolyte also cause an enhancement in the efficiency of the DSSCs for rear side illuminations.

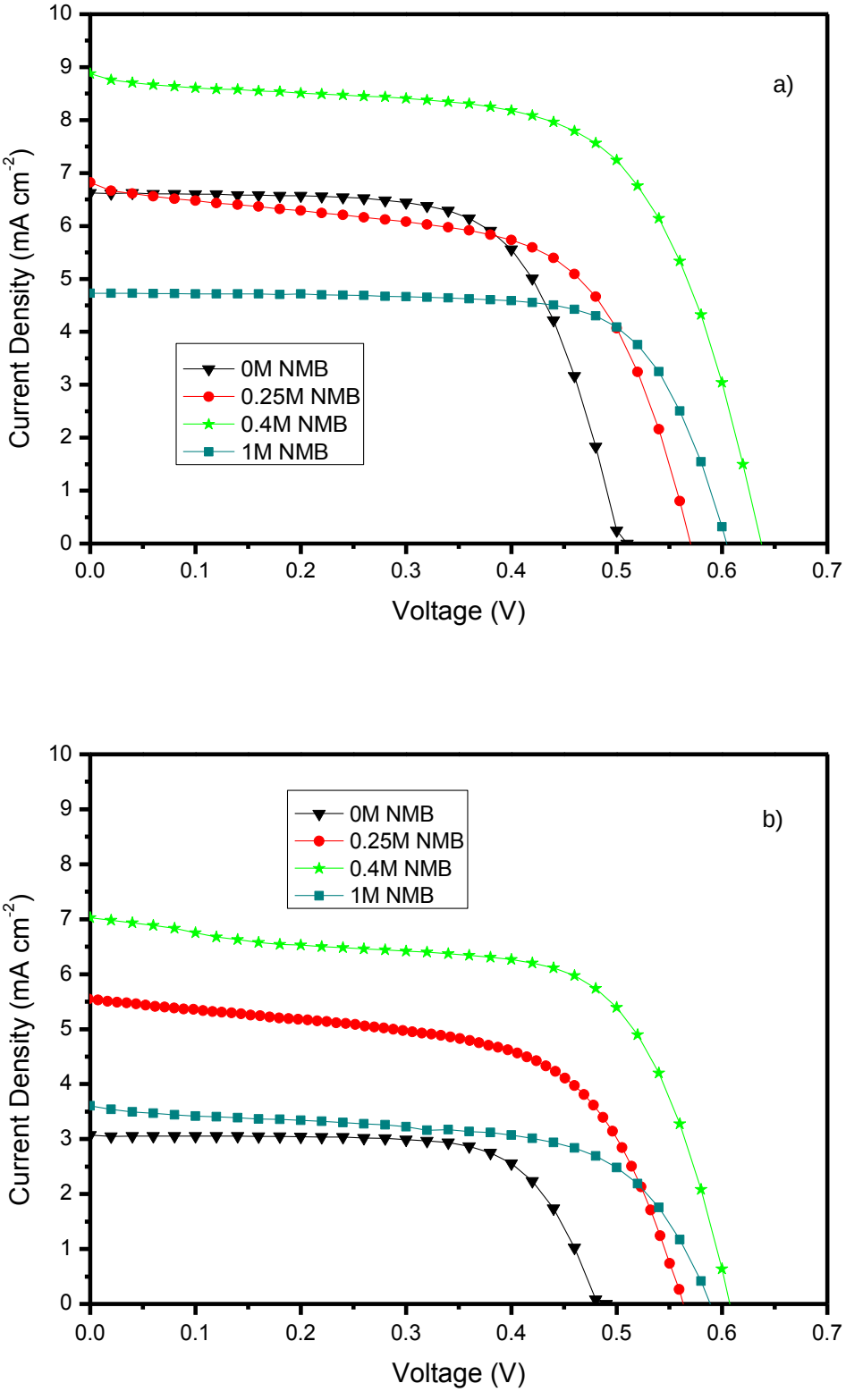

Figure 4.17 J-V characteristics curves for the DSSCs constructed using different compositions of NMB irradiated from a) front and b) rear sides [46].

Table 4.4 The photovoltaic characteristics of DSSCs constructed using different compositions of NMB [46].

	Molarity of NMB (M)	V_{oc} (V)	J_{sc} (mA cm^{-2})	FF	η (%)
Front Side Illumination	0	0.51	6.62	0.66	2.34
	0.25	0.57	6.82	0.62	2.37
	0.4	0.64	8.88	0.61	3.63
	1	0.61	4.73	0.65	2.06
Rear Side Illumination	0	0.49	3.07	0.69	1.04
	0.25	0.56	5.55	0.64	1.87
	0.4	0.61	7.03	0.63	2.76
	1	0.59	3.61	0.66	1.30

4.3.4. Effect of SiO_2 on Photovoltaic Performance

It is seen that addition of SiO_2 as dispersed particles in the electrolyte improves photocurrent density and the efficiency of the devices in front and rear side illuminated cells (Figure 4.18 and Table 4.5). IPCE measurements (Figure 4.19) reveal enhanced photon absorption with the addition of SiO_2 nanoparticles which show an increase about 41% at 540 nm with respect to the SiO_2-free electrolyte. Application of dispersed nanoparticles in the electrolyte provides enhancement in the photovoltaic efficiency of the devices better than using SiO_2 as an additional layer.

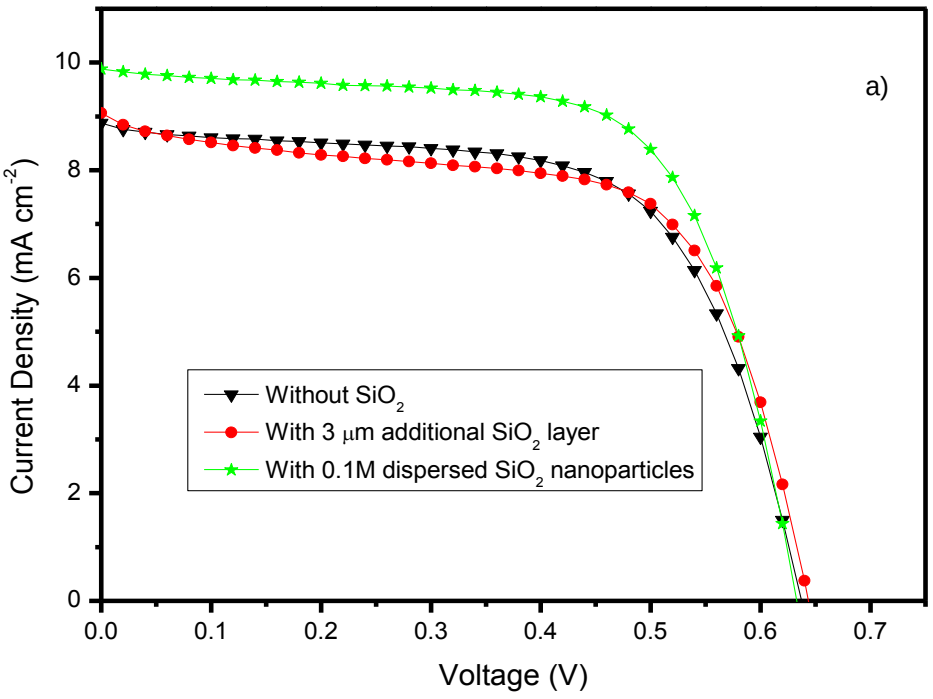

Figure 4.18 J-V characteristics curves for the DSSCs constructed using SiO_2 additions irradiated from a) front and b) rear sides.

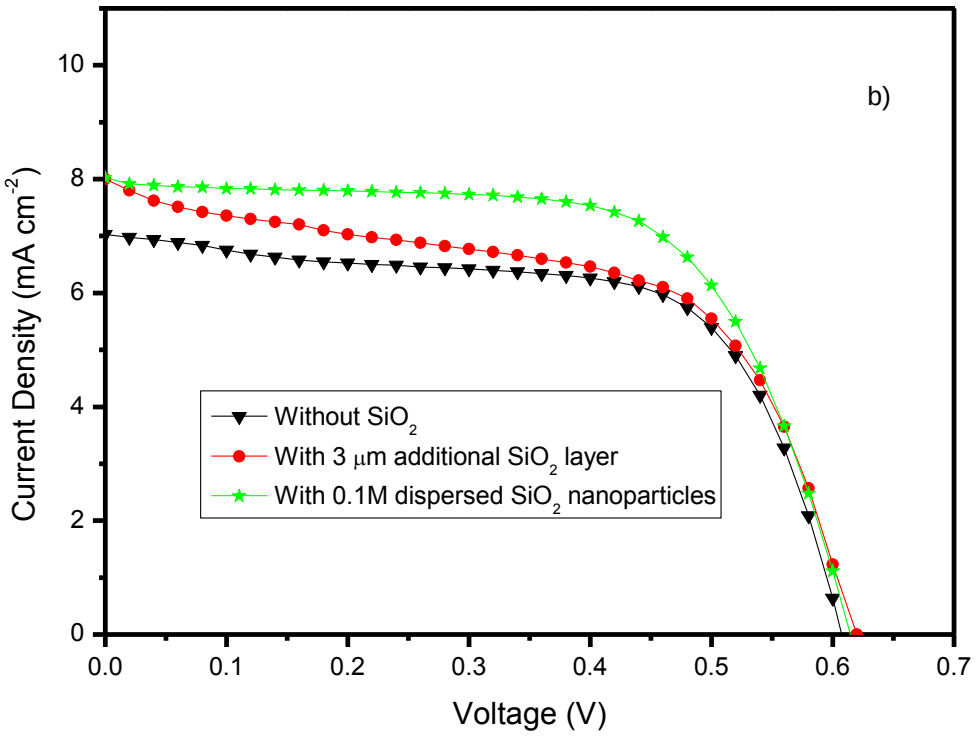

Figure 4.18 J-V characteristics curves for the DSSCs constructed using SiO_2 additions irradiated from a) front and b) rear sides. (Continued)

Table 4.5 The photovoltaic characteristics of DSSCs constructed using SiO_2 additions.

		V_{oc} (V)	J_{sc} (mA cm^{-2})	FF	η (%)
Front Side Illumination	Without SiO_2	0.64	8.88	0.61	3.63
	Additional 3 μm SiO_2 layer	0.65	9.06	0.62	3.67
	Addition of 0.1 M SiO_2 nanoparticles into electrolyte	0.63	9.88	0.66	4.21
Rear Side Illumination	Without SiO_2	0.61	7.03	0.63	2.76
	Additional 3 μm SiO_2 layer	0.62	8.02	0.58	2.83
	Addition of 0.1 M SiO_2 nanoparticles into electrolyte	0.61	8.10	0.67	3.23

Electrolyte diffusion rate can be increased by an exchange reaction which is the result of electron hopping along a continuous I^-/I_3^- chain in ionic liquid [20]. This exchange reaction, which is also called Grotthus transport, reinforces the physical diffusion. When SiO_2 nanoparticles are added to the IL electrolyte, a relative improvement in the DSSC efficiency is observed. SiO_2 nanoparticles are located at the center and they are surrounded by imidazolium cations as seen in figure 3.4. Imidazolium cations are covered by iodide and triiodide anions which carry out the exchange reaction. Thus, SiO_2 nanoparticles and electrolyte make a composite structure which provides the electron hopping in the electrolyte. SiO_2 acts as a spacing layer without adsorbing any dye molecule and does not contribute considerably to the photocurrent when deposited as an overlayer on TiO_2 compared to the dispersed SiO_2 nanoparticles in the electrolyte (Figure 4.20).

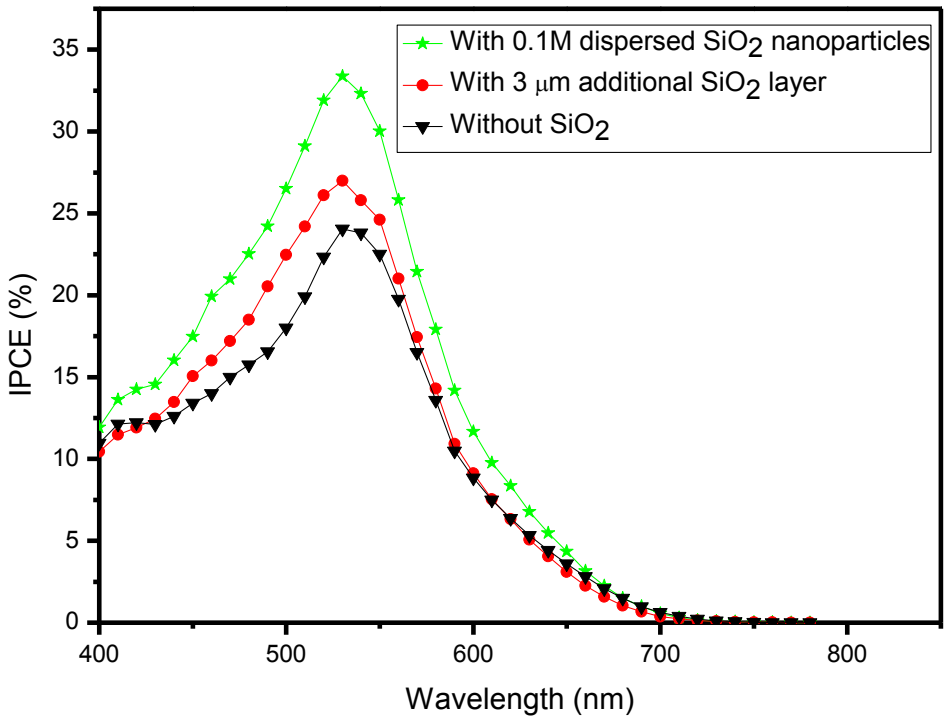

Figure 4.19 IPCE measurements of the DSSCs constructed using SiO_2 additions as 0.1M dispersed nanoparticles, 3 μm layer and without SiO_2.

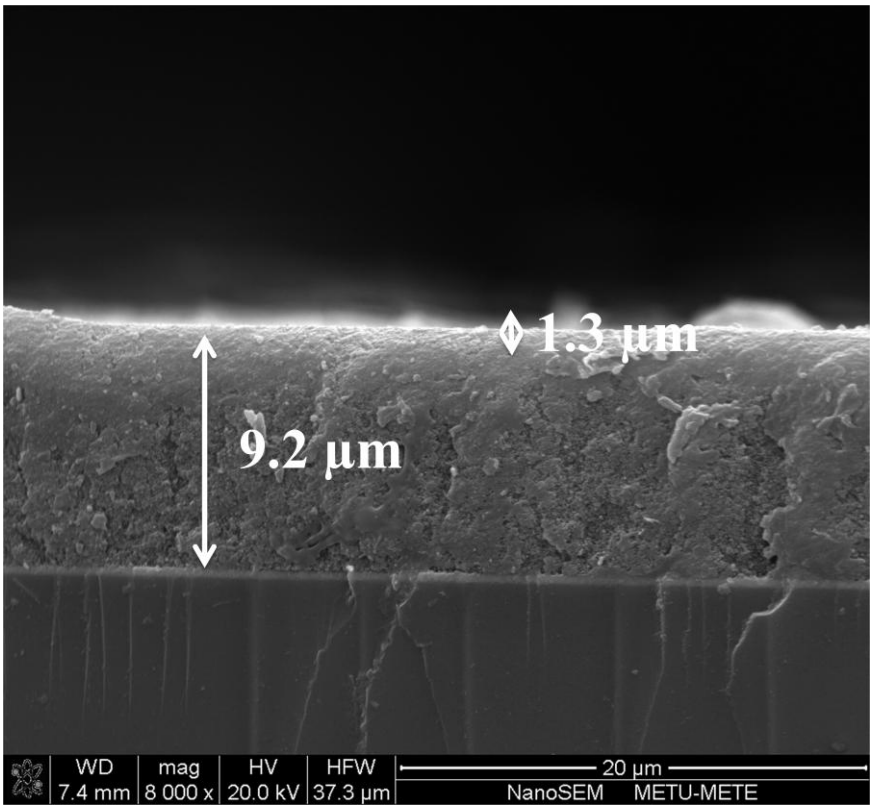

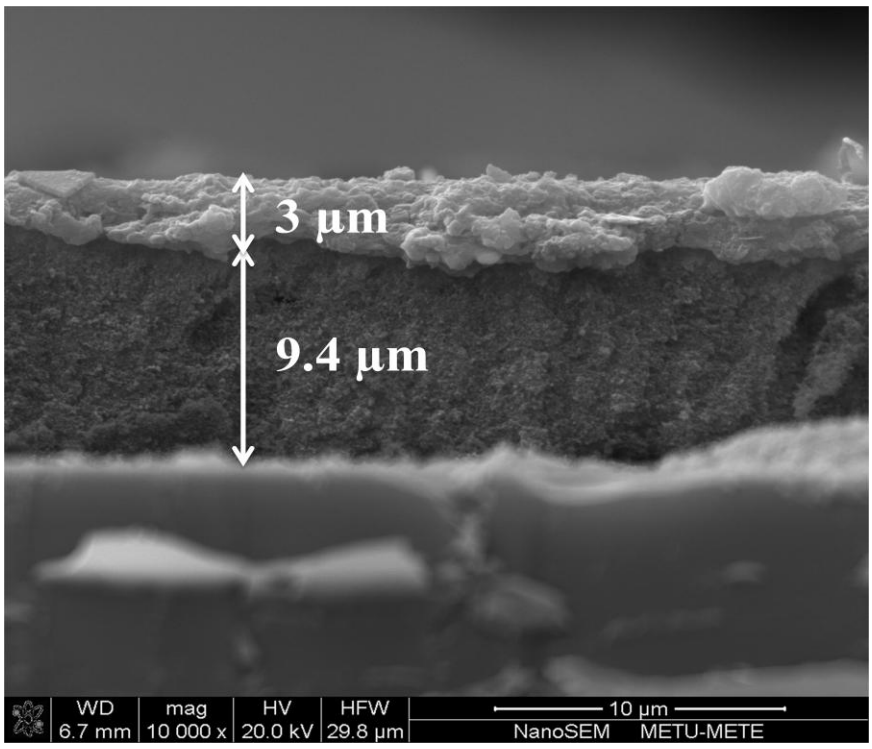

Figure 4.20 The SEM cross-sectional image of 1.3 and 3 µm SiO_2 overlayers on top of TiO_2 photoanode.

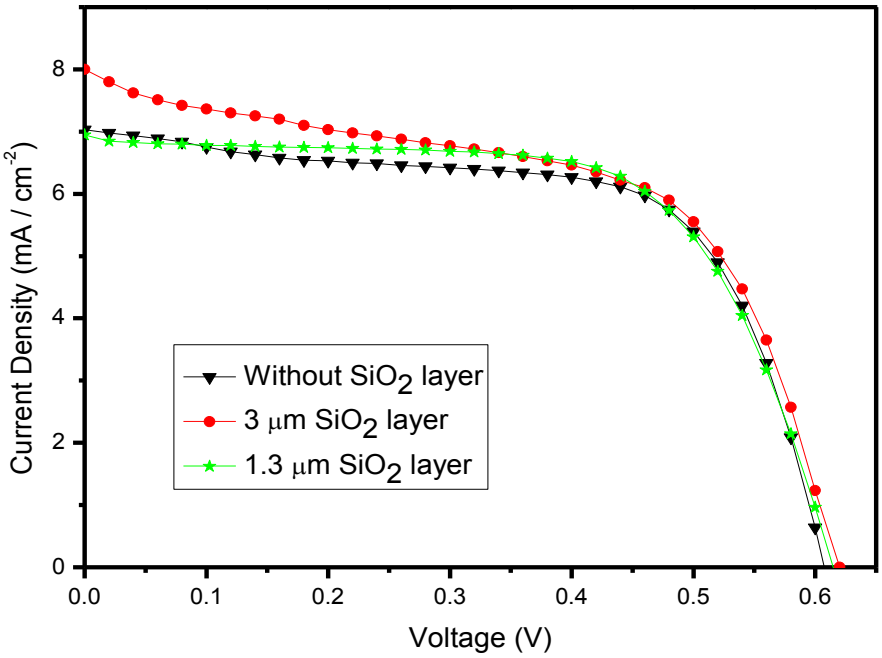

Figure 4.21 J-V characteristics curves for the DSSCs constructed using SiO_2 additions irradiated from a) front and b) rear sides.

This porous SiO_2 layer decreases optical density of the electrolyte and acts as an electrical insulator for the platinum counter electrode [1]. Porous layer is added using screen printing technique by preparing a SiO_2 paste. One layer obtained using screen printing provides about 1.3 μm thick silica layer and two layer coating gives about 3 μm thickness. The cell performances obtained using rear side illuminations in the case of 1.3 μm and 3 μm thick SiO_2 layers are given in Figure 4.21. As indicated in the figure, 1.3 μm SiO_2 layer has almost the same cell performance with the cell without SiO_2 layer. However, when using of 3 μm SiO_2 layer, cell performance increases. This is why 3 μm SiO_2 layer was used in this work for healing the performance of dye sensitized solar cells under rear side illumination.

The improvement of the photocurrent values for the rear side illuminated devices compared to the front side illuminated ones in the case of DSSCs constructed using porous SiO_2 layer can be related to less absorbed photons by the electrolyte where photons can reach photoanode part of the device and increase photocurrent. Transmission measurements were done on the DSSCs having nearly the same photoanode and counter electrode thicknesses and dye amount to ensure similar cell conditions for the devices. Transparency of the cells increased from 31.3% to 42.0% by the addition of SiO_2 nanoparticles due to the decrease in the absorption in electrolyte (Figure 4. 22). Therefore, number of photons reaching the dye molecules in the case of rear side illuminations was increased causing an enhancement in the device efficiency from 2.76% to 3.23% as given in Table 4.5.

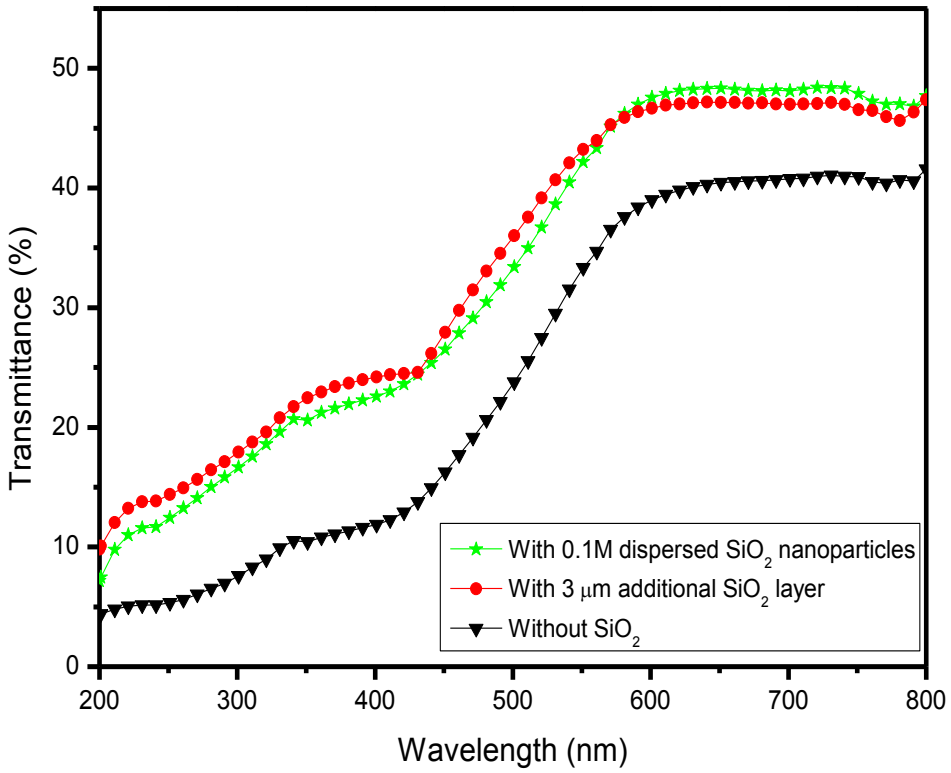

Figure 4.22 Transmittance spectra of the DSSCs constructed using SiO_2 additions as 0.1M dispersed nanoparticles, 3 μm layer and without SiO_2.

CHAPTER 5

CONCLUSIONS AND SUGGESTIONS

In this thesis, bifacial dye sensitized solar cells were constructed using transparent electrolyte layer. Due to the stability problems of the solvent based electrolytes, quasi solid electrolytes which were also critical to obtain transparent electrolyte were used in this study. Electrolytes were produced with the addition of different chemicals to obtain maxümum cell performances. Photovoltaic performances of both front and rear sides of the cells for the different electrolyte compositions were characterized using J-V and IPCE measurements. Titanium dioxide and Silicon dioxide were screen printed on FTO glass using different printing cycles as an active photoanode layer. XRD, SEM and EDX analysis give a quite important data about thick photoanode and SiO_2 layers.

XRD analysis was applied to determine the existing phases in the thick photoanode layer. Anatase and rutile phases of the titania and tin dioxide were observed in XRD spectrum. Although, the precursor composition was known before starting to work, no compositional change was observed after all the steps, especially at sintering. Many strong peaks of anatase are found in XRD spectrum. Also, particle size analyis was made using strongest peak of anatase by Debye-Scherrer equation. Particle size was calculated as 20 nm and this value was also consistent with the data sheet of the precursor. Low particle size is also a proof of existence of anatase phase, because anatase phase is the dominant phase between 10-20 nm particle sizes.

SEM studies were performed on titania thick layers coated on FTO glasses. These studies reveal that titania particles have spherical shape and they are homogenously distributed. They have good contact with each other and this supplies a good network in the photoanode layer. Average particle size was measured as 20 nm which was similar to XRD result. Images also show dense and highly porous structure of the titania film. Amount of dye absorption of titania film increases with porosity of the photoanode. Cross-sectional SEM images indicate the well adherence of the thick TiO_2 film on the substrate and these images show the average coating thicknesses. Coating thickness of the photoanode is controlled using printing cycles.When the number of screen printing cycles exceeds six, coatings start to show peeling-off on the substrate due to the stress occurring between the layers. Also, silica layer is coated on the titania layer at different coating thicknesses. A good contact between the silica and titania is supplied and complex structure behaves as a rigid body. According to EDX result, photoanode layers did not include any contaminations where the presence of them shows a dramatic decrease in the photovoltaic performance. Most critical point for the thick mesoporous photoanode layer is the agglomeration. When the agglomeration reaches to the micron levels, it creates cracks on the surface of the coated layer. These cracks damage the electron transport in the photoanode and decrease the efficiencies of the cells. Therefore, in paste production, a breaking procedure should be applied on the solution to prevent the agglomeration of the particles. Although, coatings show some cracks in this work, adherence of the layers on the substrate is quite good. However, these cracks certainly create a performance decrease.

The performance of ionic liquid electrolyte is tried to increase with some additions. For this reason, electrolyte composition, photoanode thickness, and the additions of GuSCN, NMB, and SiO_2 on the photovoltaic performance of DSSCs were studied. We have demonstrated that a bifacial DSSC can be realized. Analysis of J–V characteristics of the devices indicated that 70% PMII/ 30% ($EMIB(CN)_4$) electrolyte composition yielded the maximum efficiency.

Increase in efficiency directly related to the increase in diffusion coefficient of the electrolyte. Then, TiO_2 coatings at different thicknesses were compared and best photovoltaic efficiency was obtained using 10 μm thick coating which is considered to be the ideal coating thickness for the diffusion length of electrolyte and dye absorption. Optimum molarity of GuSCN is found as 0.1 M and for this molarity, photocurrent is dramatically improved due to decreased recombination which is believed to be surface passivation effect at photoanode electrolyte interface suppressing recombination rate. Moreover, optimum NMB molarity was found to be 0.4 for maximum efficiency. The band edge movement in NMB added electrolyte was observed with a significantly enhanced open circuit voltage.

Addition of SiO_2 to the electrolyte both as an overlayer and dispersed particles enhanced rear side illuminated cells where dispersed particles are found to be more efficient for the front side illuminated cells due to additional electron transport properties. Transparency measurements reveal the increase in transparency of the cells. More transparent cells supply more photons in the case of rear side measurements. Photocurrent of the cells increases dramatically with the increase in the amount of absorbed photons. IPCE measurements reveal enhanced photon absorption with the addition of SiO_2 nanoparticles which show an increase about 41% at 540 nm with respect to the SiO_2-free electrolyte. Application of dispersed nanoparticles in the electrolyte provides enhancement in the photovoltaic efficiency of the devices better than using SiO_2 as an additional layer.

Best rear side illuminated cell efficiency was 3.2% compared to front side illuminated cell efficiency of 4.2% which is a promising result for future rear side dye sensitized solar cell applications where front side illumination is not possible like tandem structures and for cells working from both front and rear side illuminations which seem to be one of the most promising strategies to further improve DSSC efficiency.

To conclude;

- A bifacial DSSC is realized and irradiated from front and rear sides.
- Maximum efficiency was found for 70% PMII/30% ($EMIB(CN)_4$) electrolyte composition.
- It was seen that ionic liquids provide quite sufficient photovoltaic efficiencies and therefore, they may be used as alternating electrolytes instead of solvent based electrolytes in near future.
- 10 μm thick photoanode coating is considered to be the ideal coating thickness for the diffusion length of electrolyte and maximum dye absorption.
- A significant increase in photocurrent using 0.1 M GuSCN and 0.4 M NMB was observed.
- Addition of SiO_2 nanoparticles to the electrolyte enhanced photovoltaic efficiency.
- Dispersed SiO_2 particles are found to be more efficient compared to SiO_2 overlayer for both front and rear side measurements.

To suggest;

- Bifacial cells are really an important topic for both classical and dye sensitized solar cells. Although, this work aims to increase the relative performance of the rear side to front side of the cell, collection of photons both from the front and rear sides may be possible using some specific cell designs.

- PMII electrolyte performance was increased by the addition of GuSCN, NMB and SiO_2 nanoparticles, however, tert-butylpyridine and N-alkylbenzimidazoles additions can also be used for the enhancement of photovoltaic performance.

- Although, it is known that quasi solid electrolytes have quite better stability than solvent based electrolytes, stabilities of the cells prepared using different electrolytes should be studied by electrochemical impedance measurements.

- In this work, N719 dye molecules were used due to the availability in the market, however, high extinction coefficient dye molecules can also provide an increase in cell performance.

- Due to the agglomerations occurring among overlayer silica nanoparticles, a decrease in open circuit voltage of the cell was observed. By controlling the silica paste production, cells with overlayer silica can yield higher efficiencies for the rear side measurements.

REFERENCES

[1] S. Ito, S. M. Zakeeruddin, P. Comte, P. Liska, D. Kuang, and M. Grätzel, “Bifacial dye-sensitized solar cells based on an ionic liquid electrolyte,” *Nature Photonics*, vol. 2, no. 11, pp. 693-698, Oct. 2008.

[2] G. P. Smestad, *Optoelectronics of Solar Cells*. Bellingham, Washington: SPIE Press, 2002.

[3] A. Jäger-Waldau, *PV Status Report 2010*. Ispra (VA), Italia: Luxembourg: Office for Official Publications of the European Union, 2010.

[4] B. O’Regan and M. Gratzel, “A low-cost, high-efficiency solar cell based on dye-sensitized colloidal TiO_2 films,” *Nature*, vol. 353, no. 6346, pp. 737-740, Oct. 1991.

[5] Y.-F. Chiang, C.-H. Tsai, P. Chen, and T.-F. Guo, “Bifacial transparent solid-state dye-sensitized solar cell with sputtered indium-tin-oxide counter electrode,” *Solar Energy*, Apr. 2012.

[6] Y. Liu, J. Y. Lee, and L. Hong, “In situ preparation of poly(ethylene oxide)–SiO_2 composite polymer electrolytes,” *Journal of Power Sources*, vol. 129, no. 2, pp. 303-311, Apr. 2004.

[7] A. C. Arango, L. R. Johnson, V. N. Bliznyuk, Z. Schlesinger, S. A. Carter, and H.-H. Hörhold, “Efficient Titanium Oxide/Conjugated Polymer Photovoltaics for Solar Energy Conversion,” *Advanced Materials*, vol. 12, no. 22, pp. 1689-1692, 2000.

[8] B. O’Regan, D. T. Schwartz, S. M. Zakeeruddin, and M. Grätzel, “Electrodeposited Nanocomposite n–p Heterojunctions for Solid-State Dye-Sensitized Photovoltaics,” *Advanced Materials*, vol. 12, no. 17, pp. 1263-1267, 2000.

[9] M. Gorlov and L. Kloo, “Ionic liquid electrolytes for dye-sensitized solar cells.,” *Dalton transactions (Cambridge, England : 2003)*, no. 20, pp. 2655-66, May 2008.

[10] P. Wang et al., “Charge Separation and Efficient Light Energy Conversion in Sensitized Mesoscopic Solar Cells Based on Binary Ionic Liquids,” *Journal of the American Chemical Society*, vol. 127, no. 18, pp. 6850-6856, Apr. 2005.

[11] D. Kuang, P. Wang, S. Ito, S. M. Zakeeruddin, and M. Grätzel, “Stable Mesoscopic Dye-Sensitized Solar Cells Based on Tetracyanoborate Ionic Liquid Electrolyte,” *Journal of the American Chemical Society*, vol. 128, no. 24, pp. 7732-7733, May 2006.

[12] D. Kuang et al., “High Molar Extinction Coefficient Heteroleptic Ruthenium Complexes for Thin Film Dye-Sensitized Solar Cells,” *Journal of the American Chemical Society*, vol. 128, no. 12, pp. 4146-4154, Mar. 2006.

[13] P. Bonhôte, A.-P. Dias, N. Papageorgiou, K. Kalyanasundaram, and M. Grätzel, “Hydrophobic, Highly Conductive Ambient-Temperature Molten Salts†,” *Inorganic Chemistry*, vol. 35, no. 5, pp. 1168-1178, Jan. 1996.

[14] J. Xia, N. Masaki, K. Jiang, and S. Yanagida, “Fabrication and characterization of thin Nb_2O_5 blocking layers for ionic liquid-based dye-sensitized solar cells,” *Journal of Photochemistry and Photobiology A: Chemistry*, vol. 188, no. 1, pp. 120-127, Apr. 2007.

[15] P. Wang, S. M. Zakeeruddin, R. Humphry-Baker, and M. Grätzel, “A Binary Ionic Liquid Electrolyte to Achieve ≥7% Power Conversion Efficiencies in Dye-Sensitized Solar Cells,” *Chemistry of Materials*, vol. 16, no. 14, pp. 2694-2696, Jun. 2004.

[16] P. Wang, C. Klein, R. Humphry-Baker, S. M. Zakeeruddin, and M. Grätzel, “Stable ≥8% efficient nanocrystalline dye-sensitized solar cell based on an electrolyte of low volatility,” *Applied Physics Letters*, vol. 86, no. 12, pp. 1-3, 2005.

[17] H. Matsumoto, T. Matsuda, T. Tsuda, R. Hagiwara, Y. Ito, and Y. Miyazaki, “The Application of Room Temperature Molten Salt with Low Viscosity to the Electrolyte for Dye-Sensitized Solar Cell,” *Chemistry Letters*, vol. 30, no. 1, pp. 26-27, 2001.

[18] D. Kuang et al., “Stable, High-Efficiency Ionic-Liquid-Based Mesoscopic Dye-Sensitized Solar Cells,” *Small*, vol. 3, no. 12, pp. 2094-2102, 2007.

[19] Z. Fei et al., “A Supercooled Imidazolium Iodide Ionic Liquid as a Low-Viscosity Electrolyte for Dye-Sensitized Solar Cells,” *Inorganic Chemistry*, vol. 45, no. 26, pp. 10407-10409, Nov. 2006.

[20] M. Berginc, M. Hočevar, U. Opara Krašovec, a. Hinsch, R. Sastrawan, and M. Topič, “Ionic liquid-based electrolyte solidified with SiO_2 nanoparticles for dye-sensitized solar cells,” *Thin Solid Films*, vol. 516, no. 14, pp. 4645-4650, May 2008.

[21] K. Kalyanasundaram, *Dye-Sensitized Solar Cells*, First Edition, Lausanne, Switzerland: EPFL Press, 2010.

[22] S. R. Wenham, *Applied photovoltaics*, Second Edition. London,England: Earthscan, 2007.

[23] H. Christiana and S. Bowden, “PV Education,” 2012. [Online]. Available: http://pveducation.org/. [Accessed: 12-Nov-2012].

[24] M. A. Green, *Solar Cells*. Kensington, New South Wales: Prentice-Hall, 1992.

[25] A. L. Fahrenbruch, *Fundamentals of solar cells : photovoltaic solar energy conversion*. New York: Academic Press, 1983.

[26] A. KITAI, *Principles of Solar Cells, LEDs and Diodes*. West Sussex, UK: John Wiley & Sons, Ltd, 2011.

[27] S. J. Fonash, *Solar Cell Device Physics*. Burlington,Massachusetts: Academic Press/Elsevier, 2010.

[28] J. Nelson, *The Physics of Solar Cells*. London,England: Imperial College Press, 2003.

[29] M. Ohring, *The Material Science of Thin Films*. California,USA: Academic Press, 1992.

[30] S. H. Antonio Luque, *Handbook of Photovoltaic Science and Engineering*, Second Edition. West Sussex, UK: John Wiley & Sons, Ltd, 2011.

[31] T. M. and L. Castañer, *Solar cells: materials, manufacture and operation*. Oxford: Elsevier Advanced Technology, 2005.

[32] J.-kun Lee and M. Yang, "Progress in light harvesting and charge injection of dye-sensitized solar cells," *Materials Science & Engineering B*, pp. 1-19, 2011.

[33] R. G. Gordon, "Criteria for Choosing Transparent Conductors," *MRS Bulletin* pp. 52-57, August 2000.

[34] M. Grätzel, "Conversion of sunlight to electric power by nanocrystalline dye-sensitized solar cells," *Journal of Photochemistry and Photobiology A: chemistry* vol. 164, pp. 3-14, 2004.

[35] D.-H. Lee, J.-G. Park, K. Jin Choi, H.-J. Choi, and D.-W. Kim, "Preparation of Brookite-Type TiO2/Carbon Nanocomposite Electrodes for Application to Li Ion Batteries," *European Journal of Inorganic Chemistry*, vol. 2008, no. 6, pp. 878-882, Feb. 2008.

[36] J. Krüger, "Interface Engineering in Solid-state Dye-sensitized solar cells," École Polytechnique Fédérale de Lausanne, *PhD. Thesis*, 2003.

[37] S. Ito, P. Chen, and P. Comte, "Fabrication of screen-printing pastes from TiO2 powders for dye-sensitised solar cells," *Progress in Photovoltaics: Research and Applications*, no.15, pp. 603-612, May 2007.

[38] B. Xue et al., "Highly efficient dye-sensitized solar cells using a composite electrolyte," *Comptes Rendus Chimie*, vol. 9, no. 5–6, pp. 627-630, May 2006.

[39] R. Kawano et al., "High performance dye-sensitized solar cells using ionic liquids as their electrolytes," *Journal of Photochemistry and Photobiology A: Chemistry*, vol. 164, no. 1–3, pp. 87-92, Jun. 2004.

[40] K.-M. Lee, P.-Y. Chen, C.-P. Lee, and K.-C. Ho, "Binary room-temperature ionic liquids based electrolytes solidified with SiO_2 nanoparticles for dye-sensitized solar cells," *Journal of Power Sources*, vol. 190, no. 2, pp. 573-577, May 2009.

[41] S. Ito et al., "Fabrication of thin film dye sensitized solar cells with solar to electric power conversion efficiency over 10%," *Thin Solid Films*, vol. 516, no. 14, pp. 4613-4619, May 2008.

[42] K. Ç. İçli, "Core-Shell type Nanocrystalline FTO Photoanodes for Dye Sensitized Solar Cells," Middle East Technical University, *M.Sc Thesis* 2010.

[43] J. Halme, "Dye-sensitized nanostructured and organic photovoltaic cells: technical review and preliminary tests," Helsinki University of Technology, *M.Sc. Thesis*, 2002.

[44] A. J. Frank, N. Kopidakis, and J. V. D. Lagemaat, "Electrons in nanostructured TiO_2 solar cells : transport, recombination and photovoltaic properties," *Coordination Chemistry Reviews*, vol. 248, pp. 1165-1179, 2004.

[45] I. R. Edmonds, "The performance of biracial solar cells in static solar concentrators," *Solar Energy Materials*, vol. 21, pp. 173-190, 1990.

[46] B. Cosar, K. C. Icli, H. I. Yavuz, and M. Ozenbas, “Photovoltaic performance of bifacial dye sensitized solar cell using chemically healed binary ionic liquid electrolyte solidified with SiO_2 nanoparticles,” *Electrochimica Acta*, vol. 87, pp. 425-431, Jan. 2013.

[47] Z. Yu, M. Gorlov, G. Boschloo, and L. Kloo, “Synergistic Effect of N-Methylbenzimidazole and Guanidinium Thiocyanate on the Performance of Dye-Sensitized Solar Cells Based on Ionic Liquid Electrolytes,” *The Journal of Physical Chemistry C*, vol. 114, no. 50, pp. 22330-22337, Nov. 2010.

[48] N. Kopidakis, N. R. Neale, and A. J. Frank, “Effect of an Adsorbent on Recombination and Band-Edge Movement in Dye-Sensitized TiO2 Solar Cells: Evidence for Surface Passivation,” *The Journal of Physical Chemistry B*, vol. 110, no. 25, pp. 12485-12489, Jun. 2006.

[49] C. Zhang, Y. Huang, Z. Huo, S. Chen, and S. Dai, “Photoelectrochemical Effects of Guanidinium Thiocyanate on Dye-Sensitized Solar Cell Performance and Stability,” *The Journal of Physical Chemistry C*, vol. 113, no. 52, pp. 21779-21783, Dec. 2009.